

18.S995 (Spring 2016, MWF 3-4, 2-142)
Mathematical Concepts in Biology and Biological
Physics

Jörn Dunkel

March 18, 2016

Contents

1	Diffusion, SDE models and fluctuation theorems	3
1.1	Random walks	3
1.2	Brownian motion	7
1.3	Dilute microbial suspensions	12
1.4	Escape problem	16
1.5	Stochastic resonance	21
1.6	Brownian motors	25
1.7	Fluctuation-dissipation relation	29
1.8	Fluctuation theorems	30
1.9	Problems (due Monday, March 14)	35
1.10	Solutions	37
2	Polymers	44
2.1	Persistent random walks	44
2.2	Bead-spring model	50
2.3	Continuum description	51
2.4	Problems (due Monday, April 11)	57
3	Membranes	58
3.1	Reminder: 2D differential geometry	58
3.2	Minimal surfaces	60
3.3	Thermal excitations of almost flat membranes	61
3.4	Helfrich's model	63
4	Pattern formation	65
4.1	Warm-up	65
4.2	Swift-Hohenberg model	66
4.3	Vector model for an incompressible active fluid	70
4.4	Reaction-diffusion systems (RDSs)	75
5	Microbial locomotion	79
5.1	Navier-Stokes equations	80
5.2	Stokes equations	82

5.3	Golestanian's swimmer model	84
5.4	Dimensionality	89
5.5	Force dipole and dimensionality	90
5.6	Boundary effects	92
5.7	Rheotaxis and resistive force theory	94
6	Network models	103
6.1	Graphs	103
6.2	Trees and Kirchhoff's theorem	110
6.3	Transport	111
A	Stochastic integrals and calculus	112
A.1	Ito integral	113
A.2	Stratonovich-Fisk integral	114
A.3	Backward Ito integral	117
A.4	Comparison of stochastic integrals	118
A.5	Numerical integration	119
B	Swimming Velocity for Arbitrary Deformations	121

Chapter 1

Diffusion, SDE models and fluctuation theorems

Excellent reviews of the topics discussed in this chapter can be found in Refs. [CPB08, HTB90, GHJM98, HM09].

1.1 Random walks

1.1.1 Unbiased random walk (RW)

Consider the one-dimensional unbiased RW (fixed initial position $X_0 = x_0$, N steps of length ℓ)

$$X_N = x_0 + \ell \sum_{i=1}^N S_i \quad (1.1)$$

where $S_i \in \{\pm 1\}$ are iid. random variables (RVs) with $\mathbb{P}[S_i = \pm 1] = 1/2$. Noting that ¹

$$\mathbb{E}[S_i] = -1 \cdot \frac{1}{2} + 1 \cdot \frac{1}{2} = 0, \quad (1.2)$$

$$\mathbb{E}[S_i S_j] = \delta_{ij} \mathbb{E}[S_i^2] = \delta_{ij} \left[(-1)^2 \cdot \frac{1}{2} + (1)^2 \cdot \frac{1}{2} \right] = \delta_{ij}, \quad (1.3)$$

we find for the first moment of the RW

$$\mathbb{E}[X_N] = x_0 + \ell \sum_{i=1}^N \mathbb{E}[S_i] = x_0 \quad (1.4)$$

¹By definition, for some RV X with normalized non-negative probability density $p(x) = \frac{d}{dx} \mathbb{P}[X \leq x]$, we have $\mathbb{E}[F(X)] = \int dx p(x) F(x)$. For discrete RVs, we can think of $p(x)$ as being a sum of suitably normalized δ -distributions.

and for the second moment

$$\begin{aligned}
\mathbb{E}[X_N^2] &= \mathbb{E}\left[\left(x_0 + \ell \sum_{i=1}^N S_i\right)^2\right] \\
&= \mathbb{E}\left[x_0^2 + 2x_0\ell \sum_{i=1}^N S_i + \ell^2 \sum_{i=1}^N \sum_{j=1}^N S_i S_j\right] \\
&= x_0^2 + 2x_0 \cdot 0 + \ell^2 \sum_{i=1}^N \sum_{j=1}^N \mathbb{E}[S_i S_j] \\
&= x_0^2 + 2x_0 \cdot 0 + \ell^2 \sum_{i=1}^N \sum_{j=1}^N \delta_{ij} \\
&= x_0^2 + \ell^2 N.
\end{aligned} \tag{1.5}$$

The variance (second centered moment)

$$\begin{aligned}
\mathbb{E}[(X_N - \mathbb{E}[X_N])^2] &= \mathbb{E}[X_N^2 - 2X_N\mathbb{E}[X_N] + \mathbb{E}[X_N]^2] \\
&= \mathbb{E}[X_N^2] - 2\mathbb{E}[X_N]\mathbb{E}[X_N] + \mathbb{E}[X_N]^2 \\
&= \mathbb{E}[X_N^2] - \mathbb{E}[X_N]^2
\end{aligned} \tag{1.6}$$

therefore grows linearly with the number of steps:

$$\mathbb{E}[(X_N - \mathbb{E}[X_N])^2] = \ell^2 N. \tag{1.7}$$

Continuum limit From now on, assume $x_0 = 0$ and consider an even number of steps $N = t/\tau$, where $\tau > 0$ is the time required for a single step of the RW and t the total time. The probability $P(N, K) := \mathbb{P}[X_N/\ell = K]$ to be at an even position $x/\ell = K \geq 0$ after N steps is given by the binomial coefficient

$$\begin{aligned}
P(N, K) &= \left(\frac{1}{2}\right)^N \binom{N}{\frac{N-K}{2}} \\
&= \left(\frac{1}{2}\right)^N \frac{N!}{((N+K)/2)!((N-K)/2)!}.
\end{aligned} \tag{1.8}$$

The associated probability density function (PDF) can be found by defining

$$p(t, x) := \frac{P(N, K)}{2\ell} = \frac{P(t/\tau, x/\ell)}{2\ell} \tag{1.9}$$

and considering limit $\tau, \ell \rightarrow 0$ such that

$$D := \frac{\ell^2}{2\tau} = \text{const}, \tag{1.10}$$

yielding the Gaussian

$$p(t, x) \simeq \sqrt{\frac{1}{4\pi Dt}} \exp\left(-\frac{x^2}{4Dt}\right) \quad (1.11)$$

Eq. (1.11) is the fundamental solution to the diffusion equation,

$$\partial_t p_t = D \partial_{xx} p, \quad (1.12)$$

where $\partial_t, \partial_x, \partial_{xx}, \dots$ denote partial derivatives. The mean square displacement of the continuous process described by Eq. (1.11) is

$$\mathbb{E}[X(t)^2] = \int dx x^2 p(t, x) = 2Dt, \quad (1.13)$$

in agreement with Eq. (1.7).

Remark One often classifies diffusion processes by the (asymptotic) power-law growth of the mean square displacement,

$$\mathbb{E}[(X(t) - X(0))^2] \sim t^\mu. \quad (1.14)$$

- $\mu = 0$: Static process with no movement.
- $0 < \mu < 1$: Sub-diffusion, arises typically when waiting times between subsequent jumps can be long and/or in the presence of a sufficiently large number of obstacles (e.g. slow diffusion of molecules in crowded cells).
- $\mu = 1$: Normal diffusion, corresponds to the regime governed by the standard Central Limit Theorem (CLT).
- $1 < \mu < 2$: Super-diffusion, occurs when step-lengths are drawn from distributions with infinite variance (Lévy walks; considered as models of bird or insect movements).
- $\mu = 2$: Ballistic propagation (deterministic wave-like process).

1.1.2 Biased random walk (BRW)

Consider a one-dimensional hopping process on a discrete lattice (spacing ℓ), defined such that during a time-step τ a particle at position $X(t) = \ell j \in \ell\mathbb{Z}$ can either

- (i) jump a fixed distance ℓ to the left with probability λ , or
- (ii) jump a fixed distance ℓ to the right with probability ρ , or
- (iii) remain at its position x with probability $(1 - \lambda - \rho)$.

Assuming that the process is Markovian (does not depend on the past), the evolution of the associated probability vector $P(t) = (P(t, x)) = (P_j(t))$, where $x = \ell j$, is governed by the master equation

$$P(t + \tau, x) = (1 - \lambda - \rho) P(t, x) + \rho P(t, x - \ell) + \lambda P(t, x + \ell). \quad (1.15)$$

Technically, ρ , λ and $(1 - \lambda - \rho)$ are the non-zero-elements of the corresponding transition matrix $W = (W_{ij})$ with $W_{ij} > 0$ that governs the evolution of the column probability vector $P(t) = (P_j(t)) = (P(t, y))$ by

$$P_i(t + \tau) = W_{ij} P_j(t) \quad (1.16a)$$

or, more generally, for n steps

$$P(t + n\tau) = W^n P(t). \quad (1.16b)$$

The stationary solutions are the eigenvectors of W with eigenvalue 1. To preserve normalization, one requires $\sum_i W_{ij} = 1$.

Continuum limit Define the density $p(t, x) = P(t, x)/\ell$. Assume τ, ℓ are small, so that we can Taylor-expand

$$p(t + \tau, x) \simeq p(t, x) + \tau \partial_t p(t, x) \quad (1.17a)$$

$$p(t, x \pm \ell) \simeq p(t, x) \pm \ell \partial_x p(t, x) + \frac{\ell^2}{2} \partial_{xx} p(t, x) \quad (1.17b)$$

Neglecting the higher-order terms, it follows from Eq. (1.15) that

$$\begin{aligned} p(t, x) + \tau \partial_t p(t, x) &\simeq (1 - \lambda - \rho) p(t, x) + \\ &\rho [p(t, x) - \ell \partial_x p(t, x) + \frac{\ell^2}{2} \partial_{xx} p(t, x)] + \\ &\lambda [p(t, x) + \ell \partial_x p(t, x) + \frac{\ell^2}{2} \partial_{xx} p(t, x)]. \end{aligned} \quad (1.18)$$

Dividing by τ , one obtains the advection-diffusion equation

$$\partial_t p = -u \partial_x p + D \partial_{xx} p \quad (1.19a)$$

with drift velocity u and diffusion constant D given by²

$$u := (\rho - \lambda)\frac{\ell}{\tau}, \quad D := (\rho + \lambda)\frac{\ell^2}{2\tau}. \quad (1.19b)$$

We recover the classical diffusion equation (1.12) from Eq. (1.19a) for $\rho = \lambda = 0.5$. The time-dependent fundamental solution of Eq. (1.19a) reads

$$p(t, x) = \sqrt{\frac{1}{4\pi Dt}} \exp\left(-\frac{(x - ut)^2}{4Dt}\right) \quad (1.20)$$

Remarks Note that Eqs. (1.12) and Eq. (1.19a) can both be written in the current-form

$$\partial_t p + \partial_x j_x = 0 \quad (1.21)$$

with

$$j_x = up - D\partial_x p, \quad (1.22)$$

reflecting conservation of probability. Another commonly-used representation is

$$\partial_t p = \mathcal{L}p, \quad (1.23)$$

where \mathcal{L} is a linear differential operator; in the above example (1.19b)

$$\mathcal{L} := -u\partial_x + D\partial_{xx}. \quad (1.24)$$

Stationary solutions, if they exist, are eigenfunctions of \mathcal{L} with eigenvalue 0.

1.2 Brownian motion

1.2.1 SDEs and discretization rules

The continuous stochastic process $X(t)$ described by Eq. (1.19a) or, equivalently, Eq. (1.20) can also be represented by the stochastic differential equation

$$dX(t) = u dt + \sqrt{2D} dB(t). \quad (1.25)$$

Here, $dX(t) = X(t + dt) - X(t)$ is increment of the stochastic particle trajectory $X(t)$, whilst $dB(t) = B(t + dt) - B(t)$ denotes an increment of the standard Brownian motion (or Wiener) process $B(t)$, uniquely defined by the following properties³:

²Strictly speaking, when taking the limits $\tau, \ell \rightarrow 0$, one requires that ρ and λ change such that u and D remain constant. Assuming that $\rho + \lambda = \text{const}$, this means that $(\rho - \lambda) \sim \ell$.

³Note that, since X has dimensions of length and D has dimensions length²/time, the Wiener process B in Eq. (1.25) has units time^{1/2}.

- (i) $B(0) = 0$ with probability 1.
- (ii) $B(t)$ is stationary, i.e., for $t > s \geq 0$ the increment $B(t) - B(s)$ has the same distribution as $B(t - s)$.
- (iii) $B(t)$ has independent increments. That is, for all $t_n > t_{n-1} > \dots > t_2 > t_1$, the random variables $B(t_n) - B(t_{n-1}), \dots, B(t_2) - B(t_1), B(t_1)$ are independently distributed (i.e., their joint distribution factorizes).
- (iv) $B(t)$ has Gaussian distribution with variance t for all $t \in (0, \infty)$.
- (v) $B(t)$ is continuous with probability 1.

The probability distribution \mathbb{P} governing the driving process $B(t)$ is commonly known as the Wiener measure.

Although the derivative $\xi(t) = dB/dt$ is not well-defined mathematically, Eq. (1.25) is in the physics literature often written in the form

$$\dot{X}(t) = u + \sqrt{2D} \xi(t). \quad (1.26)$$

The random driving function $\xi(t)$ is then referred to as Gaussian white noise, characterized by

$$\langle \xi(t) \rangle = 0, \quad \langle \xi(t) \xi(s) \rangle = \delta(t - s), \quad (1.27)$$

with $\langle \cdot \rangle$ denoting an average with respect to the Wiener measure.

Ito's formula Note that property (iv) implies that $\mathbb{E}[dB^2] = dt$. This justifies the following heuristic derivation of Ito's formula for the differential change of some real-valued function $F(x)$

$$\begin{aligned} dF(X(t)) &:= F(X(t + dt)) - F(X(t)) \\ &= F'(X(t)) dX + \frac{1}{2} F''(X(t)) dX^2 + \dots \\ &= F'(X(t)) dX + \frac{1}{2} F''(X(t)) \left[u dt + \sqrt{2D} dB \right]^2 + \dots \\ &= F'(X(t)) dX + DF''(X(t)) dB^2 + \mathcal{O}(dt^{3/2}); \end{aligned} \quad (1.28)$$

hence, in a probabilistic sense, one has to leading order in dt

$$\begin{aligned} dF(X(t)) &= F'(X(t)) dX + DF''(X(t)) dt \\ &= [u F'(X(t)) + DF''(X(t))] dt + F'(X(t)) \sqrt{2D} dB(t). \end{aligned} \quad (1.29)$$

It is crucial to note that, due to the choice of the expansion point, the coefficient $F'(X)$ in front of $dB(t)$ is to be evaluated at $X(t)$. This convention is the so-called Ito integration rule. In particular, it is important to keep in mind that nonlinear transformations of Ito SDEs must feature second-order derivatives.

Discretization dilemma To clarify the importance of discretization rules when dealing with SDEs, let us consider a simple generalization of Eq. (1.25), where drift u and diffusion coefficient D are position dependent. Adopting the Ito convention, the corresponding SDE reads

$$dX(t) = u(X) dt + \sqrt{2D(X)} * dB(t), \quad (1.30a)$$

where from now on the *-symbol signals that $D(X)$ is to be evaluated at $X(t)$. The simplest numerical integration procedure for Eq. (1.30a) is the stochastic Euler scheme

$$X(t + dt) = X(t) + u(X(t)) dt + \sqrt{2D(X(t))} \sqrt{dt} Z(t), \quad (1.30b)$$

where, for each time step dt , a new random number $Z(t)$ is drawn from a standard normal distribution⁴. If the driving process $B(t)$ in Eq. (1.30a) were a regular deterministic function, such as for example $B(t) = \sqrt{\tau} \sin(\Omega t)$, then Eq. (1.30a) would reduce to a standard inhomogeneous ordinary differential equation (ODE). For ODEs, it typically does not matter whether one computes the coefficients⁵ $u(x)$ and $D(x)$ at the start point $X(t)$ or the end point $X(t + dt)$. Mathematically, this is due to the fact that, for well-behaved deterministic driving functions, upper and lower Riemann sums yield the same value when letting $dt \rightarrow 0$. If, however, $B(t)$ is a rapidly varying stochastic process, such as the Brownian motion, then the corresponding lower and upper Riemann sums in general do *not* converge to the same value anymore. Therefore, when dealing with SDEs of the type (1.30a), it is important to explicitly specify the integration convention.

For instance, the so-called backward Ito SDE with coefficients u_B and D_B , denoted by

$$dX(t) = u_B(X) dt + \sqrt{2D_B(X)} \bullet dB(t), \quad (1.31a)$$

is defined as the upper Riemann sum⁶

$$X(t + dt) = X(t) + u_B(X(t + dt)) dt + \sqrt{2D_B(X(t + dt))} \sqrt{dt} Z(t). \quad (1.31b)$$

Unlike Eq. (1.30b), the backward Ito scheme (1.31b) is implicit. To reemphasize, for same functions $u \equiv u_B$ and $D \equiv D_B$, Eqs. (1.30) and (1.31) produce trajectories that follow different statistics⁷. The analog of the Ito formula (1.29) for a nonlinear transformation of the backward-Ito SDE reads simply

$$\begin{aligned} dF(X) &= F'(X) \bullet dX - D_B F''(X) dt \\ &= [u_B F'(X) - D_B F''(X)] dt + F'(X) \sqrt{2D_B} \bullet dB(t). \end{aligned} \quad (1.32)$$

⁴That is, a Gaussian distribution with mean $\mu = 0$ and variance $\sigma^2 = 1$.

⁵Assuming the functions u and D are sufficiently smooth.

⁶Note that instead of $u_B(X(t + dt))$ in (1.31b) we could in fact also have written $u_B(X(t))$, because the deterministic part of the SDE has identical lower and upper Riemann sums for $dt \rightarrow 0$.

⁷Except, of course, when $D = D_B = \text{const.}$

For sufficiently smooth coefficient functions, it is straightforward to transform back and forth between different types of SDEs (see Appendix A). That is, a given backward Ito SDE with coefficients (u_B, D_B) can be transformed into a stochastically equivalent Ito SDE by adapting the coefficients (u, D) accordingly. More precisely, by fixing

$$u = u_B + \partial_x D_B, \quad D = D_B \quad (1.33)$$

one obtains an Ito SDE that is stochastically equivalent to Eqs. (1.31).

Another discretization convention, that is popular in the physics literature is the Stratonovich-Fisk discretization, denoted by

$$dX(t) = u_S(X) dt + \sqrt{2D_S(X)} \circ dB(t), \quad (1.34a)$$

and defined as the mean value of lower and upper Riemann sum⁸

$$\begin{aligned} X(t+dt) = & X(t) + \frac{u_S(X(t)) + u_S(X(t+dt))}{2} dt + \\ & \frac{\sqrt{2D_S(X(t))} + \sqrt{2D_S(X(t+dt))}}{2} \sqrt{dt} Z(t). \end{aligned} \quad (1.34b)$$

Similarly to Eq. (1.34), by fixing

$$u = u_S + \frac{1}{2} \partial_x D_S, \quad D = D_S \quad (1.35)$$

one obtains an Ito SDE that is stochastically equivalent to Eqs. (1.31).

From a numerical perspective, the non-anticipatory Ito scheme (1.30b) is advantageous for it allows to compute the new position directly from the previous one. For analytical calculations, the Stratonovich-Fisk scheme is somewhat preferable as it preserves the rules of ordinary differential calculus,⁹

$$dF(X) = F'(X) \circ dX(t) \quad (1.36)$$

whilst the backward Ito rule bears certain conceptual advantages from a physical point of view [DH09]. However, as mentioned before, in principle one can transform back and forth between the different types of SDEs, i.e., neither of the different discretization schemes is intrinsically superior.

Various transformation formulas and their generalizations to higher space dimensions can be found in Appendix A.

⁸Note that instead of $u_B(X(t+dt))$ in (1.31b) we could in fact also have written $u_B(X(t))$, because the deterministic part of the SDE has identical lower and upper Riemann sums for $dt \rightarrow 0$.

⁹Intuitively, this follows from Eq. (1.32) and (1.32).

1.2.2 Fokker-Planck equations

Since other types of SDEs can be transformed into an equivalent Ito SDE, we shall focus in this part on discussing how one can derive a Fokker-Planck equation (FPE) for the probability density function (PDF) $p(t, x)$ for a process $X(t)$ described by the Ito SDE

$$dX(t) = u(X) dt + \sqrt{2D(X)} * dB(t). \quad (1.37)$$

The PDF can be formally defined by

$$p(t, x) = \mathbb{E}[\delta(X(t) - x)]. \quad (1.38)$$

To obtain an evolution equation for p , we consider

$$\partial_t p = \mathbb{E}\left[\frac{d}{dt}\delta(X(t) - x)\right]. \quad (1.39)$$

To evaluate the rhs., we apply Ito's formula to the differential $d[\delta(X(t) - x)]$ and find

$$\begin{aligned} \mathbb{E}[d[\delta(X - x)]] &= \mathbb{E}[(\partial_X \delta(X - x)) dX + D(X) \partial_X^2 \delta(X(t) - x) dt] \\ &= \mathbb{E}[(\partial_X \delta(X - x)) u(X) + D(X) \partial_X^2 \delta(X(t) - x)] dt. \end{aligned}$$

Here, we have used that $\mathbb{E}[g(X(t)) * dB] = 0$, which follows from the non-anticipatory definition of the Ito integral. Furthermore, by recalling that

$$\partial_X \delta(X - x) = -\partial_x \delta(X - x), \quad (1.40)$$

we may write

$$\begin{aligned} \mathbb{E}[d[\delta(X - x)]] &= \mathbb{E}[(-\partial_x \delta(X - x)) u(X) + D(X) \partial_x^2 \delta(X(t) - x)] dt \\ &= -\partial_x \mathbb{E}[\delta(X - x) u(X)] dt + \partial_x^2 \mathbb{E}[D(X) \delta(X(t) - x)] dt. \end{aligned}$$

Using another property of the δ -function

$$f(y)\delta(y - x) = f(x)\delta(y - x) \quad (1.41)$$

we obtain

$$\begin{aligned} \mathbb{E}[d[\delta(X - x)]] &= -\partial_x \mathbb{E}[\delta(X - x) u(x)] dt + \partial_x^2 \mathbb{E}[D(x) \delta(X(t) - x)] dt \\ &= -\partial_x \{u(x) \mathbb{E}[\delta(X - x)]\} dt + \partial_x^2 \{D(x) \mathbb{E}[\delta(X(t) - x)]\} dt \\ &= -\partial_x \{u(x) p - \partial_x [D(x) p]\} dt. \end{aligned}$$

Combining this with Eq. (1.39) yields the Fokker-Planck (or Smoluchowski) equation

$$\partial_t p = -\partial_x \{u(x) p - \partial_x [D(x) p]\}. \quad (1.42)$$

For comparison, an analogous calculation for the backward-Ito SDE

$$dX(t) = u_B(X) dt + \sqrt{2D_B(X)} \bullet dB(t), \quad (1.43)$$

gives

$$\partial_t p = -\partial_x [u_B(x) p - D_B(x) \partial_x p]. \quad (1.44)$$

Compared with the Ito FPE (1.42), the diffusion coefficient D_B now enters in front of the gradient $\partial_x p$. Note, however, that the two different FPEs coincide if one identifies the coefficients as in Eq. (1.33).

A summary of Fokker-Planck equations for the three different stochastic integral conventions (Ito, Stratonovich-Fisk and backward-Ito) in arbitrary space dimensions can be found in Appendix A.

1.3 Dilute microbial suspensions

A minimalist model for the locomotion of an isolated microorganism (e.g., alga or bacterium) with position $\mathbf{X}(t)$ and orientation unit vector $\mathbf{N}(t)$ is given by the coupled system of Ito SDEs

$$d\mathbf{X} = V\mathbf{N}dt + \sqrt{2D_T} * d\mathbf{B}(t), \quad (1.45a)$$

$$d\mathbf{N} = (1-d)D_R\mathbf{N}dt + \sqrt{2D_R}(\mathbf{I} - \mathbf{N}\mathbf{N}) * d\mathbf{W}(t). \quad (1.45b)$$

Here, V is the self-swimming speed of the organism, D_T the translational diffusion coefficient, and D_R the rotational diffusion coefficient, $(\mathbf{I} - \mathbf{N}\mathbf{N})$ is an orthogonal projector with d -dimensional unit matrix \mathbf{I} , and \mathbf{B} and \mathbf{W} are two independent d -dimensional Brownian motion processes. Eq. (1.45a) describes locomotion due to translational diffusion and self-swimming in the direction of the orientation \mathbf{N} , and Eq. (1.45b) models changes in orientation as diffusion on the d -dimensional unit sphere.

To confirm that Eq. (1.45b) conserves the unit length of the orientation vector, $|\mathbf{N}|^2 = 1$ for all t , it is convenient to rewrite Eqs. (1.45) in component form:

$$dX_i = VN_i dt + \sqrt{2D_T} * dB_i(t), \quad (1.46a)$$

$$dN_j = (1-d)D_R N_j dt + \sqrt{2D_R}(\delta_{jk} - N_j N_k) * dW_k(t). \quad (1.46b)$$

For the constraint $|\mathbf{N}|^2 = 1$ to be satisfied, we must have $d|\mathbf{N}|^2 = 0$. Applying the d -dimensional version of Ito's formula, see Eq. (A.12), to $F(\mathbf{N}) = |\mathbf{N}|^2$, one finds indeed that

$$\begin{aligned} d|\mathbf{N}|^2 &= 2N_j * dN_j + (\partial_{N_i} \partial_{N_j} N_k N_k) D_R(\delta_{ij} - N_i N_j) dt \\ &= 2N_j * \left[(1-d)D_R N_j dt + \sqrt{2D_R}(\delta_{jk} - N_j N_k) * dW_k(t) \right] + \\ &\quad \partial_{N_i}(\delta_{jk} N_k + N_k \delta_{jk}) D_R(\delta_{ij} - N_i N_j) dt \\ &= 2(1-d)D_R dt + \\ &\quad (\delta_{jk} \delta_{ik} + \delta_{ik} \delta_{jk}) D_R(\delta_{ij} - N_i N_j) dt \\ &= 0. \end{aligned} \quad (1.47)$$

To understand the dynamics (1.46), it is useful to compute the orientation correlation,

$$\langle \mathbf{N}(t) \cdot \mathbf{N}(0) \rangle = \mathbb{E}[\mathbf{N}(t) \cdot \mathbf{N}(0)] = \mathbb{E}[N_z(t)], \quad (1.48)$$

where we have assumed (w.l.o.g.) that $\mathbf{N}(0) = \mathbf{e}_z$. Averaging Eq. (1.46b), we find that

$$\frac{d}{dt} \mathbb{E}[N_z(t)] = (1-d)D_R \mathbb{E}[N_z(t)], \quad (1.49)$$

implying that, in this model, the memory loss about the orientation is exponential

$$\langle \mathbf{N}(t) \cdot \mathbf{N}(0) \rangle = e^{(1-d)D_R t}, \quad (1.50)$$

which is approximately true for many microorganisms. Another relevant quantity is the mean square displacement $\mathbb{E}[\mathbf{X}(t)^2]$, assuming that $\mathbf{X}(0) = 0$. Using Ito's formula,

$$\begin{aligned} d|\mathbf{X}|^2 &= 2X_j * dX_j + (\partial_{X_i} \partial_{X_j} X_k X_k) D_T \delta_{ij} dt \\ &= 2X_j * dX_j + (\delta_{jk} \delta_{ik} + \delta_{ik} \delta_{jk}) D_T \delta_{ij} dt \\ &= 2X_j * dX_j + 2d D_T dt \\ &= 2X_j [V N_j dt + \sqrt{2D_T} * dB_j(t)] + 2d D_T dt, \end{aligned} \quad (1.51)$$

averaging and dividing by dt , gives

$$\frac{d}{dt} \mathbb{E}[\mathbf{X}^2] = 2V \mathbb{E}[\mathbf{X}(t) \mathbf{N}(t)] + 2d D_T. \quad (1.52)$$

The expectation value on the rhs. can be evaluated by making use of Eq. (1.50):

$$\begin{aligned} \mathbb{E}[\mathbf{X}(t) \cdot \mathbf{N}(t)] &= \mathbb{E} \left[\int_0^t d\mathbf{X}(s) \cdot \mathbf{N}(t) \right] \\ &= V \mathbb{E} \left[\int_0^t ds \mathbf{N}(s) \cdot \mathbf{N}(t) \right] \\ &= V \int_0^t ds \langle \mathbf{N}(t) \cdot \mathbf{N}(s) \rangle \\ &= V \int_0^t ds e^{(1-d)D_R(t-s)} \\ &= \frac{V}{(d-1)D_R} [1 - e^{(1-d)D_R t}]. \end{aligned}$$

By inserting this expression into Eq. (1.52) and integrating over t , we find

$$\mathbb{E}[\mathbf{X}^2] = \frac{2V^2}{(d-1)^2 D_R^2} [(d-1)D_R t + e^{(1-d)D_R t} - 1] + 2d D_T t. \quad (1.53)$$

If D_T is small, then at short times $t \ll D_R^{-1}$ the motion is ballistic

$$\mathbb{E}[\mathbf{X}^2] \simeq V^2 t^2 + 2d D_T t, \quad (1.54)$$

At large times, the motion becomes diffusive, with asymptotic diffusion constant

$$\lim_{t \rightarrow \infty} \frac{\mathbb{E}[\mathbf{X}^2]}{t} = \frac{2V^2}{(d-1)D_R} + 2dD_T. \quad (1.55)$$

Inserting typical values for bacteria, $V \sim 10\mu\text{m/s}$ and $D_R \sim 0.1/\text{s}$, and comparing with $D_T \sim 0.2\mu\text{m}^2/\text{s}$ for a micron-sized colloids at room temperature, we see that active swimming and orientational diffusion dominate the diffusive dynamics of microorganisms at long times.

Concentration profile between two walls An interesting question that is relevant from a medical perspective concerns the spatial distribution of bacteria and other swimming microbes in the presence of confinement. Restricting ourselves to dilute suspensions¹⁰, we may obtain a simple prediction from the model (1.45) by considering the FPE for the associated PDF $p(t, \mathbf{x}, \mathbf{n})$. Given p and the total number of bacteria N_b in the solutions, we obtain the spatial concentration profile by integrating over all possible orientations

$$c(t, \mathbf{x}) = N_b \int_{\mathbb{S}_d} d\mathbf{n} p(t, \mathbf{n}, \mathbf{x}). \quad (1.56a)$$

The associated mean orientation field reads

$$\mathbf{u}(t, \mathbf{x}) = N_b \int_{\mathbb{S}_d} d\mathbf{n} p(t, \mathbf{n}, \mathbf{x}) \mathbf{n}. \quad (1.56b)$$

The FPE for the Ito-SDE (1.45) can be written as a conservation law

$$\partial_t p = -(\partial_{x_i} J_i + \partial_{n_i} \Omega_i), \quad (1.57a)$$

where

$$J_i = (Vn_i - D_T \partial_{x_i})p \quad (1.57b)$$

$$\Omega_i = D_R \left\{ (1-d)n_i p - \partial_{n_j} [(\delta_{ij} - n_i n_j)p] \right\}. \quad (1.57c)$$

Focusing on the three-dimensional case, $d = 3$, we are interested in deriving from Eq. (1.57) the stationary concentration profile c of a suspension that is confined by two quasi-infinite parallel walls, which are located $z = \pm H$. That is, we assume that the distance between the walls is much smaller than their spatial extent in the (x, y) -directions, $2H \ll L_x, L_y$. To obtain an evolution equation for c , we multiply Eq. (1.57a) by N_b and integrate over \mathbf{n} with

$$\int_{\mathbb{S}_d} d\mathbf{n} \partial_{n_i} \Omega_i = 0. \quad (1.58)$$

¹⁰The simplifying assumption that microbes can be considered as non-interacting is usually justified when their volume filling fraction is less than 1%.

This yields the mass conservation law

$$\partial_t c = -\nabla \cdot (V\mathbf{u} - D_T \nabla c). \quad (1.59)$$

To obtain also an evolution equation for \mathbf{u} , we multiply Eq. (1.57a) by n_k ,

$$\partial_t(n_k p) = -\partial_{x_i}(n_k J_i) - n_k \partial_{n_i} \Omega_i. \quad (1.60)$$

and note that

$$n_k \partial_{n_i} \Omega_i = \partial_{n_i}(n_k \Omega_i) - (\partial_{n_i} n_k) \Omega_i = \partial_{n_i}(n_k \Omega_i) - \delta_{ik} \Omega_i. \quad (1.61)$$

This allows us to rewrite (1.60) as

$$\begin{aligned} \partial_t(n_k p) &= -\partial_{x_i}(n_k J_i) + \Omega_k - \partial_{n_i}(n_k \Omega_i) \\ &= -\partial_{x_i}[V n_k n_i p - D_T \partial_{x_i}(n_k p)] + \\ &\quad D_R \{-2n_k p - \partial_{n_j}[(\delta_{kj} - n_k n_j)p]\} - \partial_{n_i}(n_k \Omega_i) \\ &= -\partial_{x_i}[V n_k n_i p - D_T \partial_{x_i}(n_k p)] - 2D_R n_k p - \\ &\quad \partial_{n_j}(n_k \Omega_j + (\delta_{kj} - n_k n_j)p). \end{aligned} \quad (1.62)$$

Multiplying by N_b and integrating over \mathbf{n} with appropriate boundary conditions gives

$$\partial_t u_k = -\partial_{x_i}[V N_b \langle n_k n_i \rangle p - D_T \partial_{x_i} u_k] - 2D_R u_k,$$

where we have abbreviated

$$\langle n_i n_k \dots \rangle = \int_{\mathbb{S}_d} d\mathbf{n} p(t, \mathbf{n}, \mathbf{x}) n_i n_k \dots. \quad (1.63)$$

To obtain a closed linear system of equations for the fields (c, \mathbf{u}) , we neglect¹¹ the higher-order moments $N_b \langle n_k n_i \rangle$ in (1.63) and find

$$\partial_t \mathbf{u} \simeq -2D_R \mathbf{u} + D_T \nabla^2 \mathbf{u}. \quad (1.64)$$

To find the stationary density and orientation profiles, we look for solutions of the form $c = \rho(z)$ and $u_x = u_y = 0, u_z = u(z)$. According to Eqs. (1.59) to (1.63), the functions ρ and u_z must satisfy

$$0 = V\rho - D_T \rho', \quad (1.65)$$

$$0 = -2D_R u + D_T u'', \quad (1.66)$$

¹¹*Ad hoc* simplifications of this type are usually referred to as ‘truncation (of the moment hierarchy)’ or ‘closure conditions’ - they are (almost) always unavoidable when one tries to derive continuum equations from ODEs, SDEs or FPEs. Closure conditions are not unique, for example, we could also have adopted the mean field approximation $N_b^2 \langle n_k n_i \rangle \simeq u_k u_i$, which leads to a nonlinear set of equations for (c, \mathbf{u}) .

and it is physically plausible that they also fulfill the symmetry¹² requirements $\rho(z) = \rho(-z)$ and $u(z) = -u(-z)$. Hence, solution takes the form

$$u(z) = A \sinh(z/\Lambda), \quad (1.67a)$$

$$\rho(z) = A \frac{V\Lambda}{D_T} [\cosh(z/\Lambda) - 1] + \rho_0, \quad (1.67b)$$

where $\Lambda = \sqrt{D_\perp/(2D_R)}$.

The cosh-profile (1.67b) agrees qualitatively with experimental measurements for dilute bacterial suspensions [BTBL08, LT09].

1.4 Escape problem

Escape problems are ubiquitous in biological, biophysical and biochemical processes. Prominent examples include, but are not restricted to,

- unbinding of molecules from receptors,
- chemical reactions,
- transfer of ion through through pores,
- evolutionary transitions between different fitness optima.

Their mathematical treatment typically involves models that are structurally very similar to the one-dimensional examples discussed in this section¹³.

1.4.1 Generic minimal model

Consider the over-damped SDE

$$dx(t) = -\partial_x U dt + \sqrt{2D} * dB(t) \quad (1.68a)$$

with a confining potential $U(x)$

$$\lim_{x \rightarrow \pm\infty} U(x) \rightarrow \infty \quad (1.68b)$$

that has two (or more) minima and maxima. A typical example is the bistable quartile double-well

$$U(x) = -\frac{a}{2}x^2 + \frac{b}{4}x^4, \quad a, b > 0 \quad (1.68c)$$

¹²Neglecting gravity is valid approximation, provided the density of the microbes roughly matches that of the surrounding fluid (which is approximately true for bacteria in water).

¹³Although things usually get more complicated in higher-dimensions.

with minima at $\pm\sqrt{a/b}$.

Generally, we are interested in characterizing the transitions between neighboring minima in terms of a rate k (units of time^{-1}) or, equivalently, by the typical time required for escaping from one of the minima. To this end, we shall first discuss the general structure of the time-dependent solution of the FPE¹⁴ for the corresponding PDF $p(t, x)$, which reads

$$\partial_t p = -\partial_x j, \quad j(t, x) = -[(\partial_x U)p + D\partial_x p], \quad (1.68d)$$

and has the stationary zero-current ($j \equiv 0$) solution

$$p_s(x) = \frac{e^{-U(x)/D}}{Z}, \quad Z = \int_{-\infty}^{+\infty} dx e^{-U(x)/D}. \quad (1.69)$$

To find the time-dependent solution, we can make the ansatz

$$p(t, x) = \varrho(t, x) e^{-U(x)/(2D)}, \quad (1.70)$$

which leads to a Schrödinger equation in imaginary time

$$-\partial_t \varrho = [-D\partial_x^2 + W(x)] \varrho =: \mathcal{H}\varrho, \quad (1.71a)$$

with an effective potential

$$W(x) = \frac{1}{4D}(\partial_x U)^2 - \frac{1}{2}\partial_x^2 U. \quad (1.71b)$$

Assuming the Hamilton operator \mathcal{H} has a discrete non-degenerate spectrum, $\lambda_0 < \lambda_1 < \dots$, the general solution $p(t, x)$ may be written as

$$p(t, x) = e^{-U(x)/(2D)} \sum_{n=0}^{\infty} c_n \phi_n(x) e^{-\lambda_n t}, \quad (1.72a)$$

where the eigenfunctions ϕ_n of \mathcal{H} satisfy

$$\int dx \phi_n^*(x) \phi_m(x) = \delta_{nm}, \quad (1.72b)$$

and the constants c_n are determined by the initial conditions

$$c_n = \int dx \phi_n^*(x) e^{U(x)/(2D)} p(0, x). \quad (1.72c)$$

At large times, $t \rightarrow \infty$, the solution (1.72a) must approach the stationary solution (1.69), implying that

$$\lambda_0 = 0, \quad c_0 = \frac{1}{\sqrt{Z}}, \quad \phi_0(x) = \frac{e^{-U(x)/(2D)}}{\sqrt{Z}}. \quad (1.73)$$

¹⁴FPEs for over-damped processes are sometimes referred to as Smoluchowski equations.

Note that $\lambda_0 = 0$ in particular means that the first non-zero eigenvalue $\lambda_1 > 0$ dominates the relaxation dynamics at large times and, therefore,

$$\tau_* = 1/\lambda_1 \quad (1.74)$$

is a natural measure of the escape time. In practice, the eigenvalue λ_1 can be computed by various standard methods (WKB approximation, Ritz method, techniques exploiting supersymmetry, etc.) depending on the specifics of the effective potential W .

1.4.2 Two-state approximation

We next illustrate a commonly used simplified description of escape problems, which can be related to (1.74). As a specific example, we can again consider the escape of a particle from the left well of a symmetric quartic double well-potential

$$U(x) = -\frac{a}{2}x^2 + \frac{b}{4}x^4, \quad p(0, x) = \delta(x - x_-) \quad (1.75a)$$

where

$$x_- = -\sqrt{a/b} \quad (1.75b)$$

is the location of the left minimum, but the general approach is applicable to other types of potentials as well.

The basic idea of the two-state approximation is to project the full FPE dynamics onto simpler set of master equations by considering the probabilities $P_{\pm}(t)$ of the coarse-grained particle-states ‘left well’ (–) and ‘right well’ (+), defined by

$$P_-(t) = \int_{-\infty}^0 dx p(t, x), \quad (1.76a)$$

$$P_+(t) = \int_0^{\infty} dx p(t, x). \quad (1.76b)$$

If all particles start in the left well, then

$$P_-(0) = 1, \quad P_+(0) = 0. \quad (1.77)$$

Whilst the exact dynamics of $P_{\pm}(t)$ is governed by the FPE (1.68d), the two-state approximation assumes that this dynamics can be approximated by the set of master equations¹⁵

$$\dot{P}_- = -k_+ P_- + k_- P_+, \quad \dot{P}_+ = k_+ P_- - k_- P_+. \quad (1.78)$$

For a symmetric potential, $U(x) = U(-x)$, forward and backward rates are equal, $k_+ = k_- = k$, and in this case, the solution of Eq. (1.78) is given by

$$P_{\pm}(t) = \frac{1}{2} \mp \frac{1}{2} e^{-2kt}. \quad (1.79)$$

¹⁵Note that Eqs. (1.78) conserve the total probability, $P_+(t) + P_-(t) = 1$.

For comparison, from the FPE solution (1.72a), we find in the long-time limit

$$p(t, x) \simeq p_s(x) + c_1 e^{-U(x)/2D} \phi_1(x) e^{-\lambda_1 t}, \quad (1.80)$$

Due to the symmetry of $p_s(x)$, we then have

$$P_-(t) \simeq \frac{1}{2} + C_1 e^{-\lambda_1 t} \quad (1.81a)$$

where

$$C_1 = c_1 \int_{-\infty}^0 e^{-U(x)/2D} \phi_1(x) dx, \quad c_1 = \phi_1^*(x_-) e^{U(x_-)/(2D)}. \quad (1.81b)$$

Since Eq. (1.81a) neglects higher-order eigenfunctions, C_1 is in general not exactly equal but usually close to $1/2$. But, by comparing the time-dependence of (1.81a) and (1.79), it is natural to identify

$$k \simeq \frac{\lambda_1}{2} = \frac{1}{2\tau_*}. \quad (1.82)$$

We next discuss, by considering in a slightly different setting, how one can obtain an explicit result for the rate k in terms of the parameters of the potential U .

1.4.3 Constant-current solution

Consider a bistable potential as in Eq. (1.75), but now with a particle source at $x_0 < x_- < 0$ and a sink¹⁶ at $x_1 > x_b = 0$. Assuming that particles are injected at x_0 at constant flux $j(t, x) \equiv J = \text{const}$, the escape rate can be defined by

$$k := \frac{J}{P_-}, \quad (1.83)$$

with P_- denoting the probability of being in the left well, as defined in Eq. (1.76a) above. To compute the rate from Eq. (1.83), we need to find a stationary constant flux solution $p_J(x)$ of Eq. (1.68d), satisfying $p_J(x_1) = 0$ and

$$J = -(\partial_x U)p_J - D\partial_x p_J \quad (1.84)$$

for some constant J . This solution is given by [HTB90]

$$p_J(x) = \frac{J}{D} e^{-U(x)/D} \int_x^{x_1} dy e^{U(y)/D}, \quad (1.85)$$

¹⁶The source could be a protein production site and the barrier could present a semi-permeable membrane.

as one can verify by differentiation

$$\begin{aligned}
-(\partial_x U)p_J - D\partial_x p_J &= -(\partial_x U)p_J - D\partial_x \left[\frac{J}{D} e^{-U(x)/D} \int_x^{x_1} dy e^{U(y)/D} \right] \\
&= -(\partial_x U)p_J - J \left[-\frac{(\partial_x U)}{D} e^{-U(x)/D} \int_x^{x_1} dy e^{U(y)/D} - 1 \right] \\
&= J.
\end{aligned} \tag{1.86}$$

Therefore, the inverse rate k^{-1} from Eq. (1.83) can be formally expressed as

$$k^{-1} = \frac{P_-}{J} = \frac{1}{D} \int_{-\infty}^{x_1} dx e^{-U(x)/D} \int_x^{x_1} dy e^{U(y)/D}, \tag{1.87}$$

and a partial integration yields the equivalent representation

$$k^{-1} = \frac{1}{D} \int_{-\infty}^{x_1} dx e^{U(x)/D} \int_{-\infty}^x dy e^{-U(y)/D}. \tag{1.88}$$

Assuming a sufficiently steep barrier, the integrals in Eq. (1.88) may be evaluated by adopting steepest descent approximations near the potential minimum at x_- and near the maximum at the barrier position x_b . More precisely, taking into account that $U'(x_-) = U'(x_b) = 0$, one can replace the potentials in the exponents by the harmonic approximations

$$U(x) \simeq U(x_-) - \frac{1}{2\tau_b} (x - x_-)^2, \tag{1.89a}$$

$$U(y) \simeq U(x_-) + \frac{1}{2\tau_-} (y - x_-)^2, \tag{1.89b}$$

where

$$\tau_- = -U''(x_0) > 0, \quad \tau_b = U''(x_b) > 0 \tag{1.90}$$

carry units of time. Inserting (1.89) into (1.88) and replacing the upper integral boundaries by $+\infty$, one thus obtains the so-called Kramers rate [HTB90, GHJM98]

$$k \simeq \frac{e^{-\Delta U/D}}{2\pi\sqrt{\tau_- \tau_b}} =: k_K, \quad \Delta U = U(x_b) - U(x_-). \tag{1.91}$$

This result agrees with the well-known empirical Arrhenius law. Note that, because typically $D \propto k_B T$ for thermal noise, binding/unbinding rates depend sensitively on temperature – this is one of the reasons why many organisms tend to function properly only within a limited temperature range.

1.5 Stochastic resonance

Noise typically impairs signal transduction, but under certain conditions an optimal dose of randomness may actually help to enhance weak signals [GHJM98]. This remarkable phenomenon is known as stochastic resonance (SR). Whilst SR was originally proposed as a possible explanation for periodically recurring climate cycles [NN81, BPSV83], experiments suggest [FSGB⁺02] that some organisms like juvenile paddle-fish might exploit SR to enhance signal detection while foraging for food.

The occurrence of SR requires three main ‘ingredients’

1. a nonlinear measurement device¹⁷,
2. a periodic signal weaker than the threshold of measurement device,
3. additional input noise, uncorrelated with the signal of interest.

To provide some intuition, assume that a weak periodic signal (frequency Ω) is detected by a particle that can move in the bistable double well-potential (1.75). For weak noise, the particle will remain trapped in one of the minima and we will be unable to infer the signal from the particle’s motion. Similarly, not much information about the underlying signal can be gained if the noise is too strong, for in this case the particle will jump randomly back and forth between the minima. If, however, the noise strength is tuned such that the Kramers escape rate (1.91) is of the order of the driving frequency,

$$k_K \sim \Omega, \tag{1.92}$$

then it is plausible to expect that the particle’s escape dynamics will be closely correlated with the driving frequency, thus exhibiting SR.

1.5.1 Generic model

To illustrate SR more quantitatively, consider the periodically driven SDE

$$dX(t) = -\partial_x U dt + A \cos(\Omega t) dt + \sqrt{2D} * dB(t), \tag{1.93a}$$

where A is the signal amplitude and

$$U(x) = -\frac{a}{2}x^2 + \frac{b}{4}x^4 \tag{1.93b}$$

a symmetric double-well potential with minima at $\pm x_* = \pm\sqrt{a/b}$ and barrier height $\Delta U = a^2/(4b)$. Introducing rescaled variables

$$x' = x/x_*, \quad t' = at, \quad A' = A/(ax_*), \quad D' = D/(ax_*^2), \quad \Omega' = \Omega/a.$$

¹⁷That is, the input-output relationship between the input signal and the observable must be nonlinear

and dropping primes. we can rewrite (1.93a) in the dimensionless form

$$dX(t) = (x - x^3) dt + A \cos(\Omega t) dt + \sqrt{2D} * dB(t), \quad (1.93c)$$

with a rescaled barrier height $\Delta U = 1/4$. The associated FPE reads

$$\partial_t p = -\partial_x \{ [-(\partial_x U) + A \cos(\Omega t)] p - D \partial_x p \}. \quad (1.94)$$

For our subsequent discussion, it is useful to rearrange terms on the rhs. as

$$\partial_t p = \partial_x [(\partial_x U) p + D \partial_x p] - A \cos(\Omega t) \partial_x p. \quad (1.95)$$

To solve Eq. (1.95) perturbatively, we insert the series ansatz

$$p(t, x) = \sum_{n=0}^{\infty} A^n p_n(t, x), \quad (1.96)$$

which gives

$$\sum_{n=0}^{\infty} A^n \partial_t p_n = \sum_{n=0}^{\infty} \{ A^n \partial_x [(\partial_x U) p_n + D \partial_x p_n] - A^{n+1} \cos(\Omega t) \partial_x p_n \} \quad (1.97)$$

Focussing on the liner response regime, corresponding to powers A^0 and A^1 , we find

$$\partial_t p_0 = \partial_x [(\partial_x U) p_0 + D \partial_x p_0] \quad (1.98a)$$

$$\partial_t p_1 = \partial_x [(\partial_x U) p_1 + D \partial_x p_1] - \cos(\Omega t) \partial_x p_0 \quad (1.98b)$$

Equation (1.98a) is just an ordinary time-independent FPE, and we know its stationary solution is just the Boltzmann distribution

$$p_0(x) = \frac{e^{-U(x)/D}}{Z_0}, \quad Z_0 = \int dx e^{-U(x)/D} \quad (1.99)$$

To obtain a formal solution to Eq. (1.98b), we make use of the following ansatz

$$p_1(t, x) = e^{-U(x)/(2D)} \sum_{m=1}^{\infty} a_{1m}(t) \phi_m(x), \quad (1.100)$$

where $\phi_m(x)$ are the eigenfunctions of the unperturbed effective Hamiltonian, cf. Eq. (1.71),

$$\mathcal{H}_0 = -D \partial_x^2 + \frac{1}{4D} (\partial_x U)^2 - \frac{1}{2} \partial_x^2 U. \quad (1.101)$$

Inserting (1.100) into Eq. (1.98b) gives

$$\sum_{m=1}^{\infty} \dot{a}_{1m} \phi_m = - \sum_{m=1}^{\infty} \lambda_m a_{1m} \phi_m - \cos(\Omega t) e^{U(x)/(2D)} \partial_x p_0. \quad (1.102)$$

Multiplying this equation by $\phi_n(x)$, and integrating from $-\infty$ to $+\infty$ while exploiting the orthonormality of the system $\{\phi_m\}$, we obtain the coupled ODEs

$$\dot{a}_{1m} = -\lambda_m a_{1m} - M_{m0} \cos(\Omega t), \quad (1.103)$$

with ‘transition matrix’ elements

$$M_{m0} = \int dx \phi_m e^{U(x)/(2D)} \partial_x p_0. \quad (1.104)$$

The asymptotic solution of Eq. (1.103) reads

$$a_{1m}(t) = -M_{m0} \left[\frac{\Omega}{\lambda_m^2 + \Omega^2} \sin(\Omega t) + \frac{\lambda_m}{\lambda_m^2 + \Omega^2} \cos(\Omega t) \right]. \quad (1.105)$$

Note that, because $\partial_x p_0$ is an antisymmetric function, the matrix elements M_{m0} vanish¹⁸ for even values $m = 0, 2, 4, \dots$, so that only the contributions from odd values $m = 1, 3, 5 \dots$ are asymptotically relevant.

Focussing on the leading order contribution, $m = 1$, and noting that $p_0(x) = p_0(-x)$, we can estimate the position mean value

$$\mathbb{E}[X(t)] = \int dx p(t, x) x \quad (1.106)$$

from

$$\begin{aligned} \mathbb{E}[X(t)] &\simeq A \int dx p_1(t, x) x \\ &\simeq A \int dx e^{-U(x)/(2D)} a_{11}(t) \phi_1(x) x \\ &= -AM_{10} \left[\frac{\Omega}{\lambda_1^2 + \Omega^2} \sin(\Omega t) + \frac{\lambda_1}{\lambda_1^2 + \Omega^2} \cos(\Omega t) \right] \int dx e^{-U(x)/(2D)} \phi_1(x) x \end{aligned}$$

Using $\lambda_1 = 2k_K$, where k_K is the Kramers rate from Eq. (1.91), we can rewrite this more compactly as

$$\mathbb{E}[X(t)] = \bar{X} \cos(\Omega t - \bar{\varphi}) \quad (1.107a)$$

with phase shift

$$\bar{\varphi} = \arctan\left(\frac{\Omega}{2k_K}\right) \quad (1.107b)$$

¹⁸The potential $U(x)$ is symmetric and, therefore, the effective Hamiltonian commutes with parity operator, implying that the eigenfunctions ϕ_{2k} are symmetric under $x \mapsto -x$, whereas eigenfunctions ϕ_{2k+1} are antisymmetric under this map.

and amplitude

$$\bar{X} = -A \frac{M_{10}}{(4k_{\text{K}}^2 + \Omega^2)^{1/2}} \int dx e^{-U(x)/(2D)} \phi_1(x) x. \quad (1.107c)$$

The amplitude \bar{X} depends on the noise strength D through k_{K} , through the integral factor and also through the matrix element

$$M_{10} = \int dx \phi_1 e^{U(x)/(2D)} \partial_x p_0. \quad (1.108)$$

To compute \bar{X} , one first needs to determine the eigenfunction ϕ_1 of \mathcal{H}_0 as defined in Eq. (1.101). For the quartic double-well potential (1.93b), this cannot be done analytically but there exist standard techniques (e.g., Ritz method) for approximating ϕ_1 by functions that are orthogonal to $\phi_0 = \sqrt{p_0/Z_0}$. Depending on the method employed, analytical estimates for \bar{X} may vary quantitatively but always show a non-monotonic dependence on the noise strength D for fixed potential-parameters (a, b) . As discussed in [GHJM98], a reasonably accurate estimate for \bar{X} is given by

$$\bar{X} \simeq \frac{Aa}{Db} \left(\frac{4k_{\text{K}}^2}{4k_{\text{K}}^2 + \Omega^2} \right)^{1/2}, \quad (1.109)$$

which exhibits a maximum for a critical value D_* determined by

$$4k_{\text{K}}^2 = \Omega^2 \left(\frac{\Delta U}{D_*} - 1 \right). \quad (1.110)$$

That is, the value D_* corresponds to the optimal noise strength, for which the mean value $\mathbb{E}[X(t)]$ shows maximal response to the underlying periodic signal – hence the name ‘stochastic resonance’ (SR).

1.5.2 Master equation approach

Similar to the case of the escape problem, one can obtain an alternative description of SR by projecting the full FPE dynamics onto a simpler set of master equations for the probabilities $P_{\pm}(t)$ of the coarse-grained particle-states ‘left well’ (–) and ‘right well’ (+), as defined by Eq. (1.76). This approach leads to the following two-state master equations with time-dependent rates

$$\dot{P}_-(t) = -k_+(t) P_- + k_-(t) P_+, \quad (1.111a)$$

$$\dot{P}_+(t) = k_+(t) P_- - k_-(t) P_+. \quad (1.111b)$$

The general solution of this pair of ODEs is given by [GHJM98]

$$P_{\pm}(t) = g(t) \left[P_{\pm}(t_0) + \int_{t_0}^t ds \frac{k_{\pm}(s)}{g(s)} \right] \quad (1.112a)$$

where

$$g(t) = \exp\left\{-\int_{t_0}^t ds [k_+(s) + k_-(s)]\right\}. \quad (1.112b)$$

To discuss SR within this framework, it is plausible to postulate time-dependent Arrhenius-type rates,

$$k_{\pm}(t) = k_K \exp\left[\pm \frac{Ax_*}{D} \cos(\Omega t)\right]. \quad (1.113)$$

Adopting these rates and considering the asymptotic limit $t_0 \rightarrow -\infty$, one can Taylor-expand the exact solution (1.112) for $Ax_* \ll D$ to obtain

$$P_{\pm}(t) = k_K \left[1 \pm \frac{Ax_*}{D} \cos(\Omega t) + \left(\frac{Ax_*}{D}\right)^2 \cos^2(\Omega t) \pm \dots \right]. \quad (1.114)$$

These approximations are valid for slow driving (adiabatic regime), and they allow us to compute expectation values to leading order in Ax_*/D . In particular, one then finds for the mean position the asymptotic linear response result [GHJM98]

$$\mathbb{E}[X(t)] = \bar{X} \cos(\Omega t - \bar{\varphi}) \quad (1.115a)$$

where

$$\bar{X} = \frac{Ax_*^2}{D} \left(\frac{4k_K^2}{4k_K^2 + \Omega^2} \right)^{1/2}, \quad \bar{\varphi} = \arctan\left(\frac{\Omega}{2k_K}\right) \quad (1.115b)$$

with k_K denoting Kramers rate as defined in Eq. (1.91). Note that Eqs. (1.115) are consistent with our earlier result (1.107).

1.6 Brownian motors

Many biophysical processes, from muscular contractions to self-propulsion of microorganisms or intracellular transport, rely on biological motors. These are, roughly speaking, collections of proteins that are capable of rectifying thermal and other random fluctuations to achieve directed motion. Here, we focus on a minimal mathematical model that captures, in a simplified manner, the main building principles of Brownian motors:¹⁹

- a spatially periodic structure (ratchet potential) that violates reflection symmetry,
- thermal or non-thermal random fluctuations, and
- a deterministic or stochastic pumping process that drives the system away from thermal equilibrium.

¹⁹For further reading, we refer to the review articles [HM09, Rei02].

Generally speaking, the combination of broken spatial symmetry and non-equilibrium driving is sufficient for generating stationary currents by means of a ratchet effect.

Most biological micro-motors operate in the low Reynolds number regime, where inertia is negligible. A minimal model can therefore be formulated in terms of an over-damped Ito-SDE

$$dX(t) = -U'(X) dt + F(t)dt + \sqrt{2D(t)} * dB(t). \quad (1.116)$$

Here, U is a periodic potential

$$U(x) = U(x + L) \quad (1.117a)$$

with broken reflection symmetry, i.e., there is no δx such that

$$U(-x) = U(x + \delta x). \quad (1.117b)$$

A typical example is

$$U = U_0[\sin(2\pi x/L) + \frac{1}{4} \sin(4\pi x/L)]. \quad (1.117c)$$

The function $F(t)$ is a deterministic driving force, and the noise amplitude $D(t)$ can be time-dependent as well.

The corresponding FPE for the associated PDF $p(t, x)$ reads

$$\partial_t p = -\partial_x j, \quad j(t, x) = -\{[U' - F(t)]p + D(t)\partial_x p\}, \quad (1.118)$$

and we assume that p is normalized to the total number of particles, i.e.

$$N_L(t) = \int_0^L dx p(t, x) \quad (1.119)$$

gives the number of particles in $[0, L]$. The quantity of interest is the mean particle velocity v_L per period defined by

$$v_L(t) := \frac{1}{N_L(t)} \int_0^L dx j(t, x). \quad (1.120)$$

Inserting the expression for j , we find for spatially periodic solutions with $p(t, x) = p(t, x + L)$ that

$$v_L = \frac{1}{N_L(t)} \int_0^L dx [F(t) - U'(x)] p(t, x). \quad (1.121)$$

1.6.1 Tilted Smoluchowski-Feynman ratchet

As a first example, assume that $F = \text{const.}$ and $D = \text{const.}$ This case can be considered as a (very) simple model for kinesin or dynein walking along a polar microtubule, with the constant force $F \geq 0$ accounting for the polarity. We would like to determine the mean transport velocity v_L for this model.

To evaluate Eq. (1.121), we focus on the long-time limit, noting that a stationary solution $p_\infty(x)$ of the corresponding FPE (1.118) must yield a constant current-density j_∞ , i.e.,

$$j_\infty = -[(\partial_x \Phi)p_\infty + D\partial_x p_\infty] \quad (1.122)$$

where

$$\Phi(x) = U(x) - xF \quad (1.123)$$

is the full effective potential acting on the walker. By comparing with (1.85), one finds that the desired constant-current solution is given by

$$p_\infty(x) = \frac{1}{Z} e^{-\Phi(x)/D} \int_x^{x+L} dy e^{\Phi(y)/D}. \quad (1.124)$$

This solution is spatially periodic, as can be seen from

$$\begin{aligned} p_\infty(x+L) &= \frac{1}{Z} e^{-[U(x+L)-(x+L)F]/D} \int_{x+L}^{x+2L} dy e^{[U(y)-yF]/D} \\ &= \frac{1}{Z} e^{-[U(x)-(x+L)F]/D} \int_x^{x+L} dz e^{[U(z+L)-(z+L)F]/D} \\ &= \frac{1}{Z} e^{-[U(x)-(x+L)F]/D} \int_x^{x+L} dz e^{[U(z)-(z+L)F]/D} \\ &= p_\infty(x), \end{aligned} \quad (1.125)$$

where we have used the coordinate transformation $z = y - L \in [x, x+L]$ after the first line. Inserting $p_\infty(x)$ into Eq. (1.121) gives

$$\begin{aligned} v_L &= -\frac{1}{N_L} \int_0^L dx (\partial_x \Phi) p_\infty \\ &= -\frac{1}{ZN_L} \int_0^L dx (\partial_x \Phi) e^{-\Phi(x)/D} \int_x^{x+L} dy e^{\Phi(y)/D} \\ &= \frac{D}{ZN_L} \int_0^L dx [\partial_x e^{-\Phi(x)/D}] \int_x^{x+L} dy e^{\Phi(y)/D}. \end{aligned} \quad (1.126)$$

Integrating by parts, this can be simplified to

$$\begin{aligned}
v_L &= -\frac{D}{ZN_L} \int_0^L dx e^{-\Phi(x)/D} \partial_x \int_x^{x+L} dy e^{\Phi(y)/D} \\
&= -\frac{D}{ZN_L} \int_0^L dx e^{-\Phi(x)/D} [e^{\Phi(x+L)/D} - e^{\Phi(x)/D}] \\
&= \frac{D}{ZN_L} \int_0^L dx \{1 - e^{[\Phi(x+L) - \Phi(x)]/D}\} \\
&= \frac{D}{ZN_L} \int_0^L dx \{1 - e^{-F[(x+L) - x]/D}\} \\
&= \frac{DL}{ZN_L} (1 - e^{-FL/D}), \tag{1.127}
\end{aligned}$$

where N_L can be expressed as

$$N_L = \frac{1}{Z} \int_0^L dx \int_x^{x+L} dy e^{-[\Phi(x) - \Phi(y)]/D}. \tag{1.128}$$

We thus obtain the final result

$$v_L = DL \frac{1 - e^{-FL/D}}{\int_0^L dx \int_x^{x+L} dy e^{-[\Phi(x) - \Phi(y)]/D}}, \tag{1.129}$$

which holds for arbitrary periodic potentials $U(x)$. Note that there is no net-current at equilibrium $F = 0$.

1.6.2 Temperature ratchet

As we have seen in the preceding sections, the combination of noise and nonlinear dynamics can yield surprising transport effects. Another example is the so-called temperature-ratchet, which can be captured by the minimal SDE model

$$dX(t) = [F - U'(X)] dt + \sqrt{2D(t)} dB(t), \tag{1.130a}$$

where $D(t) = D(t + T)$ is now a time-dependent noise amplitude, such as for instance

$$D(t) = \bar{D} \{1 + A \text{sign}[\sin(2\pi t/T)]\}, \tag{1.130b}$$

where $|A| < 1$. Such a temporally varying noise strength can be realized by heating and cooling the ratchet system periodically. Transport can be quantified in terms of the combined spatio-temporal average

$$\begin{aligned}
\langle \dot{X} \rangle &:= \frac{1}{T} \int_t^{t+T} ds \int_0^L dx j(t, x) \\
&= \frac{1}{T} \int_t^{t+T} ds \int_0^L dx [F - U'(x)] p(t, x). \tag{1.131}
\end{aligned}$$

This choice is motivated by the fact that the equations of motions are periodic in space and time, which suggests an asymptotically oscillating solution $p(t, x) = p(t, x + L) = p(t + T, L) = p(t + T, x + L)$ for the probability density. Equation (1.130) has been studied numerically (see slide and Sec. 2.6 in Ref. [Rei02]), and was found to predict an counterintuitive effect: In the presence of a small load force, optimally tuned periodic thermal pumping allows particles to climb up-hill (see slides for an illustration).

1.7 Fluctuation-dissipation relation

Until now, we focused primarily on over-damped Brownian motion processes, as sufficient to describe low-Reynolds number object. When inertia is not negligible, the above concepts can be easily extended by adding friction and noise to the Hamiltonian equation of motions. Considering a Hamiltonian $H(x_1, \dots, x_N, p_1, \dots, p_N)$, the corresponding system of SDEs reads

$$dx_i = \frac{\partial H}{\partial p_i} dt \quad (1.132a)$$

$$dp_i = -\frac{\partial H}{\partial x_i} dt - \gamma p_i dt + \sqrt{2\mathcal{D}} dB_i(t). \quad (1.132b)$$

where $(B_1(t), \dots, B_N(t))$ are standard Brownian motions, γ is the Stokes friction coefficient and \mathcal{D} the diffusion constant in momentum space. The last two terms in Eq. (1.132b) provide an effective description of the momentum transfer with a surrounding heat bath. If the Hamiltonian has the standard form

$$H = \sum_i \frac{p_i^2}{2m} + U(x_1, \dots, x_N), \quad (1.133)$$

corresponding to momentum coordinates $p_i = m\dot{x}_i$, then the overdamped SDE is formally recovered by assuming $dp_i \simeq 0$ in Eq. (1.132b) and dividing by $m\gamma$, yielding

$$dx_i = -\frac{1}{m\gamma} \frac{\partial U}{\partial x_i} dt + \sqrt{\frac{2\mathcal{D}}{m^2\gamma^2}} dB_i(t). \quad (1.134)$$

We see that the spatial diffusion constant D and the momentum diffusion constant \mathcal{D} are related by

$$D = \frac{\mathcal{D}}{m^2\gamma^2}. \quad (1.135)$$

The Fokker-Planck equation (FPE) governing the phase space PDF $f(t, x_1, \dots, x_N, p_1, \dots, p_N)$ of the stochastic process (1.132) reads

$$\partial_t f + \sum_i \left(\frac{\partial H}{\partial p_i} \frac{\partial f}{\partial x_i} - \frac{\partial H}{\partial x_i} \frac{\partial f}{\partial p_i} \right) = \sum_i \frac{\partial}{\partial p_i} \left(\gamma p_i f + \mathcal{D} \frac{\partial f}{\partial p_i} \right) \quad (1.136)$$

The lhs. vanishes if f is a function of the Hamiltonian H . The rhs. vanishes for the particular ansatz

$$f = \frac{1}{Z} \exp\left(-\frac{H}{k_B T}\right), \quad (1.137)$$

where T is the temperature of the surrounding heat bath. To see this, note that

$$\frac{\partial f}{\partial p_i} = -\frac{1}{k_B T} \frac{\partial H}{\partial p_i} \frac{1}{Z} \exp\left(-\frac{H}{k_B T}\right) = -\frac{1}{k_B T} \frac{p_i}{m} f \quad (1.138)$$

so that the components of the dissipative momentum current,

$$J_i = -\left(\gamma p_i f + \mathcal{D} \frac{\partial f}{\partial p_i}\right) = -\left(\gamma p_i f - \frac{\mathcal{D}}{k_B T} \frac{p_i}{m} f\right) = -\left(\gamma - \frac{\mathcal{D}}{m k_B T}\right) p_i f \quad (1.139)$$

vanishes if

$$\mathcal{D} = \gamma m k_B T \quad \Leftrightarrow \quad D = \frac{k_B T}{\gamma m}. \quad (1.140)$$

Equation (1.140) is the fluctuation-dissipation relation, connecting the diffusion constant (strength of the fluctuations) and the friction coefficient (dissipation) through the temperature of the bath.

1.8 Fluctuation theorems

²⁰ Microbiological systems often perform ‘thermodynamic’ operations with a mesoscopic number of degrees of freedom. To characterize biological motors, protein energetics, etc. in terms of thermodynamic quantities (work, entropy, etc.), an extension of traditional thermodynamic concepts to non-equilibrium processes is has been developed over the last decade. Theoretical work in this direction was triggered by the development of new experimental techniques [BSLS00] that make it possible to probe the folding and twisting characteristics of individual DNA molecules with the help of optical tweezers (see Fig. 1.1 for a simple schematic). These efforts led, amongst others, to the discovery of a number of exact fluctuation theorems (FTs) for non-equilibrium systems, the simplest version of which we will discuss below.

The total Hamiltonian comprising the system of interest, e.g. a DNA molecule described by coordinates $\mathbf{x}(t)$, its environment \mathbf{y} and mutual interactions reads

$$\mathcal{H}(\mathbf{x}, \mathbf{y}; \lambda(t)) = H(\mathbf{x}; \lambda(t)) + H_{\text{env}}(\mathbf{y}) + H_{\text{int}}(\mathbf{x}, \mathbf{y}) \quad (1.141)$$

where $\lambda(t)$ denotes one or more external control parameters (e.g., the force exerted by a tweezer in a molecule pulling experiments, see Fig. 1.1). The function $\lambda(t)$ defines the

²⁰The discussion in this section closely follows that in the Christopher Jarzynski’s review article [Jar11].

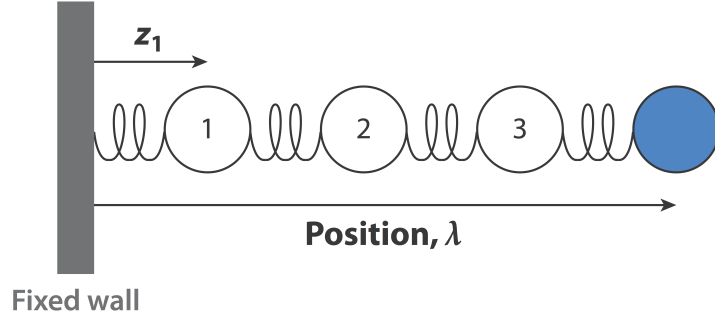


Figure 1.1: Schematic representation of a molecule pulling experiment (from Ref. [Jar11]). The molecule is modeled by a collection of masses connected by springs. The tweezer acts on one end of the molecule, e.g., via an attached gold bead (blue), whereas the other end is attached to surface.

protocol of the control parameter variation and, for simplicity, we will assume that there is only a single control parameter λ from now on. For example, for the toy model in Fig. 1.1 we have $\mathbf{x} = (z_1, z_2, z_3, p_1, p_2, p_3)$ and

$$H(\mathbf{x}; \lambda(t)) = \sum_{i=1}^3 \frac{p_i^2}{2m} + \sum_{k=0}^2 u(z_{k+1} - z_k) + u(\lambda - z_3) \quad (1.142)$$

where u is interaction potential and $z_0(t) \equiv 0$ the position of the wall. The work performed during an infinitesimal parameter variation $d\lambda$ is *defined* by

$$\delta W := d\lambda \frac{\partial H}{\partial \lambda}(\mathbf{x}; \lambda). \quad (1.143)$$

For a given protocol $\lambda(t)$ with initial condition $\lambda(0) = \lambda_0$ and final $\lambda(\tau) = \lambda_\tau$, the total work performed on the system is

$$W = \int \delta W = \int_0^\tau dt \dot{\lambda}(t) \frac{\partial H}{\partial \lambda}(\mathbf{x}(t); \lambda(t)) \quad (1.144)$$

where the integral is computed along the trajectory $\mathbf{x}(t)$ realized by the system. That is, for a given realization W depends not only on the protocol but also on the initial state \mathbf{x}_0 of the system and the initial state \mathbf{y}_0 of the environment, if we assume that $H_{\text{int}}(\mathbf{x}, \mathbf{y}) > 0$ during the process. If we repeat this process many times for the same protocol, we will observe different values of work $\{W_1, W_2, \dots\}$ that will be governed by a certain probability density $\rho(W)$. FTs are exact equalities and inequalities for certain expectation values

$$\langle G(W) \rangle := \int dW \rho(W) G(W), \quad (1.145)$$

that, under very general conditions, hold regardless of exact time dependence $\lambda(t)$.

To simplify the subsequent discussion, let us assume that we are able to decouple the system from the environment²¹ at time $t = 0$, and assume that at time $t = 0$ the PDF of the system state is given by a canonical distribution

$$f(\mathbf{x}_0; \lambda_0, T) = \frac{1}{Z(\lambda_0, T)} \exp\left[-\frac{H(\mathbf{x}_0; \lambda_0)}{k_B T}\right], \quad (1.146a)$$

where T is the *initial* equilibrium temperature of system and environment at $t = 0$, and

$$Z(\lambda_0, T) = \int d\mathbf{x}_0 \exp\left[-\frac{H(\mathbf{x}_0; \lambda_0)}{k_B T}\right] \quad (1.146b)$$

the classical partition function. In this case, the *initial* free energy of the system is given by

$$F_0 = -k_B T \ln Z(\lambda_0, T). \quad (1.147)$$

Moreover, since the dynamics for $t > 0$ is completely Hamiltonian, we have

$$\begin{aligned} \frac{dH}{dt} &= \sum_i \left(\frac{\partial H}{\partial p_i} \dot{p}_i + \frac{\partial H}{\partial z_i} \dot{z}_i \right) + \frac{\partial H}{\partial t} \\ &= \sum_i \left[\frac{\partial H}{\partial p_i} \left(-\frac{\partial H}{\partial z_i} \right) + \frac{\partial H}{\partial z_i} \left(\frac{\partial H}{\partial p_i} \right) \right] + \frac{\partial H}{\partial \lambda} \dot{\lambda} \\ &= \frac{\partial H}{\partial \lambda} \dot{\lambda} \end{aligned} \quad (1.148)$$

and, therefore,

$$W = \int_0^\tau dt \dot{\lambda} \frac{\partial H}{\partial \lambda} = \int_0^\tau dH = H(\mathbf{x}_\tau; \lambda_\tau) - H(\mathbf{x}_0; \lambda_0) \quad (1.149)$$

where $\mathbf{x}(\tau) = \mathbf{x}_\tau$. Now consider the expectation value of the function $G(W) = e^{-W/(k_B T)}$, which can be expressed as

$$\begin{aligned} \langle e^{-W/(k_B T)} \rangle &= \int d\mathbf{x}_0 f(\mathbf{x}_0; \lambda_0, T) e^{-W/(k_B T)} \\ &= \int d\mathbf{x}_0 f(\mathbf{x}_0; \lambda_0, T) e^{-[H(\mathbf{x}_\tau; \lambda_\tau) - H(\mathbf{x}_0; \lambda_0)]/(k_B T)} \\ &= \frac{1}{Z(\lambda_0, T)} \int d\mathbf{x}_0 \exp\left[-\frac{H(\mathbf{x}_0; \lambda_0)}{k_B T}\right] e^{-[H(\mathbf{x}_\tau; \lambda_\tau) - H(\mathbf{x}_0; \lambda_0)]/(k_B T)} \\ &= \frac{1}{Z(\lambda_0, T)} \int d\mathbf{x}_0 e^{-H(\mathbf{x}_\tau; \lambda_\tau)/(k_B T)} \end{aligned} \quad (1.150)$$

²¹Similar results hold for more complex dynamical models where the system remains coupled to the bath throughout the process; see discussion in Ref. [Jar11] and references therein.

Changing the integration variable from $\mathbf{x}_0 \mapsto \mathbf{x}_\tau$, we can write this as

$$\begin{aligned}
\langle e^{-W/(k_B T)} \rangle &= \frac{1}{Z(\lambda_0, T)} \int d\mathbf{x}_\tau \left| \frac{\partial \mathbf{x}_\tau}{\partial \mathbf{x}_0} \right|^{-1} e^{-H(\mathbf{x}_\tau; \lambda_\tau)/(k_B T)} \\
&= \frac{1}{Z(\lambda_0, T)} \int d\mathbf{x}_\tau e^{-H(\mathbf{x}_\tau; \lambda_\tau)/(k_B T)} \\
&= \frac{Z(\lambda_\tau, T)}{Z(\lambda_0, T)}
\end{aligned} \tag{1.151}$$

Here, we have used Liouville's theorem, which states that the phase volume is conserved under a purely Hamiltonian evolution $\mathbf{x}_0 \mapsto \mathbf{x}(\tau)$,

$$\left| \frac{\partial \mathbf{x}_\tau}{\partial \mathbf{x}_0} \right| = 1 \tag{1.152}$$

Rewriting further

$$\begin{aligned}
\langle e^{-W/(k_B T)} \rangle &= \exp \left\{ \frac{k_B T}{k_B T} \ln \left[\frac{Z(\lambda_\tau, T)}{Z(\lambda_0, T)} \right] \right\} \\
&= \exp \left\{ -\frac{1}{k_B T} [-k_B T \ln Z(\lambda_\tau, T) - (-k_B T) \ln Z(\lambda_0, T)] \right\}
\end{aligned}$$

one thus finds the FT

$$\langle e^{-W/(k_B T)} \rangle = e^{-\Delta F/(k_B T)} \tag{1.153a}$$

where

$$\Delta F = F(\lambda_\tau, T) - F(\lambda_0, T) \tag{1.153b}$$

The FT (1.153) states that, in principle, one can estimate free energy differences by measuring work W . In this context, it should be noted however that, in practice, the exponential average $\langle e^{-W/(k_B T)} \rangle$ is difficult to sample as direct estimators suffer from slow convergence.

Furthermore, using Jensen's inequality²²

$$\langle e^x \rangle \geq e^{\langle x \rangle} \tag{1.154}$$

²²Jensen's inequality states that, if $\phi(x)$ is convex then

$$\mathbb{E}[\phi(X)] \geq \phi(\mathbb{E}[X])$$

Proof: Let $L(x) = a + bx$ be a line, tangent to $\phi(x)$ at the point $x_* = \mathbb{E}[X]$. Since ϕ is convex, we have $\phi(x) \geq L(x)$. Hence

$$\mathbb{E}[\phi(X)] \geq \mathbb{E}[L(X)] = a + b\mathbb{E}[X] = L(\mathbb{E}[X]) = \phi(\mathbb{E}[X])$$

we find

$$e^{-\Delta F/(k_B T)} = \langle e^{-W/(k_B T)} \rangle \geq e^{\langle -W/(k_B T) \rangle}$$

which is equivalent to the *Clausius inequality*

$$\Delta F \leq \langle W \rangle, \tag{1.155}$$

i.e., the average work provides an upper bound for the free energy difference.

Finally, we still note that

$$\begin{aligned} \mathbb{P}[W < \Delta F - \epsilon] &:= \int_{-\infty}^{\Delta F - \epsilon} dW \rho(W) \\ &\leq \int_{-\infty}^{\Delta F - \epsilon} dW \rho(W) e^{(\Delta F - \epsilon - W)/(k_B T)} \\ &\leq e^{(\Delta F - \epsilon)/(k_B T)} \int_{-\infty}^{\infty} dW \rho(W) e^{-W/(k_B T)} \\ &= e^{(\Delta F - \epsilon)/(k_B T)} \langle e^{-W/(k_B T)} \rangle \\ &= e^{-\epsilon/(k_B T)} \end{aligned} \tag{1.156}$$

That is, the probability that a certain realization W violates the Clausius relation by an amount ϵ is exponentially small.

1.9 Problems (due Monday, March 14)

1. Provide and explain rough order-of-magnitude estimates.

- (a) How heavy is a bacterium?
- (b) How fast must a bacterium swim so that swimming makes sense?
- (c) How large is the effective diffusion constant of bacteria that perform run-and-tumble motion with run periods 1s?
- (d) How large are the self-propulsion force and the torque generated by a bacterial motor?

2. Brownian motion

- (a) Show that the probability density of the classical one-dimensional RW approaches a Gaussian PDF in the continuum limit $\ell, \tau \rightarrow 0$ such that $D = \ell^2/(2\tau) = \text{const.}$
- (b) Compute the mean square displacement of the n -dimensional BM.
- (c) Using heuristic arguments, estimate the return probability of a classical RW in $n = 1, 2, 3$ dimensions.
- (d) The Geometric BM is defined by the Ito SDE

$$dY = \mu Y dt + \sigma Y * dB(t). \quad (1.157a)$$

where μ and σ are constant parameters. Use Ito's formula to show that

$$Y(t) = Y(0) \exp \left[\left(\mu - \frac{\sigma^2}{2} \right) t + \sigma B(t) \right]. \quad (1.157b)$$

Determine mean value and variance of $Y(t)$.

3. Microcanonical fluctuation theorem

- (a) Consider a Hamiltonian system $H(\mathbf{x}; \lambda(t))$ with protocol $\lambda(t)$ such that $\lambda(0) = \lambda_0$ and $\lambda(\tau) = \lambda_\tau$. For the forward process (+), $\lambda_0 \rightarrow \lambda_\tau$, assume that the system is initially, at time $t = 0$, in the microcanonical state $H(\mathbf{x}; \lambda_0) = E_0$, corresponding to the PDF

$$p(\mathbf{x}; \lambda_0) = \frac{\delta(E_0 - H(\mathbf{x}; \lambda_0))}{\omega(E_0, \lambda_0)} \quad (1.158a)$$

Define the corresponding microcanonical PDF for the backward process (-), $\lambda_\tau \rightarrow \lambda_0$, and determine the work W_\pm performed during each realization of the forward/backward process.

- (b) Using Liouville's theorem, show that the associated work PDFs $p_{\pm}(w)$ satisfy the relation

$$\frac{p_{-}(-w)}{p_{+}(w)} = \frac{\omega(E_0, \lambda_0)}{\omega(E_0 + w, \lambda_{\tau})}. \quad (1.158b)$$

- (c) Express equation (1.158b) in terms of the Boltzmann entropy $S_B = \ln \omega$ of the final and initial state, and also in terms of the Gibbs entropy $S_G = \ln \Omega$ and the Gibbs temperature $T_G = \Omega/\omega$.

1.10 Solutions

1.10.1 Problem 1: Order-of-magnitude estimates

(a) How heavy is a bacterium? Assuming a volume $v = 1 \mu\text{m}^3$ and a mass density $\rho = 1000 \text{ kg/m}^3$ (water), we find

$$m = \rho v \sim 10^{-18} \times 10^3 \text{ kg} = 1 \text{ pg} \quad (1.159a)$$

(b) How fast must a bacterium swim so that swimming makes sense? At room temperature, $kT = 4 \times 10^{-21} \text{ J}$. Stokes drag coefficient of a sphere of radius $a = 1 \mu\text{m}$ in water

$$\gamma_S = 6\pi\eta a \sim 2 \times 10^{-8} \text{ kg/s}$$

Hence, we find for the diffusion constant

$$D \sim 0.2 \mu\text{m}^2/\text{s}$$

Assuming a run length $\sim 1 \text{ s}$, Brownian motion would move a micron-sized bacterium by approximately $0.5 \mu\text{m}$ per second. Thus a bacterium should swim at last $5\text{-}10 \mu\text{m/s}$, which is close to typical swim bacterial speeds.

(c) How large is the effective diffusion constant of bacteria that perform run-and-tumble motion with run periods $\tau \sim 1 \text{ s}$?

$$D_b \sim V^2\tau \sim 10^2 \mu\text{m}^2/\text{s}$$

(d) How large are the self-propulsion force and the torque generated by a bacterial motor?
Force

$$F \sim \gamma_S V \sim 2 \times 10^{-8} \text{ kg/s} \times 10 \mu\text{m/s} = 0.2 \text{ pN} \quad (1.159b)$$

Torque

$$T \sim (a/2) \times F \sim 10^{-19} \text{ Nm} = 10^{-12} \text{ dyn} \cdot \text{cm} \quad (1.159c)$$

Both estimates are very close to experimentally measured values.

1.10.2 Problem 2: Brownian motion

(a) The probability $P(N, K) := \mathbb{P}[X_N/\ell = K]$ to be at an even position $x/\ell = K \geq 0$ after N steps is given by the binomial coefficient

$$\begin{aligned} P(N, K) &= \left(\frac{1}{2}\right)^N \binom{N}{\frac{N-K}{2}} \\ &= \left(\frac{1}{2}\right)^N \frac{N!}{((N+K)/2)! ((N-K)/2)!} \end{aligned} \quad (1.160)$$

Defining the associated density

$$p(t, x) := \frac{P(N, K)}{2\ell} = \frac{P(t/\tau, x/\ell)}{2\ell}. \quad (1.161)$$

We wish to approximate

$$\ln[2\ell p(t, x)] = \ln P(t/\tau, x/\ell) \quad (1.162)$$

by considering limit $\tau, \ell \rightarrow 0$ such that

$$D := \frac{\ell^2}{2\tau} = \text{const.} \quad (1.163)$$

To this end, write

$$\begin{aligned} \ln[2\ell p(t, x)] &= \ln \left[\left(\frac{1}{2} \right)^{t/\tau} \frac{(t/\tau)!}{(((t/\tau) + (x/\ell))/2)! ((t/\tau) - (x/\ell))/2)!} \right] \\ &= -(t/\tau) \ln 2 + \ln(t/\tau)! \\ &\quad - \ln(((t/\tau) + (x/\ell))/2)! - \ln(((t/\tau) - (x/\ell))/2)! \end{aligned} \quad (1.164)$$

and substitute $\tau = \ell^2/(2D)$ to obtain

$$\begin{aligned} \ln[2\ell p(t, x)] &= - \left(\frac{\sigma^2}{\ell^2} \right) \ln 2 + \ln \left(\frac{\sigma^2}{\ell^2} \right)! \\ &\quad - \ln \left(\frac{\sigma^2}{2\ell^2} + \frac{x}{2\ell} \right)! - \ln \left(\frac{\sigma^2}{2\ell^2} - \frac{x}{2\ell} \right)! \end{aligned} \quad (1.165)$$

where $\sigma^2 := 2Dt$. Making use of Stirling's formula,

$$\ln n! \simeq n \ln n - n + \frac{1}{2} \ln 2\pi n, \quad (1.166)$$

we can approximate

$$\begin{aligned}
& \ln[2\ell p(t, x)] \\
\simeq & -\left(\frac{\sigma^2}{\ell^2}\right) \ln 2 \\
& + \left(\frac{\sigma^2}{\ell^2}\right) \ln\left(\frac{\sigma^2}{\ell^2}\right) - \left(\frac{\sigma^2}{\ell^2}\right) + \frac{1}{2} \ln 2\pi \left(\frac{\sigma^2}{\ell^2}\right) \\
& - \left(\frac{\sigma^2}{2\ell^2} + \frac{x}{2\ell}\right) \ln\left(\frac{\sigma^2}{2\ell^2} + \frac{x}{2\ell}\right) + \left(\frac{\sigma^2}{2\ell^2} + \frac{x}{2\ell}\right) - \frac{1}{2} \ln 2\pi \left(\frac{\sigma^2}{2\ell^2} + \frac{x}{2\ell}\right) \\
& - \left(\frac{\sigma^2}{2\ell^2} - \frac{x}{2\ell}\right) \ln\left(\frac{\sigma^2}{2\ell^2} - \frac{x}{2\ell}\right) + \left(\frac{\sigma^2}{2\ell^2} - \frac{x}{2\ell}\right) - \frac{1}{2} \ln 2\pi \left(\frac{\sigma^2}{2\ell^2} - \frac{x}{2\ell}\right) \\
= & -\left(\frac{\sigma^2}{\ell^2}\right) \ln 2 \\
& + \left(\frac{\sigma^2}{\ell^2}\right) \ln\left(\frac{\sigma^2}{\ell^2}\right) + \frac{1}{2} \ln 2\pi \left(\frac{\sigma^2}{\ell^2}\right) \\
& - \left(\frac{\sigma^2}{2\ell^2} + \frac{x}{2\ell}\right) \ln\left(\frac{\sigma^2}{2\ell^2} + \frac{x}{2\ell}\right) - \frac{1}{2} \ln 2\pi \left(\frac{\sigma^2}{2\ell^2} + \frac{x}{2\ell}\right) \\
& - \left(\frac{\sigma^2}{2\ell^2} - \frac{x}{2\ell}\right) \ln\left(\frac{\sigma^2}{2\ell^2} - \frac{x}{2\ell}\right) - \frac{1}{2} \ln 2\pi \left(\frac{\sigma^2}{2\ell^2} - \frac{x}{2\ell}\right)
\end{aligned} \tag{1.167}$$

Assuming $x\ell \ll \sigma^2$ and keeping only the leading order terms for $\ell \rightarrow 0$ gives

$$\ln[2\ell p(t, x)] \simeq -\frac{1}{2} \ln \frac{\pi\sigma^2}{2\ell^2} - \frac{x^2}{2\sigma^2} \tag{1.168}$$

and, hence,

$$p(t, x) \simeq \sqrt{\frac{1}{2\pi\sigma^2}} \exp\left(-\frac{x^2}{2\sigma^2}\right) = \sqrt{\frac{1}{4\pi Dt}} \exp\left(-\frac{x^2}{4Dt}\right). \tag{1.169}$$

(b) Assuming $\mathbf{X}(0) = \mathbf{0}$, the msd. is given by

$$\mathbb{E}[\mathbf{X}(t)^2] = n \mathbb{E}[X_1(t)^2] = n \cdot 2Dt. \tag{1.170}$$

(c) First consider 1D case. Assume RW starts at $x_0 = 0$ and denote by X_N the position after an even number N steps. The mean total number of returns $\bar{R}_{d=1}$ after an infinite number of steps is

$$\begin{aligned}
\bar{R}_{d=1} &= \sum_{N=1}^{\infty} \delta_{X_N, 0} P(N, X_N) \\
&= \sum_{N=2,4,\dots}^{\infty} P(N, 0)
\end{aligned} \tag{1.171}$$

According to Eq. (1.8), the probability of being at 0 after N steps is

$$P(N, 0) = \left(\frac{1}{2}\right)^N \binom{N}{N/2} \quad (1.172)$$

Using Stirling's formula

$$n! \simeq \sqrt{2\pi n} n^{n+\frac{1}{2}} e^{-n} \quad (1.173)$$

we can estimate

$$\begin{aligned} P(N, 0) &= \left(\frac{1}{2}\right)^N \frac{N!}{[(N/2)!]^2} \simeq \left(\frac{1}{2}\right)^N \frac{\sqrt{2\pi N} N^{N+\frac{1}{2}} e^{-N}}{[\sqrt{2\pi (N/2)} (N/2)^{N/2+\frac{1}{2}} e^{-N/2}]^2} \\ &= \left(\frac{1}{2}\right)^N \frac{N^{N+\frac{1}{2}} e^{-N}}{\sqrt{2\pi (N/2)}^{N+1} e^{-N}} \\ &= \frac{2}{\sqrt{2\pi N}} \end{aligned} \quad (1.174)$$

Hence, in 1D

$$\bar{R}_{d=1} \simeq \frac{1}{\sqrt{\pi}} \sum_{n=1}^{\infty} \frac{1}{\sqrt{n}} = +\infty. \quad (1.175)$$

In $d > 2$ dimensions, the probability of returning after $N = 2n$ steps to 0 is approximately proportional to $(\sqrt{\pi n})^d$, and therefore

$$\bar{R}_d \simeq \pi^{-d/2} \sum_{n=1}^{\infty} n^{-d/2} = \pi^{-d/2} \zeta(d/2), \quad (1.176)$$

which implies an infinite number of returns in two dimensions, $\bar{R}_{d=2} = \infty$, but gives

$$\bar{R}_{d=3} \simeq 0.47 \quad (1.177)$$

in three dimensions. That is, in 3D, returns are very rare and one needs roughly 3 particles to observe a single return during an infinite observation period.

(d) Consider $F(Y) = \ln Y$. Using Ito's formula with $D(Y) = \sigma^2 Y^2/2$

$$\begin{aligned} dF &= d(\ln Y) = F'(Y)dY + DF''(Y)dt \\ &= \frac{dY}{Y} - \frac{\sigma^2}{2}dt \\ &= \mu dt + \sigma dB(t) - \frac{\sigma^2}{2}dt. \end{aligned} \quad (1.178)$$

Hence, with $B(0) = 0$

$$\ln Y(t) - \ln Y(0) = \left(\mu - \frac{\sigma^2}{2} \right) t + \sigma B(t) \quad (1.179)$$

and therefore

$$Y(t) = Y(0) \exp \left[\left(\mu - \frac{\sigma^2}{2} \right) t + \sigma B(t) \right]. \quad (1.180)$$

We know that

$$B(t) = \frac{\ln Y(t) - \ln Y(0) - \left(\mu - \frac{\sigma^2}{2} \right) t}{\sigma} \quad (1.181)$$

follows a normal distribution with variance t , i.e., the PDF of $b = B(t)$ is

$$p(b) = \frac{1}{\sqrt{2\pi t}} e^{-b^2/(2t)} \quad (1.182)$$

Denoting $y = Y(t)$ and using the standard transformation formula

$$\hat{p}(y) = p(b(y)) \frac{db}{dy}, \quad (1.183)$$

with $db/dy = (y\sigma)^{-1}$, one finds

$$\hat{p}(y) = \frac{1}{y\sigma\sqrt{2\pi t}} \exp \left\{ -\frac{1}{2\sigma^2 t} \left[\ln y - \ln Y(0) - \left(\mu - \frac{\sigma^2}{2} \right) t \right]^2 \right\}. \quad (1.184)$$

We may use this to compute mean value and variance

$$\mathbb{E}[Y(t)] = \int_0^\infty dy \hat{p}(y) y = \int_{-\infty}^\infty db p(b) y(b) = Y(0) e^{\mu t} \quad (1.185)$$

and similarly

$$\mathbb{E}[Y(t)^2] = \int_0^\infty dy \hat{p}(y) y^2 = \int_{-\infty}^\infty db p(b) y(b)^2 = Y(0)^2 e^{(2\mu + \sigma^2)t} \quad (1.186a)$$

which yields the variance

$$\mathbb{E}[Y(t)^2] - \mathbb{E}[Y(t)]^2 = Y(0)^2 e^{2\mu t} (e^{\sigma^2 t} - 1). \quad (1.187)$$

1.10.3 Problem 3: Microcanonical fluctuation theorem

(a) The work performed during the forward process (+) and the backward process (−) is given by

$$W_+ = H(\mathbf{x}_\tau; \lambda_\tau) - H(\mathbf{x}_0; \lambda_0) = -W_- \quad (1.188)$$

(b) We start from the definition of the forward probability density

$$\begin{aligned}
p_+(w) &= \langle \delta(W_+ - w) \rangle_{\lambda_0 \rightarrow \lambda_\tau} \\
&= \frac{1}{\omega(E_0, \lambda_0)} \int d\mathbf{x}_0 \delta(E_0 - H(\mathbf{x}_0; \lambda_0)) \delta(W_+ - w) \\
&= \frac{1}{\omega(E_0, \lambda_0)} \int d\mathbf{x}_0 \delta(E_0 - H(\mathbf{x}_0; \lambda_0)) \delta(H(\mathbf{x}_\tau; \lambda_\tau) - H(\mathbf{x}_0; \lambda_0) - w) \\
&= \frac{1}{\omega(E_0, \lambda_0)} \int d\mathbf{x}_0 \delta(E_0 - H(\mathbf{x}_0; \lambda_0)) \delta(H(\mathbf{x}_\tau; \lambda_\tau) - E_0 - w),
\end{aligned}$$

where we have inserted (1.188) in the argument of second δ -function.

We next insert (1.188) in the argument of first δ -function, and replace the integration variable $\mathbf{x}_0 \rightarrow \mathbf{x}_\tau$ using Liouville's theorem

$$\begin{aligned}
p_+(w) &= \frac{1}{\omega(E_0, \lambda_0)} \int d\mathbf{x}_0 \delta(E_0 - H(\mathbf{x}_\tau; \lambda_\tau) + W_+) \delta(H(\mathbf{x}_\tau; \lambda_\tau) - E_0 - w) \\
&= \frac{1}{\omega(E_0, \lambda_0)} \int d\mathbf{x}_\tau \left| \frac{\partial \mathbf{x}_\tau}{\partial \mathbf{x}_0} \right|^{-1} \delta(E_0 - H(\mathbf{x}_\tau; \lambda_\tau) + W_+) \delta(H(\mathbf{x}_\tau; \lambda_\tau) - (E_0 + w)) \\
&= \frac{1}{\omega(E_0, \lambda_0)} \int d\mathbf{x}_\tau \delta(E_0 - H(\mathbf{x}_\tau; \lambda_\tau) + W_+) \delta(H(\mathbf{x}_\tau; \lambda_\tau) - (E_0 + w)) \\
&= \frac{1}{\omega(E_0, \lambda_0)} \int d\mathbf{x}_\tau \delta(E_0 - (E_0 + w) + W_+) \delta(H(\mathbf{x}_\tau; \lambda_\tau) - (E_0 + w))
\end{aligned}$$

We can now reexpress the integrand as MC average at final energy $E_\tau = E_0 + w$

$$\begin{aligned}
p_+(w) &= \frac{1}{\omega(E_0, \lambda_0)} \int d\mathbf{x}_\tau \delta(-w + W_+) \delta(H(\mathbf{x}_\tau; \lambda_\tau) - (E_0 + w)) \\
&= \frac{\omega(E_0 + w, \lambda_\tau)}{\omega(E_0, \lambda_0)} \int d\mathbf{x}_\tau \delta(-w + W_+) \frac{\delta(H(\mathbf{x}_\tau; \lambda_\tau) - (E_0 + w))}{\omega(E_0 + w, \lambda_\tau)} \\
&= \frac{\omega(E_0 + w, \lambda_\tau)}{\omega(E_0, \lambda_0)} \int d\mathbf{x}_\tau \delta(-w - W_-) \frac{\delta(H(\mathbf{x}_\tau; \lambda_\tau) - (E_0 + w))}{\omega(E_0 + w, \lambda_\tau)} \\
&= \frac{\omega(E_0 + w, \lambda_\tau)}{\omega(E_0, \lambda_0)} \langle \delta(W_- + w) \rangle_{\lambda_\tau \rightarrow \lambda_0, E_\tau = E_0 + w} \\
&= \frac{\omega(E_0 + w, \lambda_\tau)}{\omega(E_0, \lambda_0)} p_-(-w)
\end{aligned}$$

Hence, we obtain the final result

$$\frac{p_-(-w)}{p_+(w)} = \frac{\omega(E_0, \lambda_0)}{\omega(E_0 + w, \lambda_\tau)} \tag{1.189}$$

(c) We can rewrite the rhs. of Eq. (1.189) in terms of the Boltzmann entropy $S_B = \ln \omega$ as

$$\begin{aligned}
\frac{p_-(-w)}{p_+(w)} &= \exp [\ln \omega(E_0, \lambda_0) - \ln \omega(E_0 + w, \lambda_\tau)] \\
&= e^{-[S_B(E_0+w, \lambda_\tau) - S_B(E_0, \lambda_0)]} \\
&= e^{-\Delta S_B}
\end{aligned} \tag{1.190}$$

Alternatively, in terms of the Gibbs entropy $S_G = \ln \Omega$ and Gibbs temperature $T_G = \Omega/\omega$, we find

$$\begin{aligned}
\frac{p_-(-w)}{p_+(w)} &= \frac{\omega(E_0, \lambda_0)/\Omega(E_0, \lambda_0)}{\omega(E_0 + w, \lambda_\tau)/\Omega(E_0 + w, \lambda_\tau)} \times \frac{\Omega(E_0, \lambda_0)}{\Omega(E_0 + w, \lambda_\tau)} \\
&= \frac{T_G(E_0 + w, \lambda_\tau)}{T_G(E_0, \lambda_0)} \times e^{-[S_G(E_0+w, \lambda_\tau) - S_G(E_0, \lambda_0)]} \\
&= \frac{T_G(E_0 + w, \lambda_\tau)}{T_G(E_0, \lambda_0)} \times e^{-\Delta S_G}
\end{aligned} \tag{1.191}$$

Chapter 2

Polymers

2.1 Persistent random walks

2.1.1 von Mises-Fisher (vMF) distribution

The PDF of the vMF distribution on the unit sphere $\mathbf{n} \in \mathbb{S}$ reads

$$f(\mathbf{n}|\boldsymbol{\mu}) = C_2 e^{\kappa \mathbf{n} \cdot \boldsymbol{\mu}}. \quad (2.1)$$

The parameter $\boldsymbol{\mu} \in \mathbb{S}$ determines the mean direction and κ the spread, with $\kappa = 0$ corresponding to a uniform distribution and $\kappa \rightarrow \infty$ to a δ -distribution at $\mathbf{n} = \boldsymbol{\mu}$. Assuming w.l.o.g. $\boldsymbol{\mu} = (0, 0, 1)$ and using spherical coordinates $\mathbf{n} = (\cos \phi \sin \theta, \sin \phi \sin \theta, \cos \theta)$ with $(\phi, \theta) \in [0, 2\pi) \times [0, \pi]$, the normalization constant C_2 can be computed from

$$\begin{aligned} 1 &= C_2 \int_0^{2\pi} d\phi \int_0^\pi d\theta \sin \theta f(\mathbf{n}|\boldsymbol{\mu}) \\ &= C_2 \int_0^{2\pi} d\phi \int_0^\pi d\theta \sin \theta e^{\kappa \cos \theta} \\ &= C_2 \frac{4\pi \sinh \kappa}{\kappa}, \end{aligned} \quad (2.2)$$

yielding

$$C_2 = \frac{\kappa}{4\pi \sinh \kappa}. \quad (2.3)$$

Similarly, one finds for the mean

$$\mathbb{E}[\mathbf{n}|\boldsymbol{\mu}] = C_2 \int d\mathbf{n} \mathbf{n} e^{\kappa \mathbf{n} \cdot \boldsymbol{\mu}} = \left(\frac{1}{\tanh \kappa} - \frac{1}{\kappa} \right) \boldsymbol{\mu} =: \sigma \boldsymbol{\mu}, \quad (2.4a)$$

where the scale-factor $\sigma(\kappa)$ exhibits the following limiting behaviors

$$\lim_{\kappa \rightarrow 0} \sigma(\kappa) = 0, \quad (2.4b)$$

$$\lim_{\kappa \rightarrow \infty} \sigma(\kappa) = 1. \quad (2.4c)$$

2.1.2 vMF polymer model

Consider an idealized polymer consisting of $i = 1, \dots, N$ segments of length λ . Each segment has an orientation $\boldsymbol{\mu}_i$, so that the vector connecting the two polymer ends is given by

$$\mathbf{R}(N) = \sum_{i=1}^N \mathbf{R}_i = \lambda \sum_{i=1}^N \boldsymbol{\mu}_i. \quad (2.5)$$

The total length of the polymer is $L = N\lambda$ and w.l.o.g. we choose $\mathbf{R}(0)$ and $\boldsymbol{\mu}_1 = (0, 0, 1)$. We assume that the conditional PDF of $\boldsymbol{\mu}_i$ for a given $\boldsymbol{\mu}_{i-1}$, is a vMF-distribution with spread parameter κ ,

$$f(\boldsymbol{\mu}_i | \boldsymbol{\mu}_{i-1}) = C_2 e^{\kappa \boldsymbol{\mu}_i \cdot \boldsymbol{\mu}_{i-1}}. \quad (2.6)$$

We would like to compute correlation functions and statistical moments of $\mathbf{R}(N)$ in the limit of large N . Of particular interest are the mean end-position

$$\mathbb{E}[\mathbf{R}(N) | \boldsymbol{\mu}_1] = \lambda \sum_{n=1}^N \mathbb{E}[\boldsymbol{\mu}_n | \boldsymbol{\mu}_1], \quad (2.7a)$$

the squared end-to-end distance

$$\mathcal{D}(N) = \mathbb{E}[\mathbf{R}(N) \cdot \mathbf{R}(N)], \quad (2.7b)$$

and the excursion PDF

$$p_N(\mathbf{r}) = \mathbb{E}[\delta(\mathbf{r} - \mathbf{R}(N))]. \quad (2.7c)$$

Mean end-position and persistence length

To compute the mean end-position $\mathbb{E}[\mathbf{R}(N) | \boldsymbol{\mu}_1]$ for a given initial condition $\boldsymbol{\mu}_1$, let us first note that the conditional expectation value $\mathbb{E}[\boldsymbol{\mu}_n | \boldsymbol{\mu}_1]$ can be computed as

$$\begin{aligned} \mathbb{E}[\boldsymbol{\mu}_n | \boldsymbol{\mu}_1] &= C_2^{n-1} \int \boldsymbol{\mu}_n e^{\kappa \sum_{i=2}^n \boldsymbol{\mu}_i \cdot \boldsymbol{\mu}_{i-1}} \prod_{i=2}^n d\boldsymbol{\mu}_i \\ &= \sigma C_2^{n-2} \int \boldsymbol{\mu}_{n-1} e^{\kappa \sum_{i=2}^{n-1} \boldsymbol{\mu}_i \cdot \boldsymbol{\mu}_{i-1}} \prod_{i=2}^{n-1} d\boldsymbol{\mu}_i \\ &\dots \\ &= \sigma^{n-1} \boldsymbol{\mu}_1, \end{aligned} \quad (2.8)$$

yielding

$$\mathbb{E}[\mathbf{R}(N) | \boldsymbol{\mu}_1] = \lambda \sum_{n=1}^N \sigma^{n-1} \boldsymbol{\mu}_1 = \lambda \sum_{n=0}^{N-1} \sigma^n \boldsymbol{\mu}_1 = \lambda \frac{1 - \sigma^N}{1 - \sigma} \boldsymbol{\mu}_1. \quad (2.9)$$

In the limit case of a uniform distribution, $\kappa \rightarrow 0$, we find at fixed N

$$\mathbb{E}[\mathbf{R}(N)|\boldsymbol{\mu}_1] = \lambda\boldsymbol{\mu}_1 \quad (2.10a)$$

whereas for an infinitely stiff polymer with $\kappa \rightarrow \infty$

$$\mathbb{E}[\mathbf{R}(N)|\boldsymbol{\mu}_1] = \lambda N\boldsymbol{\mu}_1, \quad (2.10b)$$

illustrating that the vMF-model interpolates between undirected random walking and ballistic motion.

An important quantity that characterizes the stiffness of a polymer is the *persistence length* L_P , intuitively defined in terms of the asymptotically exponential decay of the orientation correlation function

$$\langle \cos \theta_N \rangle \equiv \mathbb{E}[\boldsymbol{\mu}_N \cdot \boldsymbol{\mu}_1] \simeq e^{-L/L_P} \quad (2.11)$$

for large polymer length $L = N\lambda$. Noting that

$$\mathbb{E}[\boldsymbol{\mu}_N \cdot \boldsymbol{\mu}_1] = \mathbb{E}[\boldsymbol{\mu}_N|\boldsymbol{\mu}_1] \cdot \boldsymbol{\mu}_1, \quad (2.12)$$

we can obtain L_P from (2.8) by

$$\begin{aligned} \frac{1}{L_P} &= - \lim_{L \rightarrow \infty} \frac{1}{L} \ln \mathbb{E}[\boldsymbol{\mu}_N \cdot \boldsymbol{\mu}_1] \\ &= - \lim_{N \rightarrow \infty} \frac{1}{\lambda N} \ln \sigma^{N-1} \\ &= - \frac{1}{\lambda} \ln \sigma. \end{aligned} \quad (2.13)$$

Inserting the explicit expression $\sigma(\kappa)$ from (2.4a), we find for $\kappa \ll 1$

$$L_P \simeq \frac{\lambda}{\ln(3/\kappa)}, \quad (2.14a)$$

whereas for $\kappa \gg 1$

$$L_P \simeq \lambda\kappa. \quad (2.14b)$$

Squared end-to-end distance

To compute the squared end-to-end distance

$$\mathcal{D}(N) = \mathbb{E}[\mathbf{R}(N) \cdot \mathbf{R}(N)] = \lambda^2 \sum_{i,j=1}^N \mathbb{E}[\boldsymbol{\mu}_i \cdot \boldsymbol{\mu}_j], \quad (2.15)$$

we may use that the orientation correlation is translation-invariant

$$\mathbb{E}[\boldsymbol{\mu}_i \cdot \boldsymbol{\mu}_j] = \sigma^{|i-j|}. \quad (2.16)$$

Computing the double sum (2.15), one obtains

$$\mathcal{D}(N) = \lambda^2 \frac{N - \sigma (2 - 2\sigma^N + \sigma N)}{(\sigma - 1)^2}, \quad (2.17)$$

and from this the limiting behaviors

$$\lim_{\kappa \rightarrow 0} \mathcal{D}(N) = \lim_{\sigma \rightarrow 0} \mathcal{D}(N) = \lambda^2 N, \quad (2.18a)$$

$$\lim_{\kappa \rightarrow \infty} \mathcal{D}(N) = \lim_{\sigma \rightarrow 1} \mathcal{D}(N) = \lambda^2 N^2, \quad (2.18b)$$

corresponding to normal diffusion and ballistic growth. Conversely, when keeping $\kappa < \infty$ fixed but letting the number of monomers $N \rightarrow \infty$, then

$$D(\kappa) := \lim_{N \rightarrow \infty} \frac{\mathcal{D}}{N} = \lambda^2 \frac{1 + \sigma}{1 - \sigma}, \quad (2.18c)$$

This means that, for finite κ , the end-to-end distance increases with $N^{1/2}$ corresponding to normal diffusion. For floppy polymers with $\kappa \rightarrow 0$, one finds that $D \rightarrow \lambda^2$, whereas for large κ

$$\lim_{\kappa \rightarrow \infty} \frac{D}{\kappa} = 2\lambda^2. \quad (2.19)$$

That is, for long stiff polymers with $\kappa \gg 1$, we have

$$D \simeq 2\lambda^2 \kappa = 2\lambda L_P. \quad (2.20)$$

Excursion PDF & thermodynamics

Unfortunately, it is not possible to compute the excursion PDF (2.7c) exactly for the vMF model¹. However, the central limit theorem combined with (2.18c) implies that, for large N , the excursion PDF will approach a Gaussian

$$p(\mathbf{r}) \simeq \left(\frac{3}{2\pi DN} \right)^{3/2} e^{-3r^2/(2DN)}. \quad (2.21)$$

For the remainder of this section, we will assume that the end-points of the polymer are fixed at $\mathbf{0}$ and \mathbf{r} . To make the connection with thermodynamics, we may consider \mathbf{r} as a *macroscopic* state-variable, that can be realized by a number of different polymer configurations referred to as *microstates*. If no other constraints are known, it is plausible that each microstate is equally likely and, for large N , the number of microstates realizing a specific the macrostate \mathbf{r} is $\lambda^3 p(\mathbf{r})$, assuming the spatial resolution is of the order of the segment length λ . The corresponding microcanonical entropy is given by

$$S \simeq k_B \ln[\lambda^3 p(\mathbf{r})] = S_0 - k_B \frac{3r^2}{2DN}. \quad (2.22)$$

¹The vMF polymer model is equivalent to a classical Heisenberg spin model [Fis64].

To obtain a prediction for the mean force \mathbf{f} required to stretch the polymer by a small amount $d\mathbf{r}$, we can exploit the general thermodynamic relation

$$dE = \delta W + \delta Q, \quad (2.23a)$$

where work and heat increments are defined as usual by

$$\delta W = -\mathbf{f} \cdot d\mathbf{r}, \quad \delta Q = TdS, \quad (2.23b)$$

with T denoting temperature. If one neglect self-avoidance interactions, which are present in real polymers, the energy remains constant during a change of conformation, $dE = 0$. Hence,

$$dS = \frac{\mathbf{f}}{T} \cdot d\mathbf{r} \quad (2.24)$$

and the stretch force components are obtained as

$$f_i = T \left(\frac{\partial S}{\partial r_i} \right) = -\frac{3k_B T}{DN} r_i. \quad (2.25)$$

Thus far, our calculations implicitly assumed a microcanonical setting, since we focussed on an isolated polymer. In most experiments, polymers are surrounded by liquid molecules that may act as a canonical bath. If the polymer is sufficiently long (thermodynamic limit) and if the coupling between polymer and bath is sufficiently weak, then one can safely assume that microcanonical and canonical ensembles become equivalent. In this case, $-\mathbf{f}$ is the force needed to stretch a polymer in a solvent bath of temperature T .

Furthermore, it is also instructive to compute the corresponding free-energy

$$F := E - TS = E - TS_0 + k_B T \frac{3\mathbf{r}^2}{2DN}. \quad (2.26)$$

This is essentially a thermodynamic version of Hooke's law

$$F = F_0 + \frac{K}{2} \mathbf{r}^2, \quad K = \frac{3k_B T}{DN}. \quad (2.27)$$

For long stiff polymers we have $DN \simeq 2\lambda N L_P = 2LL_P$, we find for the spring-constant

$$K = \frac{3k_B T}{2LL_P}. \quad (2.28)$$

This means, for example, that the persistence length L_p can be inferred from force measurements if temperature T and polymer length L are known.

Self-avoidance (Flory's scaling argument)

The simplest way of accounting for self-avoidance is to include in Eq. (2.27) a free-energy contribution F_e that accounts for excluded volume effects. Consider a polymer consisting of $N \gg 1$ monomers of volume v_d with fixed end-to-end distance \mathbf{r} . Flory's scaling argument assumes that for a fixed $|\mathbf{r}|$, the N monomers may (very roughly) explore a volume of $|\mathbf{r}|^d$, where d is the space dimension. The overlap probability for a single monomer is given by the volume filling fraction $\phi = v_d N / |\mathbf{r}|^d$. Assuming short-range repulsion, so that F is extensive, we have for N particles

$$F_e \simeq N k_B T \phi = N k_B T \frac{v_d N}{|\mathbf{r}|^d}, \quad (2.29)$$

where $k_B T$ accounts for the thermal kinetic energy. Adding F_e to Eq. (2.27), we find in d dimensions

$$F = F_0 + N k_B T \left(\frac{v_d N}{|\mathbf{r}|^d} + \frac{|\mathbf{r}|^{2d}}{2D_d N^2} \right). \quad (2.30)$$

To obtain the equilibrium distance r_* , we must minimize this expression with respect to $r = |\mathbf{r}|$, which gives

$$0 = \frac{dF}{d|\mathbf{r}|} = -d \frac{v_d N}{r_*^{d+1}} + \frac{d}{D_d N^2} r_* \quad (2.31)$$

and therefore

$$r_* = (D_d v_d)^{1/d+2} N^{3/(d+2)}. \quad (2.32)$$

Thus, explicitly

$$d = 1 : \quad r_* \propto N \quad (2.33a)$$

$$d = 2 : \quad r_* \propto N^{3/4}, \quad (2.33b)$$

$$d = 3 : \quad r_* \propto N^{3/5}. \quad (2.33c)$$

The result is trivial for $d = 1$, seems to be exact for $d = 2$ when compared to simulations, and is very close to best numerical results $N^{0.589\dots}$ for $d = 3$.

2.2 Bead-spring model

To obtain a simple dynamical model for the motion of a polymer in a solvent fluid, we can consider a chain consisting of $\alpha = 1, \dots, N$ beads, representing monomers at positions $\mathbf{X}_\alpha(t)$. Neglecting inertial effects and hydrodynamic interactions, we may assume that the dynamics of a single bead is governed by the over-damped Langevin equation

$$d\mathbf{X}_\alpha(t) = -\nabla_{\mathbf{x}_\alpha} U(\{\mathbf{X}_\alpha\}) dt + \sqrt{2D} * d\mathbf{B}_\alpha(t), \quad (2.34)$$

where D is the thermal diffusion constant of a bead. The potential U contains contributions from elastic nearest neighbor interactions U_e , from bending U_b and, to implement self-avoidance, steric short-range repulsion U :

$$U = U_e + U_b + U_s \quad (2.35)$$

Defining $(N - 1)$ chain link vectors \mathbf{R}_α and their orientations $\boldsymbol{\mu}_\alpha$ by

$$\mathbf{R}_\alpha = \mathbf{X}_{\alpha+1} - \mathbf{X}_\alpha, \quad \boldsymbol{\mu}_\alpha = \frac{\mathbf{R}_\alpha}{\|\mathbf{R}_\alpha\|} \quad (2.36)$$

the potentials can be written as sums over 2-body and 3-body interactions

$$U_e = \sum_{\alpha=1}^{N-1} u(\|\mathbf{R}_\alpha\|), \quad (2.37a)$$

$$U_b = \sum_{\alpha=1}^{N-2} b(\boldsymbol{\mu}_\alpha \cdot \boldsymbol{\mu}_{\alpha+1}), \quad (2.37b)$$

$$U_s = \sum_{\alpha=1}^N \sum_{\beta=1, \beta \neq \alpha}^N s(\|\mathbf{X}_\alpha - \mathbf{X}_\beta\|). \quad (2.37c)$$

Specifically, the elastic spring potential $u(r)$ and the steric repulsion potential $s(r)$ encode 2-body interactions, whereas the bending potential $b(q)$ involves 3-body interactions.² Plausible choices are

$$u(r) = \frac{K}{2}(r - \lambda)^2, \quad b(q) = \frac{B}{2}(q - 1)^2, \quad s(r) = \frac{S e^{-r/\sigma}}{r^\nu} \quad (2.38)$$

for some $\nu > 1$. Although (2.34) can only be solved numerically, we know that the associated stationary equilibrium distribution is given by

$$p_N(\{\mathbf{x}_\alpha\}) = \frac{1}{Z_N} \exp\left[-\frac{U(\{\mathbf{X}_\alpha\})}{D}\right], \quad (2.39)$$

where

$$Z_N = \int \left(\prod_{\alpha=1}^N d^3x_\alpha \right) \exp\left[-\frac{U(\{\mathbf{x}_\alpha\})}{D}\right]. \quad (2.40)$$

²In principle, one could still include a potential contribution U_t that penalizes twisting, which would have to involve 4-bead interactions, for defining ‘twist’ requires three subsequent vectors $\{\boldsymbol{\mu}_{\alpha-1}, \boldsymbol{\mu}_\alpha, \boldsymbol{\mu}_{\alpha+1}\}$.

2.3 Continuum description

2.3.1 Differential geometry of curves

Consider a continuous curve $\mathbf{r}(t) \in \mathbb{R}^3$, where $t \in [0, T]$. Assume that the first three derivatives $\dot{\mathbf{r}}(t), \ddot{\mathbf{r}}(t), \dddot{\mathbf{r}}(t)$ are linearly independent. The length of the curve is given by

$$L = \int_0^T dt \|\dot{\mathbf{r}}(t)\| \quad (2.41)$$

where $\dot{\mathbf{r}}(t) = d\mathbf{r}/dt$ and $\|\cdot\|$ denotes the Euclidean norm. The local unit tangent vector is defined by

$$\mathbf{t} = \frac{\dot{\mathbf{r}}}{\|\dot{\mathbf{r}}\|}. \quad (2.42)$$

The unit normal vector, or unit curvature vector, is

$$\mathbf{n} = \frac{(\mathbf{I} - \mathbf{t}\mathbf{t}) \cdot \ddot{\mathbf{r}}}{\|(\mathbf{I} - \mathbf{t}\mathbf{t}) \cdot \ddot{\mathbf{r}}\|}. \quad (2.43)$$

Unit tangent vector $\hat{\mathbf{t}}(t)$ and unit normal vector $\hat{\mathbf{n}}(t)$ span the *osculating* ('kissing') plane at point t . The unit binormal vector is defined by

$$\mathbf{b} = \frac{(\mathbf{I} - \mathbf{t}\mathbf{t}) \cdot (\mathbf{I} - \mathbf{n}\mathbf{n}) \cdot \ddot{\mathbf{r}}}{\|(\mathbf{I} - \mathbf{t}\mathbf{t}) \cdot (\mathbf{I} - \mathbf{n}\mathbf{n}) \cdot \ddot{\mathbf{r}}\|}. \quad (2.44)$$

The orthonormal basis $\{\mathbf{t}(t), \mathbf{n}(t), \mathbf{b}(t)\}$ spans the local Frenet frame. For *plane* curves, $\ddot{\mathbf{r}}(t)$ is not linearly independent of $\dot{\mathbf{r}}$ and $\ddot{\mathbf{r}}$. In this case, we set $\mathbf{b} = \mathbf{t} \wedge \mathbf{n}$.

The local curvature $\kappa(t)$ and the associated radius of curvature $\rho(t) = 1/\kappa$ are defined by

$$\kappa(t) = \frac{\dot{\mathbf{t}} \cdot \mathbf{n}}{\|\dot{\mathbf{r}}\|}, \quad (2.45)$$

and the local torsion $\tau(t)$ by

$$\tau(t) = \frac{\dot{\mathbf{n}} \cdot \mathbf{b}}{\|\dot{\mathbf{r}}\|}. \quad (2.46)$$

For plane curves with constant \mathbf{b} , we have $\tau = 0$.

Given $\|\dot{\mathbf{r}}\|$, $\kappa(t)$, $\tau(t)$ and the initial values $\{\mathbf{t}(0), \mathbf{n}(0), \mathbf{b}(0)\}$, the Frenet frames along the curve can be obtained by solving the Frenet-Serret system

$$\frac{1}{\|\dot{\mathbf{r}}\|} \begin{pmatrix} \dot{\mathbf{t}} \\ \dot{\mathbf{n}} \\ \dot{\mathbf{b}} \end{pmatrix} = \begin{pmatrix} 0 & \kappa & 0 \\ -\kappa & 0 & \tau \\ 0 & -\tau & 0 \end{pmatrix} \begin{pmatrix} \mathbf{t} \\ \mathbf{n} \\ \mathbf{b} \end{pmatrix}. \quad (2.47a)$$

The above formulas simplify if t is the arc length, for in this case $\|\dot{\mathbf{r}}\| = 1$.

2.3.2 Stretchable polymers: Minimal model and equipartition

As a simple example, consider a polymer confined in a plane. Assume the polymer's endpoints are fixed at $(x, y) = (0, 0)$ and $(x, y) = (0, L)$, respectively, and that the ground-state configuration corresponds to a straight line connecting these two points. Denoting the tension³ by γ , adopting the parameterization $y = h(x)$ for the polymer and assuming that the bending energy is negligible, the energy relative to the ground-state is given by

$$E = \gamma \left[\int_0^L dx \sqrt{1 + h_x^2} - L \right], \quad (2.48)$$

where $h_x = h'(x)$. Restricting ourselves to small deformations, $|h_x| \ll 1$, we may approximate

$$E \simeq \frac{\gamma}{2} \int_0^L dx h_x^2. \quad (2.49)$$

Taking into account that $h(0) = h(L) = 0$, we may represent $h(x)$ and its derivative through the Fourier-sine series

$$h(x) = \sum_{n=1}^{\infty} A_n \sin\left(\frac{n\pi x}{L}\right) \quad (2.50a)$$

$$h_x(x) = \sum_{n=1}^{\infty} A_n \frac{n\pi}{L} \cos\left(\frac{n\pi x}{L}\right). \quad (2.50b)$$

Exploiting orthogonality

$$\int_0^L dx \sin\left(\frac{n\pi x}{L}\right) \sin\left(\frac{m\pi x}{L}\right) = \frac{L}{2} \delta_{nm} \quad (2.51)$$

we may rewrite the energy (2.49) as

$$\begin{aligned} E &\simeq \frac{\gamma}{2} \sum_n \sum_m \int_0^L dx A_n A_m \left(\frac{n\pi}{L}\right) \left(\frac{m\pi}{L}\right) \cos\left(\frac{n\pi x}{L}\right) \cos\left(\frac{m\pi x}{L}\right) \\ &= \frac{\gamma}{2} \sum_n \sum_m A_n A_m \left(\frac{n\pi}{L}\right) \left(\frac{m\pi}{L}\right) \frac{L}{2} \delta_{nm} \\ &= \sum_{n=1}^{\infty} E_n, \end{aligned} \quad (2.52a)$$

where the energy E_n stored in Fourier mode n is

$$E_n = A_n^2 \left(\frac{\gamma n^2 \pi^2}{4L}\right). \quad (2.52b)$$

³ γ carries units of energy/length.

Now assume the polymer is coupled to a bath and the stationary distribution is canonical

$$\begin{aligned} p(\{A_n\}) &= \frac{1}{Z} \exp(-\beta E) \\ &= \frac{1}{Z} \exp\left[-\beta \sum_{n=1}^{\infty} A_n^2 \left(\frac{\gamma n^2 \pi^2}{4L}\right)\right] \end{aligned} \quad (2.53)$$

with $\beta = (k_B T)^{-1}$. The PDF factorizes and, therefore, also the normalization constant

$$Z = \prod_{i=1}^{\infty} Z_n, \quad (2.54a)$$

where

$$Z_n = \int_{-\infty}^{\infty} dA_n \exp\left[-\beta A_n^2 \left(\frac{\gamma n^2 \pi^2}{4L}\right)\right] = \left(\frac{4\pi L}{\beta \gamma n^2 \pi^2}\right)^{1/2}. \quad (2.54b)$$

We thus find for the first to moments of A_n

$$\mathbb{E}[A_n] = 0 \quad (2.55a)$$

$$\mathbb{E}[A_n^2] = \frac{2k_B T L}{\gamma n^2 \pi^2}, \quad (2.55b)$$

and from this for the mean energy per mode

$$\mathbb{E}[E_n] = \left(\frac{\gamma n^2 \pi^2}{4L}\right) \mathbb{E}[A_n^2] = \frac{1}{2} k_B T. \quad (2.56)$$

That is, each mode absorbs the same amount of thermal energy, which is just a manifestation of the canonical equipartition theorem for harmonic degrees of freedom.

We may use the equipartition result to compute the variance of the polymer at the position $x \in [0, L]$

$$\begin{aligned} \mathbb{E}[h(x)^2] &:= \sum_{n=1}^{\infty} \sum_{m=1}^{\infty} \mathbb{E}[A_n A_m] \sin\left(\frac{n\pi x}{L}\right) \sin\left(\frac{m\pi x}{L}\right) \\ &= \sum_{n=1}^{\infty} \sum_{m=1}^{\infty} \mathbb{E}[A_n^2] \delta_{nm} \sin\left(\frac{n\pi x}{L}\right) \sin\left(\frac{m\pi x}{L}\right) \\ &= \left(\frac{2k_B T L}{\gamma \pi^2}\right) \sum_{n=1}^{\infty} \frac{\sin^2(n\pi x/L)}{n^2}. \end{aligned} \quad (2.57)$$

If we additionally average along x

$$\langle \mathbb{E}[h(x)^2] \rangle = \left(\frac{k_B T L}{\gamma \pi^2}\right) \sum_{n=1}^{\infty} \frac{1}{n^2} = \left(\frac{k_B T L}{\gamma \pi^2}\right) \frac{\pi^2}{6} = \frac{k_B T L}{6\gamma}. \quad (2.58)$$

Thus, by measuring fluctuations along the polymer we may infer γ .

2.3.3 Rigid polymers: Euler-Bernoulli equation

Consider a rigid polymer whose motion is confined to the (x, y) -plane, with one end fixed at $(x, y) = (0, 0)$ and the other moving freely. As before, we adopt the parameterization $h(x)$ and assume that the energy can be expressed in terms of fundamental geometric properties. At zero-temperature and in the absence of other forces, the groundstate of the polymer is a straight configuration along the positive the x -axis, i.e., $h_0(x) = 0, x \in [0, L]$.

Since one end of the polymer can move freely, tension is negligible, and the main contribution to the polymers energy comes from curvature κ ,

$$E \simeq \frac{A}{2} \int_0^L dx \kappa^2, \quad (2.59)$$

where A is the bending modulus (units energy \times length). For plane curves $h(x)$, the curvature can be expressed as

$$\kappa = \frac{h_{xx}}{(1 + h_x^2)^{3/2}}. \quad (2.60)$$

Focussing on the limit of weak deformations, $h_x \ll 1$, we may approximate $\kappa \simeq h_{xx}$, and the energy simplifies to

$$E \simeq \frac{A}{2} \int_0^L dx (h_{xx})^2. \quad (2.61)$$

The exact form of the boundary conditions depend on how the polymer is attached to the plane $x = 0$. Assuming that polymer is rigidly anchored at an angle 90° , the boundary conditions at the fixed end at $x = 0$ are

$$h(0) = 0, \quad h_x(0) = 0. \quad (2.62a)$$

At the free end, we will consider flux conditions

$$h_{xx}(L) = 0, \quad h_{xxx}(L) = 0. \quad (2.62b)$$

Intuitively, because of $\kappa = h_{xx}$, these last two conditions mean that the polymer tries to maintain minimal absolute curvature at the free end. By means of the BCs (2.62) and two partial integrations, we may rewrite (2.61) as

$$\begin{aligned} E &\simeq \frac{A}{2} \left[h_x h_{xx} \Big|_0^L - \int_0^L dx h_x h_{xxx} \right] \\ &= \frac{A}{2} \left[- \int_0^L dx h_x h_{xxx} \right] \\ &= \frac{A}{2} \left[-h h_{xxx} \Big|_0^L + \int_0^L dx h h_{xxxx} \right] = \frac{A}{2} \left[\int_0^L dx h h_{xxxx} \right]. \end{aligned} \quad (2.63)$$

If the polymer is surrounded by a viscous solvent, an initial perturbation $h(0, x)$ will relax to the ground-state. Neglecting fluctuations due to thermal noise, the relaxation dynamics $h(t, x)$ will be of the over-damped form⁴

$$\eta h_t = -\frac{\delta E}{\delta h}, \quad (2.64)$$

where η is a damping constant, and the variational derivative is defined by

$$\frac{\delta E[h(x)]}{\delta h(y)} := \lim_{\epsilon \rightarrow 0} \frac{E[h(x) + \epsilon \delta(x - y)] - E[h(x)]}{\epsilon}. \quad (2.65)$$

Keeping terms up to order ϵ , we find for the energy functional (2.61)

$$\begin{aligned} E[h(x) + \epsilon \delta(x - y)] - E[h(x)] &= \frac{A}{2} \int_0^L dx [(h + \epsilon \delta)_{xx}(h + \epsilon \delta)_{xx} - (h_{xx})^2] \\ &= \frac{A}{2} \int_0^L dx [2\epsilon h_{xx} \delta_{xx} + \mathcal{O}(\epsilon^2)] \end{aligned}$$

Using the integral identity

$$g(x) \partial_x^n \delta(x - y) = (-1)^n \delta(x - y) \partial_x^n g(x) \quad (2.66)$$

for any smooth function g , one obtains

$$\frac{\delta E[h(x)]}{\delta h(y)} = A \int_0^L dx h_{xxxx}(x) \delta(x - y) = A h_{xxxx}(y), \quad (2.67)$$

so that Eq. (2.64) becomes a linear fourth-order equation

$$h_t = -\alpha h_{xxxx}, \quad \alpha = \frac{A}{\eta}. \quad (2.68)$$

Inserting the ansatz

$$h = e^{-t/\tau} \phi(x), \quad h_t = -\frac{1}{\tau} e^{-t/\tau} \phi, \quad h_{xxxx} = e^{-t/\tau} \phi_{xxxx}, \quad (2.69)$$

gives the eigenvalue problem

$$\frac{1}{\tau \alpha} \phi = \phi_{xxxx}. \quad (2.70)$$

for the one-dimensional biharmonic operator $(\partial_x^2)^2$, which has the general solution

$$\phi(x) = B_1 \cosh(x/\lambda) + B_2 \sinh(x/\lambda) + B_3 \cos(x/\lambda) + B_4 \sin(x/\lambda) \quad (2.71a)$$

⁴If inertia is important then one would need to term of the form μh_{tt} on the lhs. of Eq. (2.64).

where

$$\lambda = (\alpha\tau)^{1/4}. \quad (2.71b)$$

From the boundary conditions (2.62), we have

$$\begin{aligned} 0 &= B_1 + B_3 \\ 0 &= B_2 + B_4 \\ 0 &= B_1 \cosh(L/\lambda) + B_2 \sinh(L/\lambda) - B_3 \cos(L/\lambda) - B_4 \sin(L/\lambda) \\ 0 &= B_1 \sinh(L/\lambda) + B_2 \cosh(L/\lambda) + B_3 \sin(L/\lambda) - B_4 \cos(L/\lambda) \end{aligned}$$

Inserting the first two conditions into the last two, we obtain the linear system

$$0 = B_1[\cosh(L/\lambda) + \cos(L/\lambda)] + B_2[\sinh(L/\lambda) + \sin(L/\lambda)] \quad (2.73a)$$

$$0 = B_1[\sinh(L/\lambda) - \sin(L/\lambda)] + B_2[\cosh(L/\lambda) + \cos(L/\lambda)]. \quad (2.73b)$$

For nontrivial solutions to exist, we must have

$$0 = \det \begin{pmatrix} [\cosh(L/\lambda) + \cos(L/\lambda)] & [\sinh(L/\lambda) + \sin(L/\lambda)] \\ [\sinh(L/\lambda) - \sin(L/\lambda)] & [\cosh(L/\lambda) + \cos(L/\lambda)] \end{pmatrix} \quad (2.74)$$

which gives us the eigenvalue condition

$$0 = \cosh(L/\lambda) \cos(L/\lambda) + 1. \quad (2.75)$$

This equation has solutions for discrete values $\lambda_n > 0$ that can be computed numerically, and one finds for the first few eigenvalues

$$\frac{L}{2\lambda_n} = \{0.94, 2.35, 3.93, 5.50, \dots\}. \quad (2.76)$$

For comparison, for purely sinusoidal excitations of a harmonic string one would expect that $L/\lambda_n \propto n$. The full time-dependent solution can thus be written as

$$\begin{aligned} h(t, x) = \sum_{n=1}^{\infty} B_{1n} e^{-t/\tau_n} \left\{ \cosh(x/\lambda_n) - \cos(x/\lambda_n) + \right. \\ \left. \frac{\cos(L/\lambda_n) + \cosh(L/\lambda_n)}{\sin(L/\lambda_n) + \sinh(L/\lambda_n)} [\sin(x/\lambda_n) - \sinh(x/\lambda_n)] \right\}, \quad (2.77) \end{aligned}$$

where $\tau_n = \lambda_n^4/\alpha = \lambda_n^4\eta/A$, and the coefficients B_{1n} are determined by the initial condition.

To obtain an estimate for the energy per mode, let us consider the quasi-stationary limit, which can be formally defined by $\eta \rightarrow \infty$. In this case, we have the mode-expansion

$$\begin{aligned} h(x) = \sum_{n=1}^{\infty} B_{1n} \left\{ \cosh(x/\lambda_n) - \cos(x/\lambda_n) + \right. \\ \left. \frac{\cos(L/\lambda_n) + \cosh(L/\lambda_n)}{\sin(L/\lambda_n) + \sinh(L/\lambda_n)} [\sin(x/\lambda_n) - \sinh(x/\lambda_n)] \right\}. \quad (2.78) \end{aligned}$$

This expression can be inserted into (2.63), and after exploiting orthogonality of the bi-harmonic eigenfunctions

$$E \simeq \sum_{n=1} E_n, \quad E_n = \frac{A L}{2 \lambda_n^4} B_n^2, \quad (2.79)$$

i.e., the energy per mode is proportional to the square of the amplitude, just as in the stretching case discussed in Sec. 2.3.2. It is therefore possible to compute thermal expectation values exactly from Gaussian integrals. In particular, from equipartition

$$\mathbb{E}[E_n] = \frac{A L}{2 \lambda_n^4} \mathbb{E}[B_n^2] = \frac{1}{2} k_B T. \quad (2.80)$$

If we combine this with the (crude) harmonic approximation $\lambda_n \propto n$, then

$$\mathbb{E}[B_n^2] \propto \frac{k_B T}{n^4}, \quad (2.81)$$

whereas in the stretching case we had found that $\mathbb{E}[B_n^2] \propto k_B T/n^2$.

2.4 Problems (due Monday, April 11)

1. Implement the torsion-free bead-spring model from Sec. 2.2 in MATLAB.
 - (a) Explain your choice of the discretization time-step.
 - (b) Compute, for suitable parameter choices/combinations, the orientation correlation functions and the mean squared end-to-end distance.
 - (c) How do your results compare with the theoretical predictions (2.33)?

Chapter 3

Membranes

The discussion in this section builds on the review article [Sei97] and the textbook [OLXY99].

3.1 Reminder: 2D differential geometry

We consider an orientable surface in \mathbb{R}^3 . Possible local parameterizations are

$$\mathbf{F}(s_1, s_2) \in \mathbb{R}^3 \quad (3.1)$$

where $(s_1, s_2) \in U \subseteq \mathbb{R}^2$. Alternatively, if one chooses Cartesian coordinates $(s_1, s_2) = (x, y)$, then it suffices to specify

$$z = f(x, y) \quad (3.2a)$$

or, equivalently, the implicit representation

$$\Phi(x, y, z) = z - f(x, y). \quad (3.2b)$$

The vector representation (3.1) can be related to the ‘height’ representation (3.2a) by

$$\mathbf{F}(x, y) = \begin{pmatrix} x \\ y \\ f(x, y) \end{pmatrix} \quad (3.3)$$

Denoting derivatives by $\mathbf{F}_i = \partial_{s_i} \mathbf{F}$, we introduce the surface metric tensor $g = (g_{ij})$ by

$$g_{ij} = \mathbf{F}_i \cdot \mathbf{F}_j, \quad (3.4a)$$

abbreviate its determinant by

$$|g| := \det g, \quad (3.4b)$$

and define the associated Laplace-Beltrami operator ∇^2 by

$$\nabla^2 h = \frac{1}{\sqrt{|g|}} \partial_i (g_{ij}^{-1} \sqrt{|g|} \partial_j h), \quad (3.4c)$$

for some function $h(s_1, s_2)$. For the Cartesian parameterization (3.3), one finds explicitly

$$\mathbf{F}_x(x, y) = \begin{pmatrix} 1 \\ 0 \\ f_x \end{pmatrix}, \quad \mathbf{F}_y(x, y) = \begin{pmatrix} 0 \\ 1 \\ f_y \end{pmatrix} \quad (3.5)$$

and, hence, the metric tensor

$$g = (g_{ij}) = \begin{pmatrix} \mathbf{F}_x \cdot \mathbf{F}_x & \mathbf{F}_x \cdot \mathbf{F}_y \\ \mathbf{F}_y \cdot \mathbf{F}_x & \mathbf{F}_y \cdot \mathbf{F}_y \end{pmatrix} = \begin{pmatrix} 1 + f_x^2 & f_x f_y \\ f_y f_x & 1 + f_y^2 \end{pmatrix} \quad (3.6a)$$

and its determinant

$$|g| = 1 + f_x^2 + f_y^2, \quad (3.6b)$$

where $f_x = \partial_x f$ and $f_y = \partial_y f$. For later use, we still note that the inverse of the metric tensor is given by

$$g^{-1} = (g_{ij}^{-1}) = \frac{1}{1 + f_x^2 + f_y^2} \begin{pmatrix} 1 + f_y^2 & -f_x f_y \\ -f_y f_x & 1 + f_x^2 \end{pmatrix}. \quad (3.6c)$$

Assuming the surface is regular at (s_1, s_2) , which just means that the tangent vectors \mathbf{F}_1 and \mathbf{F}_2 are linearly independent, the local unit normal vector is defined by

$$\mathbf{N} = \frac{\mathbf{F}_1 \wedge \mathbf{F}_2}{\|\mathbf{F}_1 \wedge \mathbf{F}_2\|}. \quad (3.7)$$

In terms of the Cartesian parameterization, this can also be rewritten as

$$\mathbf{N} = \frac{\nabla \Phi}{\|\nabla \Phi\|} = \frac{1}{\sqrt{1 + f_x^2 + f_y^2}} \begin{pmatrix} -f_x \\ -f_y \\ 1 \end{pmatrix}. \quad (3.8)$$

Here, we have adopted the convention that $\{\mathbf{F}_1, \mathbf{F}_2, \mathbf{N}\}$ form a right-handed system.

To formulate ‘geometric’ energy functionals for membranes, we still require the concept of curvature, which quantifies the local bending of the membrane. We define a 2×2 -curvature tensor $R = (R_{ij})$ by

$$R_{ij} = \mathbf{N} \cdot (\mathbf{F}_{ij}) \quad (3.9)$$

and local *mean curvature* H and local *Gauss curvature* K by

$$H = \frac{1}{2} \text{tr}(g^{-1} \cdot R), \quad K = \det(g^{-1} \cdot R). \quad (3.10)$$

Adopting the Cartesian representation (3.2a), we have

$$\mathbf{F}_{xx} = \begin{pmatrix} 0 \\ 0 \\ f_{xx} \end{pmatrix}, \quad \mathbf{F}_{xy} = \mathbf{F}_{yx} = \begin{pmatrix} 0 \\ 0 \\ f_{xy} \end{pmatrix}, \quad \mathbf{F}_{yy} = \begin{pmatrix} 0 \\ 0 \\ f_{yy} \end{pmatrix} \quad (3.11a)$$

yielding the curvature tensor

$$(R_{ij}) = \begin{pmatrix} \mathbf{N} \cdot \mathbf{F}_{xx} & \mathbf{N} \cdot \mathbf{F}_{xy} \\ \mathbf{N} \cdot \mathbf{F}_{yx} & \mathbf{N} \cdot \mathbf{F}_{yy} \end{pmatrix} = \frac{1}{\sqrt{1 + f_x^2 + f_y^2}} \begin{pmatrix} f_{xx} & f_{xy} \\ f_{yx} & f_{yy} \end{pmatrix} \quad (3.11b)$$

Denoting the eigenvalues of the matrix $g^{-1} \cdot R$ by κ_1 and κ_2 , we obtain for the mean curvature

$$H = \frac{1}{2}(\kappa_1 + \kappa_2) = \frac{(1 + f_y^2)f_{xx} - 2f_x f_y f_{xy} + (1 + f_x^2)f_{yy}}{2(1 + f_x^2 + f_y^2)^{3/2}} \quad (3.12)$$

and for the Gauss curvature

$$K = \kappa_1 \cdot \kappa_2 = \frac{f_{xx}f_{yy} - f_{xy}^2}{(1 + f_x^2 + f_y^2)^2}. \quad (3.13)$$

An important result that relates curvature and topology is the Gauss-Bonnet theorem, which states that any compact two-dimensional Riemannian manifold M with smooth boundary ∂M , Gauss curvature K and geodesic curvature k_g of ∂M satisfies the integral equation

$$\int_M K dA + \oint_{\partial M} k_g ds = 2\pi \chi(M). \quad (3.14)$$

Here, dA is the area element on M , ds the line element along ∂M , and $\chi(M)$ the Euler characteristic of M . The latter is given by $\chi(M) = 2 - 2g$, where g is the *genus* (number of handles) of M . For example, the 2-sphere $M = \mathbb{S}^2$ has $g = 0$ handles and hence $\chi(\mathbb{S}^2) = 2$, whereas a two-dimensional torus $M = \mathbb{T}^2$ has $g = 1$ handle and therefore $\chi(\mathbb{T}^2) = 0$.

Equation (3.14) implies that, for any closed surface, the integral over K is always a constant. That is, for closed membranes, the first integral in Eq. (3.14) represents just a trivial (constant) energetic contribution.

3.2 Minimal surfaces

Minimal surfaces are surfaces that minimize the area within a given contour ∂M ,

$$A(M|\partial M) = \int_M dA = \min! \quad (3.15)$$

Assuming a Cartesian parameterization $z = f(x, y)$ and abbreviating $f_i = \partial_i f$ as before, we have

$$dA = \sqrt{|g|} dx dy = \sqrt{1 + f_x^2 + f_y^2} dx dy =: \mathcal{L} dx dy, \quad (3.16)$$

and the minimum condition (3.15) can be expressed in terms of the Euler-Lagrange equations

$$0 = \frac{\delta A}{\delta f} = -\partial_i \frac{\partial \mathcal{L}}{\partial f_i}. \quad (3.17)$$

Inserting the Lagrangian $\mathcal{L} = \sqrt{|g|}$, one finds

$$0 = - \left[\partial_x \left(\frac{f_x}{\sqrt{1 + f_x^2 + f_y^2}} \right) + \partial_y \left(\frac{f_y}{\sqrt{1 + f_x^2 + f_y^2}} \right) \right] \quad (3.18)$$

which may be recast in the form

$$0 = \frac{(1 + f_y^2)f_{xx} - 2f_x f_y f_{xy} + (1 + f_x^2)f_{yy}}{(1 + f_x^2 + f_y^2)^{3/2}} = -2H. \quad (3.19)$$

Thus, minimal surfaces satisfy

$$H = 0 \quad \Leftrightarrow \quad \kappa_1 = -\kappa_2, \quad (3.20)$$

implying that each point of a minimal surface is a saddle point.

3.3 Thermal excitations of almost flat membranes

Assuming that a quasi-infinite membrane prefers a flat configuration, we postulate the energy functional

$$E = \int dA f_c, \quad f_c = \frac{k_c}{2}(2H)^2. \quad (3.21a)$$

The constant k_c is the bending rigidity and carries dimensions of energy. For an almost planar membrane with $|f_x|, |f_y| \ll 1$, we may approximate

$$2H \simeq f_{xx} + f_{yy}, \quad (3.22)$$

which gives to leading order for the energy

$$E \simeq \frac{k_c}{2} \int dx dy (f_{xx} + f_{yy})^2. \quad (3.23)$$

Similar to our earlier discussion of polymers, we would like to express the energy in terms of contributions from elementary excitations. To this end, we abbreviate $\mathbf{x} = (x, y)$ and consider the Fourier ansatz

$$f(\mathbf{x}) = \int \frac{d^2 q}{(2\pi)^2} \hat{f}_{\mathbf{q}} \exp(i\mathbf{q} \cdot \mathbf{x}), \quad (3.24)$$

demanding $\hat{f}_{-\mathbf{q}} = \hat{f}_{\mathbf{q}}^*$ to ensure real-valued solutions. Inserting the Fourier expansion into (3.23) gives

$$\begin{aligned}
E &\simeq \frac{k_c}{2} \int \frac{d^2q}{(2\pi)^2} \int \frac{d^2q'}{(2\pi)^2} \int dx dy (i\mathbf{q})^2 (i\mathbf{q}')^2 \hat{f}_{\mathbf{q}} \hat{f}_{\mathbf{q}'} \exp[i(\mathbf{q} + \mathbf{q}') \cdot \mathbf{x}] \\
&= \frac{k_c}{2} \int \frac{d^2q}{(2\pi)^2} \int d^2q' (\mathbf{q}^2) (\mathbf{q}'^2) \hat{f}_{\mathbf{q}} \hat{f}_{\mathbf{q}'} \delta(\mathbf{q} + \mathbf{q}') \\
&= \frac{k_c}{2} \int \frac{d^2q}{(2\pi)^2} |\mathbf{q}|^4 \hat{f}_{\mathbf{q}} \hat{f}_{-\mathbf{q}} \\
&= \frac{k_c}{2} \int \frac{d^2q}{(2\pi)^2} |\mathbf{q}|^4 \hat{f}_{\mathbf{q}} \hat{f}_{\mathbf{q}}^*.
\end{aligned} \tag{3.25}$$

We see that each bending mode contributes an energy $E(\mathbf{q}) \propto |\mathbf{q}|^4$ to the total bending energy, in agreement with our results for the bending of rigid polymers. Using standard Gaussian path integral formulas, we can compute the thermal correlation function¹

$$\begin{aligned}
\langle \hat{f}_{\mathbf{q}} \hat{f}_{\mathbf{q}'}^* \rangle &= \int D\hat{f} \hat{f}_{\mathbf{q}} \hat{f}_{\mathbf{q}'}^* \frac{e^{-\beta E}}{Z} \\
&= \frac{1}{Z} \int D\hat{f} \hat{f}_{\mathbf{q}} \hat{f}_{\mathbf{q}'}^* e^{-\beta \frac{k_c}{2(2\pi)^2} \int d^2q d^2q' \delta(\mathbf{q} - \mathbf{q}') |\mathbf{q}|^4 \hat{f}_{\mathbf{q}} \hat{f}_{\mathbf{q}'}^*} \\
&= \frac{k_B T}{k_c |\mathbf{q}|^4} (2\pi)^2 \delta(\mathbf{q} - \mathbf{q}').
\end{aligned} \tag{3.27}$$

This result can be used to calculate the thermal mean squared deviations of the derivatives

$$\begin{aligned}
\langle f_x^2 + f_y^2 \rangle &= - \int \frac{d^2q}{(2\pi)^2} \int \frac{d^2q'}{(2\pi)^2} (\mathbf{q} \cdot \mathbf{q}') \langle \hat{f}_{\mathbf{q}} \hat{f}_{\mathbf{q}'}^* \rangle \\
&= - \int \frac{d^2q}{(2\pi)^2} \int \frac{d^2q'}{(2\pi)^2} (\mathbf{q} \cdot \mathbf{q}') \frac{k_B T}{k_c |\mathbf{q}|^4} (2\pi)^2 \delta(\mathbf{q} - \mathbf{q}') \\
&= \int \frac{d^2q}{(2\pi)^2} \frac{k_B T}{k_c |\mathbf{q}|^2} \\
&= \int \frac{d|\mathbf{q}|}{2\pi} \frac{k_B T}{k_c |\mathbf{q}|},
\end{aligned} \tag{3.28}$$

¹Recall that for a d -dimensional Gaussian integral with positive-definite diagonal matrix $A = \text{diag}(A_{11}, \dots, A_{dd}) = (A_{ii} \delta_{ij})$

$$\int d^d x \left(\frac{\det A}{2\pi} \right)^{1/2} e^{-\frac{1}{2} \mathbf{x} \cdot A \cdot \mathbf{x}} = 1 \tag{3.26a}$$

$$\int d^d x \left(\frac{\det A}{2\pi} \right)^{1/2} e^{-\frac{1}{2} \mathbf{x} \cdot A \cdot \mathbf{x}} x_i x_j = \frac{\delta_{ij}}{A_{ii}}. \tag{3.26b}$$

Eq. (3.27) is the infinite-dimensional generalization of this relation, obtained by rewriting the complex path integral in terms of real and imaginary part and by noting that $\int d\mathbf{q}' \delta(\mathbf{q} - \mathbf{q}') \delta(\mathbf{q}' - \mathbf{q}'') = \delta(\mathbf{q} - \mathbf{q}'')$, hence $\delta^{-1} = \delta$ in this sense.

where we have transformed to polar coordinates in the last step. To obtain a meaningful result, we need to specific upper and lower bounds for the $|\mathbf{q}|$ -range. These bounds are provided naturally by the molecular length scale a and the linear extension $L \gg a$ of the membrane, yielding

$$\langle f_x^2 + f_y^2 \rangle = \frac{k_B T}{2\pi k_c} \int_{(2\pi)/L}^{(2\pi)/a} \frac{d|\mathbf{q}|}{|\mathbf{q}|} = \frac{k_B T}{2\pi k_c} \ln(L/a). \quad (3.29)$$

Recalling our initial assumption $|f_x|, |f_y| \ll 1$, we see that the notion of planar membrane is only meaningful as long as $\langle f_x^2 + f_y^2 \rangle \ll 1$, or equivalently if

$$L \ll L_P = a e^{2\pi k_c / (k_B T)}, \quad (3.30)$$

where L_P is the persistence length, defined by the condition $\langle f_x^2 + f_y^2 \rangle = 1$.

3.4 Helfrich's model

Assuming that lipid bilayer membranes can be viewed as two-dimensional surfaces, Helfrich [Hel73] proposed in 1973 the following geometric curvature energy per unit area for a closed membrane

$$f_c = \frac{k_c}{2} (2H - c_0)^2 + k_G K, \quad (3.31)$$

where constants k_c, k_G are bending rigidities and c_0 is the spontaneous curvature of the membrane. The full free energy for a closed membrane can then be written as

$$F_c = \int dA f_c + \sigma \int dA + \Delta p \int dV, \quad (3.32)$$

where σ is the surface tension and Δp the osmotic pressure (outer pressure minus inner pressure). Minimizing F with respect to the surface shape, one finds after some heroic manipulations the shape equation²

$$\Delta p - 2\sigma H + k_c(2H - c_0)(2H^2 + c_0 H - 2K) + k_c \nabla^2(2H - c_0) = 0, \quad (3.33)$$

where ∇^2 is the Laplace-Beltrami operator on the surface. The derivation of Eq. (3.33) uses our earlier result

$$\frac{\delta A}{\delta f} = -2H, \quad (3.34)$$

and the fact that the volume integral may be rewritten as³

$$V = \int dV = \int dA \frac{1}{3} \mathbf{F} \cdot \mathbf{N}, \quad (3.35)$$

²The full derivation can be found in Chapter 3 of Ref. [OLXY99].

³Here, we made use of the volume formula $dV = \frac{1}{3} h dA$ for a cone or pyramid of height $h = \mathbf{F} \cdot \mathbf{N}$.

which gives

$$\frac{\delta V}{\delta f} = 1. \quad (3.36)$$

For open membranes with boundary ∂M , a plausible energy functional is given by

$$F_o = \int dA f_c + \sigma \int dA + \gamma \oint_{\partial M} ds, \quad (3.37)$$

where γ is the line tension of the boundary. In this case, variation yields not only the corresponding shape equation but also a non-trivial set of boundary conditions.

Chapter 4

Pattern formation

4.1 Warm-up

Consider a scalar density $\rho(t, x)$, governed by the simple diffusion equation

$$\rho_t = D\rho_{xx} \tag{4.1a}$$

with reflecting boundary conditions on $[0, L]$,

$$\rho_x(t, 0) = \rho_x(t, L) = 0. \tag{4.1b}$$

This dynamics defined by Eqs. (4.1) conserves the total ‘mass’

$$M(t) = \int_0^L dx \rho(t, x) \equiv M_0, \tag{4.2}$$

and a spatially homogeneous stationary solution is given by

$$\rho_0 = M_0/L. \tag{4.3}$$

To evaluate its stability, we can consider wave-like perturbations

$$\rho(t, x) = \rho_0 + \delta\rho(t, x), \quad \delta\rho = \epsilon e^{\sigma t - ikx}. \tag{4.4}$$

Inserting this perturbation ansatz into (4.1) gives

$$\sigma(k) = -Dk^2 \geq 0 \tag{4.5}$$

signaling that ρ_0 is a stable solution, because all modes with $|k| > 0$ become exponentially damped.

4.2 Swift-Hohenberg model

As a simple generalization of (4.1), we consider the simplest isotropic fourth-order model [DHBG13] for a non-conserved scalar or pseudo-scalar order-parameter $\psi(t, \mathbf{x})$, given by

$$\partial_t \psi = F(\psi) + \gamma_0 \Delta \psi - \gamma_2 \Delta^2 \psi, \quad (4.6)$$

where $\partial_t = \partial/\partial t$ denotes the time derivative, and $\Delta = \nabla^2$ is the d -dimensional Laplacian. The force F is derived from a Landau-potential $U(\psi)$

$$F = -\frac{\partial U}{\partial \psi}, \quad U(\psi) = \frac{a}{2}\psi^2 + \frac{b}{3}\psi^3 + \frac{c}{4}\psi^4, \quad (4.7)$$

where $c > 0$ to ensure stability.

The derivative terms on the rhs. of (4.6) can also be obtained by variational methods from a suitably defined energy functional,¹

$$\partial_t \psi = -\frac{\delta \mathcal{F}}{\delta \psi}, \quad (4.10)$$

where

$$\mathcal{F}[\psi] = \int d^d x \left[\frac{1}{2} \gamma_0 (\nabla \psi) \cdot (\nabla \psi) + \frac{1}{2} \gamma_2 (\Delta \psi)(\Delta \psi) + U(\psi) \right]. \quad (4.11)$$

In the context of active suspensions, ψ could, for example, quantify local energy fluctuations, local alignment, phase differences, or vorticity. In this case, the transport coefficients ($a, b, c, \gamma_1, \gamma_2$) in Equations (4.6) and (4.7) will contain passive contributions due to steric or other physical interactions as well as active motility-related contributions. In general, it is very challenging to derive the exact functional dependence between macroscopic transport coefficients and microscopic interaction and motility parameters for active non-equilibrium systems. With regard to practical applications, however, it is often sufficient to view transport coefficients as purely phenomenological parameters that can be determined by matching the solutions of continuum models, such as the one defined by Equations (4.6)

¹To see this, consider a functional \mathcal{F} that depends on some real-valued fields $\phi_k(x_1, \dots, x_d), k = 1, \dots, N$, and their first and second derivatives, and can be written as

$$\mathcal{F}[\phi] = \int d^d x F(\phi_k, \partial_i \phi_k, \partial_{ij} \phi_k), \quad (4.8)$$

where $\phi = (\phi_k)$ and $\partial_i = \partial/\partial x_i$, $\partial_{ij} = \partial^2/\partial x_i \partial x_j$. Assuming $F(\eta_k, \xi_{ik}, \zeta_{ijk})$ is a quadratic polynomial in ξ_{ik} and ζ_{ijk} , the functional derivative of \mathcal{F} with respect to ϕ_k is given by

$$\frac{\delta \mathcal{F}}{\delta \phi_k} = \frac{\partial F}{\partial \phi_k} - \partial_i \frac{\partial F}{\partial (\partial_i \phi_k)} + \partial_{ij} \frac{\partial F}{\partial (\partial_{ij} \phi_k)}, \quad (4.9)$$

with a summation convention for identical indices $i, j = 1, \dots, d$.

and (4.7), to experimental data. This is analogous to treating the viscosity in the classical Navier-Stokes equations as a phenomenological fit parameter. The actual predictive strength of a continuum model lies in the fact that, once the parameter values have been determined for a given set-up, the theory can be used to obtain predictions for how the system should behave in different geometries or under changes of the boundary conditions (externally imposed shear, etc.). In some cases, it may also be possible to deduce qualitative parameter dependencies from physical or biological considerations. For instance, if ψ describes vorticity or local angular momentum in an isolated active fluid, say a bacterial suspension, then transitions from $a > 0$ to $a < 0$ or $\gamma_0 > 0$ to $\gamma_0 < 0$, which both lead to non-zero flow patterns, must be connected to the microscopic self-swimming speed v_0 of the bacteria. Assuming a linear relation, this suggests that, to leading order, $a_0 = \delta - \alpha v_0$ where $\delta > 0$ is a passive damping contribution and $\alpha v_0 > 0$ the active part, and similarly for γ_0 . It may be worthwhile to stress at this point that higher-than-second-order spatial derivatives can also be present in passive systems, but their effects on the dynamics will usually be small as long as $\gamma_0 > 0$. If, however, physical or biological mechanisms can cause γ_0 to become negative, then higher-order damping terms, such as the γ_2 -term in (4.6), cannot be neglected any longer as they are essential for ensuring stability at large wave-numbers.²

4.2.1 Linear stability analysis

The fixed points of (4.6) are determined by the zeros of the force $F(\psi)$, corresponding to the minima of the potential U , yielding

$$\psi_0 = 0 \tag{4.13a}$$

²For completeness, one should also note that in the case of a conserved order-parameter field ϱ the field equations would either have to take the current-form $\partial_t \varrho = -\nabla \cdot \mathbf{J}(\varrho)$ or, alternatively, one can also implement conservation laws globally by means of Lagrange multipliers. To illustrate this briefly, let us consider a system that is confined to a finite spatial domain $\Omega \subset \mathbb{R}^d$ of volume

$$|\Omega| = \int_{\Omega} d^d x \tag{4.12}$$

and described by a density ϱ that is subject to a global ‘mass’ constraint

$$M = \int_{\Omega} d^d x \varrho = \text{const.}$$

Assuming the dynamics of ϱ is governed by an equation similar to (4.6), the Lagrange-multiplier approach yields the non-local equation

$$\begin{aligned} \partial_t \varrho &= F(\varrho) + \gamma_0 \Delta \varrho - \gamma_2 \Delta^2 \varrho - \lambda_1, \\ \lambda_1 &= \frac{1}{|\Omega|} \int_{\Omega} d^d x [F(\varrho) + \gamma_0 \Delta \varrho - \gamma_2 \Delta^2 \varrho]. \end{aligned}$$

and

$$\psi_{\pm} = -\frac{b}{2c} \pm \sqrt{\frac{b^2}{4c^2} - \frac{a}{c}}, \quad \text{if } b^2 > 4ac. \quad (4.13b)$$

Linearization of (4.6) near ψ_0 for small perturbations

$$\delta\psi = \epsilon_0 \exp(\sigma_0 t - i\mathbf{k} \cdot \mathbf{x}) \quad (4.14)$$

gives

$$\sigma_0(\mathbf{k}) = -(a + \gamma_0|\mathbf{k}|^2 + \gamma_2|\mathbf{k}|^4). \quad (4.15)$$

Similarly, one finds for

$$\psi = \psi_{\pm} + \epsilon_{\pm} \exp(\sigma_{\pm} t - i\mathbf{k} \cdot \mathbf{x}) \quad (4.16)$$

the dispersion relation

$$\sigma_{\pm}(\mathbf{k}) = -[-(2a + b\psi_{\pm}) + \gamma_0|\mathbf{k}|^2 + \gamma_2|\mathbf{k}|^4]. \quad (4.17)$$

In both cases, k -modes with $\sigma > 0$ are unstable. From Eqs. (4.15) and (4.17), we see immediately that $\gamma_2 > 0$ is required to ensure small-wavelength stability of the theory and, furthermore, that non-trivial dynamics can be expected if a and/or γ_0 take negative values. In particular, all three fixed points can become simultaneously unstable if $\gamma_0 < 0$.

4.2.2 Symmetry breaking

With regard to microbial suspensions, the minimal model (4.6) is useful for illustrating how microscopic symmetry-breaking mechanisms that affect the motion of individual organisms or cells [DTM⁺05, LTT08, EKG10, DMCS12] can be implemented into macroscopic field equations. To demonstrate this, we interpret ψ as a vorticity-like 2D pseudo-scalar field that quantifies local angular momentum in a dense microbial suspension, assumed to be confined to a thin quasi-2D layer of fluid. If the confinement mechanism is top-bottom symmetric, as for example in a thin free-standing bacterial film [SAKG07], then one would expect that vortices of either handedness are equally likely. In this case, (4.6) must be invariant under $\psi \rightarrow -\psi$, implying that $U(\psi) = U(-\psi)$ and, therefore, $b = 0$ in (4.7). Intuitively, the transformation $\psi \rightarrow -\psi$ corresponds to a reflection of the observer position at the midplane of the film (watching the 2D layer from above *vs.* watching it from below).

The situation can be rather different, however, if we consider the dynamics of microorganisms close to a liquid-solid interface, such as the motion of bacteria or sperms cells in the vicinity of a glass slide (Fig. 4.2). In this case, it is known that the trajectory of a swimming cell can exhibit a preferred handedness [DTM⁺05, LTT08, EKG10, DMCS12]. For example, the bacteria *Escherichia coli* [DTM⁺05] and *Caulobacter* [LTT08] have been observed to swim in circles when confined near to a solid surface. More precisely, due to an

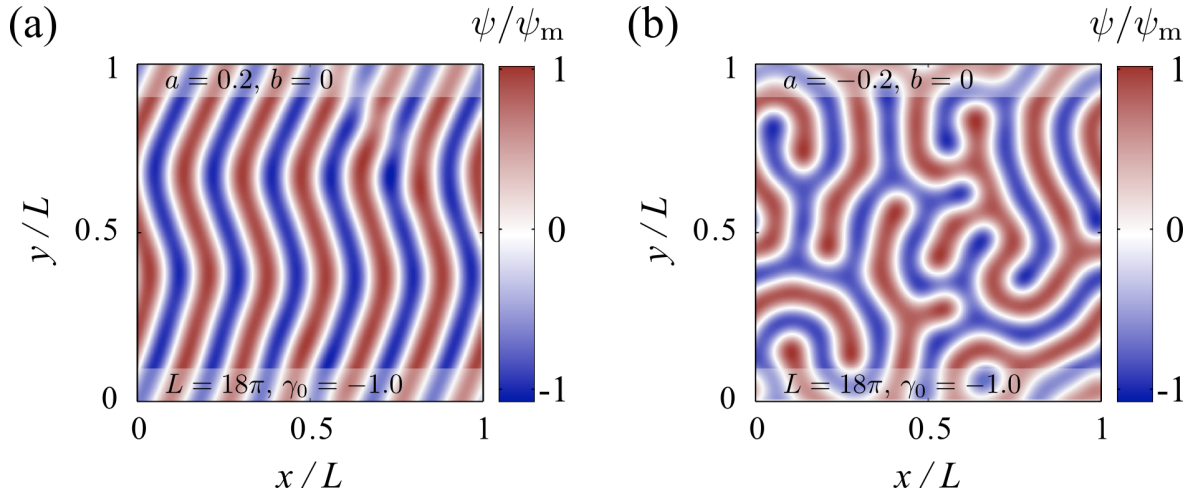


Figure 4.1: Numerical illustration of structural transitions in the order-parameter ψ for symmetric (a) mono-stable and (b) bi-stable potentials $U(\psi)$ with $b = 0$; for details see Ref. [DHBG13]. (c) Snapshots of the order-parameter field ψ at $t = 500$, scaled by the maximum value ψ_m , for a mono-stable potential $U(\psi)$ and homogeneous random initial conditions. (b) Snapshots of the order-parameter at $t = 500$ for a bi-stable potential. For $\gamma_0 \ll -(2\pi)^2\gamma_2/L^2$, increasingly more complex quasi-stationary structures arise; see References [AT06, POS97] for similar patterns in excited granular media and chemical reaction systems.

intrinsic chirality in their swimming apparatus, these organisms move on circular orbits in clockwise (anticlockwise) direction when viewed from inside the bulk fluid (glass surface). Qualitatively similar behavior has also been reported for sea urchin sperm swimming close to solid surfaces [Gib80].

Hence, for various types of swimming microorganisms, the presence of the near-by no-slip boundary breaks the reflection symmetry, $\psi \not\leftrightarrow -\psi$. The simplest way of accounting for this in a macroscopic continuum model is to adapt the potential $U(\psi)$ by permitting values $b \neq 0$ in (4.7). The result of a simulation with $b > 0$ is shown in Fig. 4.2a. In contrast to the symmetric case $b = 0$ (compare Fig. 4.1c), an asymmetric potential favors the formation of stable hexagonal patterns (Fig. 4.2a) – such self-assembled hexagonal vortex lattices have indeed been observed experimentally by Riedel *et al.* [RKH05] for highly concentrated spermatozoa of sea urchins (*Strongylocentrotus droebachiensis*) near a glass surface (Fig. 4.2b).³

³Note that although (4.6) can serve as a heuristic model for vortex formation it is not a conservation law, implying that angular momentum must be exchanged with a background medium and/or with the boundary.

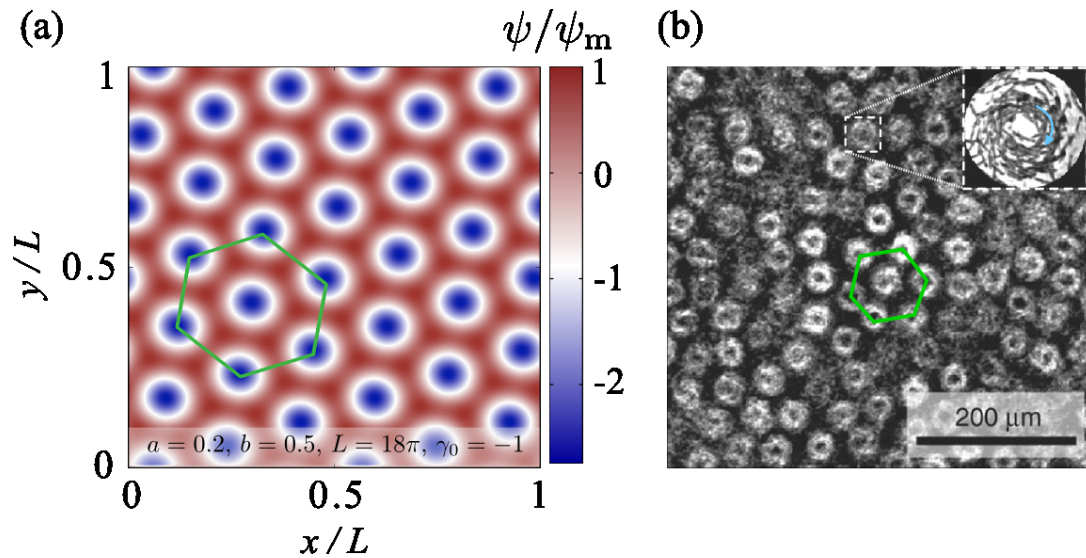


Figure 4.2: Effect of symmetry-breaking in the Swift-Hohenberg model. (a) Stationary hexagonal lattice of the pseudo-scalar angular momentum order-parameter ψ , scaled by the maximum value ψ_m , as obtained in simulations [DHBG13] of Eqs. (4.6) and (4.7) with $b > 0$, corresponding to a broken reflection symmetry $\psi \not\leftrightarrow -\psi$. Blue regions correspond to clockwise motions. (b) Hexagonal vortex lattice formed spermatozoa of sea urchins (*Strongylocentrotus droebachiensis*) near a glass surface [RKH05]. At high densities, the spermatozoa assemble into vortices that rotate in clockwise direction (inset) when viewed from the bulk fluid.

4.3 Vector model for an incompressible active fluid

We now generalize the preceding considerations to identify a minimal vector-field model for dense bacterial suspensions [WDH⁺12, DHD⁺13]. Popular continuum theories [Ram10, TTR05, TT98, Wol08, BM09, Ped10, SR02, SS08] of microbial fluids typically distinguish solvent concentration, bacterial density, solvent velocity, bacterial velocity, and various orientational order-parameter fields (polarization, \mathbf{Q} -tensors, etc.). Aiming to identify a minimal hydrodynamic model, we construct a simplified higher-order theory by focussing exclusively on the dynamics of the mean bacterial⁴ velocity field $\mathbf{v}(t, \mathbf{x})$ and restricting ourselves to the incompressible limit. By construction, the resulting \mathbf{v} -only theory, which is essentially a minimal Swift-Hohenberg-type [SH77] extension of the Toner-Tu model [TTR05, TT98], may not be applicable to swarming or flocking regimes, where density fluctuations are dominant, but it can provide a useful basis for quantitative comparisons with experiments and simulations on highly concentrated active suspensions [WDH⁺12, DHD⁺13]. Another assumption implicit to the vector model below is that the energy input, required to maintain non-zero velocity patterns, is quasi-stationary.

⁴Whilst the joint momentum of a bacteria-solvent mixture is conserved, the dynamics of the active (bacterial) component alone, as considered here, does not satisfy such a conservation law.

Relaxation of this assumption would imply the need for additional energy balance equations that account for spatial and temporal variations in the conversion of chemical into kinetic energy of motion. In other words, the \mathbf{v} -only theory formulated below only applies to situations where concentrations of nutrients, oxygen, etc. in a microbial suspension are approximately constant during the observation period. In practice, \mathbf{v} can be determined applying suitable coarse-graining procedures (PIV algorithms, local averaging, etc.) to discrete experimental or numerical velocity data [WDH⁺12, HGBH03].

4.3.1 Model equations

Postulating incompressibility, which is a good approximation for sufficiently dense suspensions [WDH⁺12],⁵

$$\nabla \cdot \mathbf{v} = \partial_i v_i = 0, \quad (4.18)$$

we assume that the dynamics of the bacterial mean velocity-field \mathbf{v} is governed by the generalized Navier-Stokes equation

$$(\partial_t + \mathbf{v} \cdot \nabla) \mathbf{v} = -\nabla p - (A + C|\mathbf{v}|^2) \mathbf{v} + \nabla \cdot \mathbf{E}. \quad (4.19)$$

The pressure $p(t, \mathbf{x})$ is the Lagrange multiplier for the incompressibility constraint. Similar to the scalar case, (4.7) above, the (A, C) -terms in Equation (4.19) represent a quartic Landau velocity potential [Ram10, TTR05, TT98]

$$U(\mathbf{v}) = \frac{A}{2} |\mathbf{v}|^2 + \frac{C}{4} |\mathbf{v}|^4. \quad (4.20)$$

Physically, the inclusion of a polar ordering potential accounts for the fact that microorganisms typically exhibit head-tail asymmetries that may favor polar alignment, as manifested in the ‘bionematic’ jets that form in bacterial suspensions [CCD⁺07, CKGG11]. For $A > 0$ and $C > 0$, the potential is mono-stable and the fluid is damped towards a disordered state with $\mathbf{v} = 0$. By contrast, for $A < 0$, (4.20) describes a d -dimensional mexican-hat (sombbrero) potential with fixed-points $|\mathbf{v}| = \sqrt{-A/C}$ corresponding to global polar order. However, the fact that polar ordering appears only locally but not globally in suspensions of swimming bacteria [DCC⁺04, CCD⁺07, CKGG11] suggests that other instability mechanisms must be at work [SR02]. To capture this mathematically, one must either introduce additional order parameters [Ram10, TTR05, TT98] or destabilize the theory by identifying a suitable phenomenological ansatz for the effective stresses [SH77].

Adopting the latter approach, we postulate that the components of the symmetric and traceless rate-of-strain \mathbf{E} tensor are given by

$$E_{ij} = \Gamma_0 (\partial_i v_j + \partial_j v_i) - \Gamma_2 \Delta (\partial_i v_j + \partial_j v_i) + S q_{ij}, \quad (4.21)$$

⁵We adopt a summation convention for equal indices throughout.

where

$$q_{ij} = v_i v_j - \frac{\delta_{ij}}{d} |\mathbf{v}|^2 \quad (4.22)$$

is a $d \times d$ -dimensional mean-field approximation to the \mathbf{Q} -tensor, representing active nematic stresses [SR02, BM08] due to swimming (δ_{ij} is the Kronecker tensor). Although the S -term does not affect the linear stability of the model, general hydrodynamic arguments [Ped10] imply that $S < 0$ for pusher-swimmers like *E. coli* [DDC⁺11] or *B. subtilis*, whereas $S > 0$ for puller-type microswimmers such as *Chlamydomonas* algae [DGM⁺10]. The Γ_0 -term in (4.21) is dictated by the requirement that the model contains the Navier-Stokes equations as a limit case, and the Γ_2 -damping term is motivated by generic stability considerations, as recent experiments [WDH⁺12, DHD⁺13] suggest that Γ_0 can become negative in dense bacterial suspensions. Inserting Equations (4.21) and (4.22) into (4.19), and defining

$$\lambda_0 = 1 - S, \quad \lambda_1 = -S/d, \quad (4.23)$$

we obtain

$$(\partial_t + \lambda_0 \mathbf{v} \cdot \nabla) \mathbf{v} = -\nabla p + \lambda_1 \nabla \mathbf{v}^2 - (A + C |\mathbf{v}|^2) \mathbf{v} + \Gamma_0 \Delta \mathbf{v} - \Gamma_2 \Delta^2 \mathbf{v}. \quad (4.24)$$

The standard Navier-Stokes equations for a passive fluid are recovered for $S = A = C = \Gamma_2 = 0$ and $\Gamma_0 > 0$.

For $\Gamma_0 > 0$ and $\Gamma_2 = 0$, (4.24) reduces to an incompressible version of the classical Toner-Tu model [Ram10, TTR05, TT98]. It is, however, the combination of the two Γ -terms with the non-variational convective derivative that turns out to be crucial for the formation of self-sustained quasi-chaotic flow patterns. The linear Γ -terms are reminiscent of the higher-order spatial derivatives in the classical Swift-Hohenberg theory [SH77], see (4.6), and (4.24) with $\Gamma_0 < 0$ and $\Gamma_2 > 0$ yields a simple – if not the simplest – generic continuum description of turbulent meso-scale instabilities observed in dense bacterial suspensions [WDH⁺12]. More generally, (4.24) can provide a satisfactory phenomenological model whenever interaction terms in more complex field theories, that lead to instabilities in the \mathbf{v} -field, can be effectively approximated by a fourth-order Taylor expansion in Fourier space. This is likely to be the case for a wide range of active systems. Phrased differently, the last two terms in (4.24) may be regarded as the Fourier-space analogue of the Toner-Tu driving terms, which correspond to a series expansion in terms of the order-parameter. Hence, similar to the higher-order gradient terms in the scalar theory from (4.6), the (Γ_0, Γ_2) -terms in (4.24) describe intermediate-range interactions, and their role in Fourier-space is similar to that of the Landau potential in velocity space.

4.3.2 Linear stability analysis

To support the qualitative statements in the preceding paragraph, we now perform a stability analysis for the 2D case, assuming $\Gamma_0 < 0$ and $C > 0, \Gamma_2 > 0$.

The fixed points of Equations (4.18) and (4.24) are given by the extrema of the quartic velocity potential $U(\mathbf{v})$. For arbitrary values of A , Equations (4.18) and (4.24) have a fixed point that corresponds to a disordered isotropic state $(\mathbf{v}, p) = (\mathbf{0}, p_0)$ where p_0 is a constant pressure. For $A < 0$, an additional class of fixed points arises, corresponding to a manifold of globally ordered polar states $(\mathbf{v}, p) = (\mathbf{v}_0, p_0)$, where \mathbf{v}_0 is constant vector with arbitrary orientation and fixed swimming speed $|\mathbf{v}_0| = \sqrt{-A/C} =: v_0$.

Linearizing Equations (4.18) and (4.24) for small velocity and pressure perturbations around the isotropic state, $\mathbf{v} = \epsilon$ and $p = p_0 + \eta$ with $|\eta| \ll |p_0|$, and considering perturbations of the form

$$(\eta, \epsilon) = (\hat{\eta}, \hat{\epsilon}) \exp(\sigma_0 t - i\mathbf{k} \cdot \mathbf{x}), \quad (4.25)$$

we find

$$0 = \mathbf{k} \cdot \hat{\epsilon}, \quad (4.26)$$

$$\sigma_0 \hat{\epsilon} = i\hat{\eta}\mathbf{k} - (A + \Gamma_0|\mathbf{k}|^2 + \Gamma_2|\mathbf{k}|^4)\hat{\epsilon}. \quad (4.27)$$

Multiplying the second equation by \mathbf{k} and using the incompressibility condition implies that $\hat{\eta} = 0$ and, therefore,

$$\sigma_0(\mathbf{k}) = - (A + \Gamma_0|\mathbf{k}|^2 + \Gamma_2|\mathbf{k}|^4). \quad (4.28)$$

Assuming $\Gamma_0 < 0$ and $\Gamma_2 > 0$, and provided that $4A < |\Gamma_0|^2/\Gamma_2$, we find an unstable band of modes with $\sigma_0(\mathbf{k}) > 0$ for $k_-^2 < |\mathbf{k}|^2 < k_+^2$, where

$$k_{\pm}^2 = \frac{|\Gamma_0|}{\Gamma_2} \left(\frac{1}{2} \pm \sqrt{\frac{1}{4} - \frac{A\Gamma_2}{|\Gamma_0|^2}} \right). \quad (4.29)$$

For $A < 0$ the isotropic state is generally unstable with respect to long-wavelength (i.e., small- $|\mathbf{k}|$) perturbations.

We next perform a similar analysis for the polar state (\mathbf{v}_0, p_0) , which is energetically preferred for $A < 0$ and corresponds to all active particles swimming in the same direction ('global order'). In this case, when considering small deviations

$$\mathbf{v} = \mathbf{v}_0 + \epsilon, \quad p = p_0 + \eta, \quad (4.30)$$

it is useful to distinguish perturbations perpendicular and parallel to \mathbf{v}_0 , by writing $\epsilon = \epsilon_{\parallel} + \epsilon_{\perp}$ where $\mathbf{v}_0 \cdot \epsilon_{\perp} = 0$ and $\mathbf{v}_0 \cdot \epsilon_{\parallel} = v_0 \epsilon_{\parallel}$. Without loss of generality, we may choose \mathbf{v}_0 to point along the x -axis, $\mathbf{v}_0 = v_0 \mathbf{e}_x$. Adopting this convention, we have $\epsilon_{\parallel} = (\epsilon_{\parallel}, 0)$ and $\epsilon_{\perp} = (0, \epsilon_{\perp})$, and to leading order

$$|\mathbf{v}|^2 \simeq v_0^2 + 2v_0 \epsilon_{\parallel}. \quad (4.31)$$

Linearization for exponential perturbations of the form

$$(\eta, \epsilon_{\parallel}, \epsilon_{\perp}) = (\hat{\eta}, \hat{\epsilon}_{\parallel}, \hat{\epsilon}_{\perp}) \exp(\sigma t - i\mathbf{k} \cdot \mathbf{x}) \quad (4.32)$$

yields

$$0 = \mathbf{k} \cdot \hat{\epsilon}, \quad (4.33a)$$

$$\sigma \hat{\epsilon} = i(\hat{\eta} - 2v_0\lambda_1\hat{\epsilon}_{\parallel})\mathbf{k} + \mathbf{M}\hat{\epsilon}, \quad (4.33b)$$

where

$$\mathbf{M} = \begin{pmatrix} 2A & 0 \\ 0 & 0 \end{pmatrix} - (\Gamma_0|\mathbf{k}|^2 + \Gamma_2|\mathbf{k}|^4 - i\lambda_0k_xv_0)\mathbf{I} \quad (4.34)$$

with $\mathbf{I} = (\delta_{ij})$ denoting the identity matrix. Multiplying Equation (4.33b) with $i\mathbf{k}$, and using the incompressibility condition (4.33a), gives

$$\hat{\eta} = 2v_0\lambda_1\hat{\epsilon}_{\parallel} + i\frac{\mathbf{k} \cdot (\mathbf{M}\hat{\epsilon})}{|\mathbf{k}|^2}. \quad (4.35)$$

Inserting this into Equation (4.33b) and defining $\mathbf{M}_{\perp} = \mathbf{\Pi}(\mathbf{k})\mathbf{M}$, where

$$\Pi_{ij}(\mathbf{k}) = \delta_{ij} - \frac{k_i k_j}{|\mathbf{k}|^2} \quad (4.36)$$

is the orthogonal projector of \mathbf{k} , we obtain

$$\sigma \hat{\epsilon} = \mathbf{M}_{\perp} \hat{\epsilon}. \quad (4.37)$$

The eigenvalue spectrum of the matrix \mathbf{M}_{\perp} is given by

$$\sigma(\mathbf{k}) \in \left\{ 0, i\lambda_0v_0k_x - \left(\Gamma_0|\mathbf{k}|^2 + \Gamma_2|\mathbf{k}|^4 - 2A\frac{k_x^2}{|\mathbf{k}|^2} \right) \right\}. \quad (4.38)$$

The zero eigenvalues correspond to the Goldstone modes. The non-zero eigenvalues have eigenvectors $(-k_y, k_x)$, implying that, for $\Gamma_0 < 0$, there will be a range of exponentially growing modes in the direction perpendicular to \mathbf{k} .

Equations (4.28) and (4.38) predict that, when $A < 0$ and $\Gamma_0 < 0$, isotropic and polar fixed points become simultaneously unstable, thereby signaling the existence of spatially inhomogeneous dynamic attractors. More generally, within the class of standard PDEs, the two Γ -terms in (4.24) appear to provide the simplest ‘linear way’ of obtaining a \mathbf{v} -only theory that exhibits non-trivial stationary dynamics. In principle, one could also try to model instabilities by combining odd or fractional powers of $|\mathbf{k}|$ in Equations (4.28) and (4.38); this would be analogous to replacing the quartic Landau potential by a more general function of $|\mathbf{v}|$. However, when considering eigenvalue spectra based on odd or non-integer powers of $|\mathbf{k}|$, the underlying dynamical equations in position space would become fractional PDEs. Such fractional models could potentially be useful for describing active suspensions with long-range or other types of more complex interactions.

4.4 Reaction-diffusion systems (RDSs)

RDSs constitute a class of generic mathematical models of structure formation, which can be represented in the form

$$\partial_t \mathbf{q}(t, \mathbf{x}) = D \nabla^2 \mathbf{q} + \mathbf{R}(\mathbf{q}), \quad (4.39)$$

where

- $\mathbf{q}(t, \mathbf{x})$ as an n -dimensional vector field describing the concentrations of n chemical substances, species etc.
- D is a *diagonal* $n \times n$ -diffusion matrix, and
- the n -dimensional vector $\mathbf{R}(\mathbf{q})$ accounts for all *local* reactions.

4.4.1 One-dimensional examples

Assuming $\mathbf{q}(t, \mathbf{x}) = u(t, x)$, the class of one-dimensional RDSs

$$u_t = D u_{xx} + R(u), \quad (4.40)$$

includes the following well-known models:

- (i) Fisher's equation [Fis30]

$$R(u) = \alpha u(u_0 - u), \quad \alpha > 0, u_0 > 0 \quad (4.41a)$$

originally proposed to describe the spreading of biological species.

- (ii) The Newell-Whitehead-Segel equation

$$R(u) = \beta u(u_0^2 - u^2), \quad \beta > 0, \quad (4.41b)$$

which provides an effective description of Rayleigh-Benard convection.

- (iii) The Zeldovich equation

$$R(u) = \beta u(u_0 - u)(u - a), \quad \beta > 0, u_0 > a > 0, \quad (4.41c)$$

which arises in combustion theory.

A rather generic feature of RDSs is that they admit wave-like solutions when complemented with suitable boundary conditions. As an example, consider the Fisher equation (4.41a), which after rescaling of (t, x, u) , can be rewritten as

$$u_t = u_{xx} + u(1 - u). \quad (4.42)$$

Looking for travelling wave solutions

$$u(t, x) = w(z), \quad z = x - ct, \quad (4.43a)$$

and using

$$u_t = \frac{dw}{dz} \frac{dz}{dt} = -cw', \quad u_x = \frac{dw}{dz} \frac{dz}{dx} = w', \quad u_{xx} = w'' \quad (4.43b)$$

we may rewrite (4.42) as

$$w'' + cw' + w(1 - w) = 0. \quad (4.44a)$$

One can show [AZ79] that, for every wave-speed $c \geq 2$, Eq. (4.44a) possesses solutions $w(z)$ that satisfy

$$\lim_{z \rightarrow -\infty} w(z) = 1, \quad \lim_{z \rightarrow +\infty} w(z) = 0. \quad (4.44b)$$

Note that these solutions interpolate between the two fixed points $u = 1$ and $u = 0$. No such solution exists for $c < 2$, and for $c \geq 2$ the exact shape of the wave depends on the value of c . Closed analytical solutions can be found for the particular value $c = 5/\sqrt{6}$; in this case [AZ79]

$$w(z) = \frac{1}{[1 + r \exp(z/\sqrt{6})]^2} \quad (4.44c)$$

for all $r > 0$.

4.4.2 Two species in one space dimension

As a slightly more complex case, let us now consider $\mathbf{q}(t, \mathbf{x}) = (u(t, x), v(t, x))$, $D = \text{diag}(D_u, D_v)$ and $\mathbf{R} = (F(u, v), G(u, v))$, then

$$u_t = D_u u_{xx} + F(u, v) \quad (4.45a)$$

$$v_t = D_v v_{xx} + G(u, v) \quad (4.45b)$$

In general, (F, G) can be derived from the reaction/reproduction kinetics, and conservation laws may impose restrictions on permissible functions (F, G) . The fixed points (u_*, v_*) of (4.45) are determined by the condition

$$\mathbf{R}(u_*, v_*) = \begin{pmatrix} F(u_*, v_*) \\ G(u_*, v_*) \end{pmatrix} = \mathbf{0}. \quad (4.46)$$

Expanding (4.45) for small plane-wave perturbations

$$\begin{pmatrix} u(t, x) \\ v(t, x) \end{pmatrix} = \begin{pmatrix} u_* \\ v_* \end{pmatrix} + \boldsymbol{\epsilon}(t, x) \quad (4.47a)$$

with

$$\boldsymbol{\epsilon} = \hat{\boldsymbol{\epsilon}} e^{\sigma t - ikx} = \begin{pmatrix} \hat{\epsilon} \\ \hat{\eta} \end{pmatrix} e^{\sigma t - ikx}, \quad (4.47b)$$

we find the linear equation

$$\sigma \hat{\boldsymbol{\epsilon}} = - \begin{pmatrix} k^2 D_u & 0 \\ 0 & k^2 D_v \end{pmatrix} \hat{\boldsymbol{\epsilon}} + \begin{pmatrix} F_u^* & F_v^* \\ G_u^* & G_v^* \end{pmatrix} \hat{\boldsymbol{\epsilon}} \equiv M \hat{\boldsymbol{\epsilon}}, \quad (4.48)$$

where

$$F_u^* = \partial_u F(u_*, v_*), \quad F_v^* = \partial_v F(u_*, v_*), \quad G_u^* = \partial_u G(u_*, v_*), \quad G_v^* = \partial_v G(u_*, v_*).$$

Solving this eigenvalue equation for σ , we obtain

$$\sigma_{\pm} = \frac{1}{2} \left\{ -(D_u + D_v)k^2 + (F_u^* + G_v^*) \pm \sqrt{4F_v^*G_u^* + [F_u^* - G_v^* + (D_v - D_u)k^2]^2} \right\}, \quad (4.49)$$

which gives

$$\det M = \sigma_+ \sigma_- = (F_u^* - D_u k^2)(G_v^* - D_v k^2) - F_v^* G_u^*, \quad (4.50a)$$

$$\text{tr } M = \sigma_+ + \sigma_- = F_u^* + G_v^* - (D_u + D_v)k^2. \quad (4.50b)$$

In order to have an instability for some finite value k , at least one of the two eigenvalues must have a positive real part. If the eigenvalues are real, this means that either the condition

$$\det M < 0, \quad (4.51a)$$

or the conditions

$$\det M > 0 \quad \wedge \quad \text{tr } M > 0 \quad (4.51b)$$

must be satisfied. These criteria can be easily tested for a given reaction kinetics (F, G) . We briefly summarize two popular examples.

Lotka-Volterra model This model describes a simple predator-prey dynamics, defined by

$$F(u, v) = Au - Buv, \quad (4.52a)$$

$$G(u, v) = -Cv + Euv \quad (4.52b)$$

with positive rate parameters $A, B, C, E > 0$. The field $u(t, x)$ measures the concentration of prey and $v(t, x)$ that of the predators. The model has two fixed points

$$(u_0, v_0) = (0, 0), \quad (u_*, v_*) = (C/E, A/B), \quad (4.53)$$

with Jacobians

$$\begin{pmatrix} F_u(u_0, v_0) & F_v(u_0, v_0) \\ G_u(u_0, v_0) & G_v(u_0, v_0) \end{pmatrix} = \begin{pmatrix} A & 0 \\ 0 & -C \end{pmatrix} \quad (4.54a)$$

and

$$\begin{pmatrix} F_u(u_*, v_*) & F_v(u_*, v_*) \\ G_u(u_*, v_*) & G_v(u_*, v_*) \end{pmatrix} = \begin{pmatrix} A - \frac{BC}{E} & -A \\ C & -C + \frac{AE}{B} \end{pmatrix}. \quad (4.54b)$$

It is straightforward to verify that, for suitable choices of A, B, C, D , the model exhibits a range of unstable k -modes.

FitzHugh-Nagumo model This model aims to describe the propagation of an action potential through nerve cells, and is defined by

$$F(u, v) = \lambda u - \mu u^3 - \eta v + \kappa, \quad (4.55a)$$

$$G(u, v) = \frac{1}{\tau}(u - \beta v) \quad (4.55b)$$

with positive parameters $\lambda, \mu, \tau, \eta, \beta$. The field $u(t, x)$ measures the membrane voltage, and $v(t, x)$ is a slower gate voltage that controls relaxation of u . The parameter κ represents external currents that cause an increase of u . Similar to the Lotka-Volterra model, the FitzHugh-Nagumo model exhibits a range of unstable k -modes for biologically relevant parameters choices.

Chapter 5

Microbial locomotion

Microswimmers are tiny devices (e.g., bacteria or eukaryotic cells) that achieve locomotion in a fluid through a self-induced change of shape. Biological examples are manifold: Some bacteria like *Escherichia coli* propel themselves by rotating helically shaped bundle of flagella, much like a corkscrew penetrating into a cork. Sperm cells move by inducing a wave-like deformation in a thin flagellum or cilium, whereas organisms move by beating two or more cilia in a synchronized manner (Fig. 5.1).

Because of their tiny size, the microswimmers operate at low Reynolds number, i.e., inertial and turbulent effects are negligible¹. In this regime, swimming mechanisms are very different from employed by humans and other animals. In particular, any microbial swimming strategy must involve time-irreversible motion. Whilst moving through the liquid, a swimmer modifies the flow of the surrounding liquid. This can lead to an effective hydrodynamic interactions between nearby organisms, which can be attractive or repulsive depending on the details of the swimming mechanism. However, such deterministic forces are usually perturbed by a considerable amount of thermal or intrinsic noise.

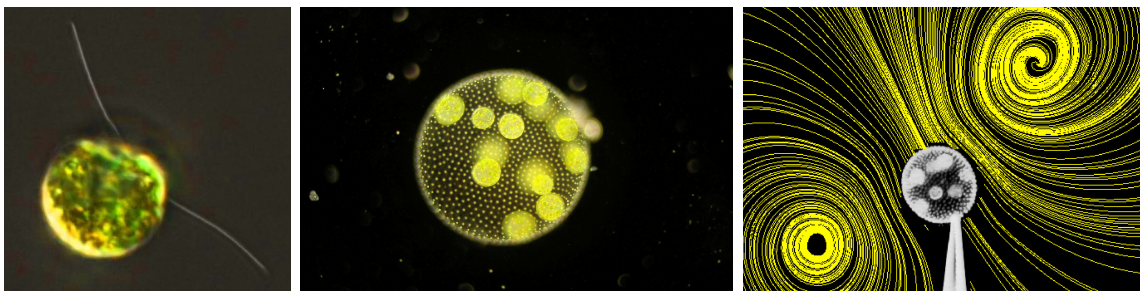


Figure 5.1: (left) *Chlamydomonas* alga with two cilia. (middle) A multicellular *Volvox* colony swims by beating several hundreds of cilia on their surface in synchronized manner. (right) Flow field created by a *Volvox* when held fixed with a pipette (photos: Knut Drescher).

¹This is equivalent to larger animals swimming through a bath of treacle.

5.1 Navier-Stokes equations

Consider a fluid of conserved mass density $\varrho(t, \mathbf{x})$, governed by continuity equation

$$\partial_t \varrho + \nabla \cdot (\varrho \mathbf{u}) = 0, \quad (5.1)$$

where $\mathbf{u}(t, \mathbf{x})$ is local flow velocity. According to standard hydrodynamic theory, the dynamics of \mathbf{u} is described by the Navier-Stokes equations (NSEs)

$$\varrho [\partial_t \mathbf{u} + (\mathbf{u} \cdot \nabla) \mathbf{u}] = \mathbf{f} - \nabla p + \nabla \cdot \hat{T}, \quad (5.2)$$

where $p(t, \mathbf{x})$ the pressure in the fluid, $\hat{T}(t, \mathbf{x})$ the deviatoric² stress-energy tensor of the fluid, and $\mathbf{f}(t, \mathbf{x})$ an external force-density field. A typical example of an external force \mathbf{f} , that is also relevant in the biological context, is the gravitational force

$$\mathbf{f} = \varrho \mathbf{g}, \quad (5.3)$$

where $\mathbf{g}(t, \mathbf{x})$ is the gravitational acceleration field.

Considering a Cartesian coordinate frame, Eqs. (5.1) and (5.2) can also be rewritten in the component form

$$\partial_t \varrho + \nabla_i (\varrho u_i) = 0, \quad (5.4a)$$

$$\varrho (\partial_t u_i + u_j \partial_j u_i) = F_i - \partial_i p + \partial_j \hat{T}_{ji}. \quad (5.4b)$$

To close the system of equations (5.4), one still needs to

- (i) fix the equation of state

$$p = p[\varrho, \dots],$$

- (ii) choose an ansatz the symmetric stress-energy tensor

$$\hat{T} = (\hat{T}_{ij}[\varrho, \mathbf{u}, \dots]),$$

- (iii) specify an appropriate set of initial and boundary conditions.

²‘deviatoric’:= without hydrostatic stress (pressure); a ‘full’ stress-energy tensor $\hat{\sigma}$ may be defined by

$$\hat{\sigma}_{ij} := -p \delta_{ij} + \hat{T}_{ij}.$$

Simplifications In the case of a *homogeneous* fluid with ³

$$\partial_t \varrho = 0 \quad \text{and} \quad \nabla \varrho = 0, \quad (5.5)$$

the associated flow is *incompressible* (isochoric)

$$\nabla \cdot \mathbf{u} = 0. \quad (5.6)$$

A *Newtonian* fluid is a fluid that can, by definition, be described by

$$\hat{T}_{ij} := \lambda (\nabla \cdot \mathbf{u}) \delta_{ij} + \mu (\partial_i u_j + \partial_j u_i). \quad (5.7)$$

where λ the first coefficient of viscosity (related to *bulk* viscosity), and μ is the second coefficient of viscosity (shear viscosity). Thus, for an incompressible Newtonian fluid, the Navier-Stokes system (5.4) simplifies to

$$0 = \nabla \cdot \mathbf{u}, \quad (5.8a)$$

$$\varrho [\partial_t \mathbf{u} + (\mathbf{u} \cdot \nabla) \mathbf{u}] = -\nabla p + \mu \nabla^2 \mathbf{u} + \mathbf{f}. \quad (5.8b)$$

Dynamic viscosity The SI physical unit of *dynamic* viscosity μ is the Pascal \times second

$$[\mu] = 1 \text{ Pa} \cdot \text{s} = 1 \text{ kg}/(\text{m} \cdot \text{s}) \quad (5.9)$$

If a fluid with a viscosity $\mu = 1 \text{ Pa} \cdot \text{s}$ is placed between two plates, and one plate is pushed sideways with a shear stress of one pascal, it moves a distance equal to the thickness of the layer between the plates in one second. The dynamic viscosity of water ($T = 20^\circ\text{C}$) is $\mu = 1.0020 \times 10^{-3} \text{ Pa} \cdot \text{s}$.

Kinematic viscosity Below we will be interested in comparing viscous and inertial forces. Their ratio is characterized by the *kinematic* viscosity ν , defined as

$$\nu = \frac{\mu}{\varrho}, \quad [\nu] = \text{m}^2/\text{s} \quad (5.10)$$

The kinematic viscosity of water with mass density $\varrho = 1 \text{ g}/\text{cm}^3$ is $\nu = 10^{-6} \text{ m}^2/\text{s} = 1 \text{ mm}^2/\text{s} = 1 \text{ cSt}$.

³By virtue of the conservation law (5.1), a homogeneous material is always incompressible, but in general the converse is not true.

5.2 Stokes equations

5.2.1 Motivation

Consider an object of characteristic length L , moving at absolute velocity $U = |\mathbf{U}|$ through (relative to) an incompressible, homogeneous Newtonian fluid of constant viscosity μ and constant density ρ . The object can be imagined as a moving boundary (condition), which induces a flow field $\mathbf{u}(t, \mathbf{x})$ in the fluid. The ratio of the inertial (dynamic) pressure ρU^2 and viscous shearing stress $\mu U/L$ can be characterized by the Reynolds number⁴

$$\mathcal{R} = \frac{|\rho(\partial_t \mathbf{u} + (\mathbf{u} \cdot \nabla) \mathbf{u})|}{|\mu \nabla^2 \mathbf{u}|} \simeq \frac{\rho U^2/L}{\mu U/L^2} = \frac{UL\rho}{\mu} = \frac{UL}{\nu}. \quad (5.11)$$

For example, when considering swimming in water ($\nu = 10^{-6} \text{ m}^2/\text{s}$), one finds for fish or humans:

$$L \simeq 1 \text{ m}, \quad U \simeq 1 \text{ m/s} \quad \Rightarrow \quad \mathcal{R} \simeq 10^6,$$

whereas for bacteria:

$$L \simeq 1 \text{ }\mu\text{m}, \quad U \simeq 10 \text{ }\mu\text{m/s} \quad \Rightarrow \quad \mathcal{R} \simeq 10^{-5}.$$

If the Reynolds number is very small, $\mathcal{R} \ll 1$, the nonlinear NSEs (5.8) can be approximated by the linear *Stokes equations*⁵

$$0 = \nabla \cdot \mathbf{u}, \quad (5.12a)$$

$$0 = \mu \nabla^2 \mathbf{u} - \nabla p + \mathbf{f}. \quad (5.12b)$$

The four equations (5.12) determine the four unknown functions (\mathbf{u}, p) . However, to uniquely identify such solutions, these equations must still be endowed with appropriate initial and boundary conditions, such as for example

$$\begin{cases} \mathbf{u}(t, \mathbf{x}) = 0, \\ p(t, \mathbf{x}) = p_\infty, \end{cases} \quad \text{as} \quad |\mathbf{x}| \rightarrow \infty. \quad (5.13)$$

Note that, by neglecting the explicit time-dependent inertial terms in NSEs, *the time-dependence of the flow is determined exclusively and instantaneously by the motion of the boundaries and/or time-dependent forces* as generated by the swimming objects.

⁴Actually, the (local) Reynolds number is defined in terms of the fluid velocity \mathbf{u} relative to an ‘appropriately’ chosen reference frame (e.g., the restframe of a confining body). Eq. (5.11) implicitly assumes that $\mathbf{u} \simeq \mathbf{U}$ on the surface of the object. Moreover, the value of the Reynolds number depends on the choice of a – somewhat arbitrary – characteristic length scale L , sometimes expressed through the notation \mathcal{R}_L . Specifically, one uses the approximations $|(\mathbf{u} \cdot \nabla) \mathbf{u}| \simeq |\mathbf{U} \cdot \mathbf{U}/L|$ and, similarly, $|\partial_t \mathbf{u}| \simeq \mathbf{U}/\tau$ with a characteristic timescale $\tau = L/|\mathbf{U}|$, yielding $|(\mathbf{u} \cdot \nabla) \mathbf{u}| \simeq |\partial_t \mathbf{u}| \simeq U^2/L$.

⁵More precisely, by replacing Eq. (5.8) with Eq. (5.12), it is assumed that for small Reynolds numbers $\tilde{\mathcal{R}}(t, \mathbf{x}) := |\rho(\mathbf{u} \cdot \nabla) \mathbf{u}|/(\mu \nabla^2 \mathbf{u}) \simeq UL(\rho/\mu) \ll 1$ one can approximate

$$\rho [\partial_t \mathbf{u} + (\mathbf{u} \cdot \nabla) \mathbf{u}] - \mu \nabla^2 \mathbf{u} \simeq -\mu \nabla^2 \mathbf{u}$$

The consistency of this approximation can be checked *a posteriori* by inserting the solution for \mathbf{u} into the lhs. of Eq. (5.8).

5.2.2 Special solutions

Oseen solution Consider the Stokes equations (5.12) for a point-force

$$\mathbf{f}(\mathbf{x}) = \mathbf{F} \delta(\mathbf{x}). \quad (5.14)$$

In this case, the solution with standard boundary conditions (5.13) reads⁶

$$u_i(\mathbf{x}) = G_{ij}(\mathbf{x}) F_j, \quad p(\mathbf{x}) = \frac{F_j x_j}{4\pi|\mathbf{x}|^3} + p_\infty, \quad (5.15a)$$

where the Greens function G_{ij} is given by the Oseen tensor

$$G_{ij}(\mathbf{x}) = \frac{1}{8\pi\mu|\mathbf{x}|} \left(\delta_{ij} + \frac{x_i x_j}{|\mathbf{x}|^2} \right), \quad (5.15b)$$

which has the inverse

$$G_{jk}^{-1}(\mathbf{x}) = 8\pi\mu|\mathbf{x}| \left(\delta_{jk} - \frac{x_j x_k}{2|\mathbf{x}|^2} \right), \quad (5.16)$$

as can be seen from

$$\begin{aligned} G_{ij} G_{jk}^{-1} &= \left(\delta_{ij} + \frac{x_i x_j}{|\mathbf{x}|^2} \right) \left(\delta_{jk} - \frac{x_j x_k}{2|\mathbf{x}|^2} \right) \\ &= \delta_{ik} - \frac{x_i x_k}{2|\mathbf{x}|^2} + \frac{x_i x_k}{|\mathbf{x}|^2} - \frac{x_i x_j}{|\mathbf{x}|^2} \frac{x_j x_k}{2|\mathbf{x}|^2} \\ &= \delta_{ik} - \frac{x_i x_k}{2|\mathbf{x}|^2} + \frac{x_i x_k}{2|\mathbf{x}|^2} \\ &= \delta_{ik}. \end{aligned} \quad (5.17)$$

Stokes solution (1851) Consider a sphere of radius a , which at time t is located at the origin, $\mathbf{X}(t) = \mathbf{0}$, and moves at velocity $\mathbf{U}(t)$. The corresponding solution of the Stokes equation with standard boundary conditions (5.13) reads⁷

$$u_i(t, \mathbf{x}) = U_j \left[\frac{3}{4} \frac{a}{|\mathbf{x}|} \left(\delta_{ji} + \frac{x_j x_i}{|\mathbf{x}|^2} \right) + \frac{1}{4} \frac{a^3}{|\mathbf{x}|^3} \left(\delta_{ji} - 3 \frac{x_j x_i}{|\mathbf{x}|^2} \right) \right], \quad (5.18a)$$

$$p(t, \mathbf{x}) = \frac{3}{2} \mu a \frac{U_j x_j}{|\mathbf{x}|^3} + p_\infty. \quad (5.18b)$$

If the particle is located at $\mathbf{X}(t)$, one has to replace x_i by $x_i - X_i(t)$ on the rhs. of Eqs. (5.18). Parameterizing the surface of the sphere by

$$\mathbf{a} = a \sin \theta \cos \phi \mathbf{e}_x + a \sin \theta \sin \phi \mathbf{e}_y + a \cos \theta \mathbf{e}_z = a_i \mathbf{e}_i$$

⁶Proof by insertion.

⁷Proof by insertion.

where $\theta \in [0, \pi], \phi \in [0, 2\pi)$, one finds that on this boundary

$$\mathbf{u}(t, \mathbf{a}(\theta, \phi)) = \mathbf{U}, \quad (5.19a)$$

$$p(t, \mathbf{a}(\theta, \phi)) = \frac{3}{2} \frac{\mu}{a^2} U_j a_j(\theta, \phi) + p_\infty, \quad (5.19b)$$

corresponding to a no-slip boundary condition on the sphere's surface. The $\mathcal{O}(a/|\mathbf{x}|)$ -contribution in (5.18a) coincides with the Oseen result (5.15), if we identify

$$\mathbf{F} = 6\pi\mu a \mathbf{U}. \quad (5.20)$$

The prefactor $\gamma = 6\pi\mu a$ is the well-known Stokes drag coefficient for a sphere.

The $\mathcal{O}[(a/|\mathbf{x}|)^3]$ -part in (5.18a) corresponds to the finite-size correction, and defining the Stokes tensor by

$$S_{ij} = G_{ij} + \frac{1}{24\pi\mu} \frac{a^2}{|\mathbf{x}|^3} \left(\delta_{ji} - 3 \frac{x_j x_i}{|\mathbf{x}|^2} \right), \quad (5.21)$$

we may rewrite (5.18a) as⁸

$$u_i(t, \mathbf{x}) = S_{ij} F_j. \quad (5.22)$$

5.3 Golestanian's swimmer model

This part is copied (with very minor adaptations) from the article of Golestanian and Ajdari [GA07], for their excellent discussion is difficult, if not impossible, to improve.

5.3.1 Three-sphere swimmer: simplified analysis

As a minimal model of a low Reynolds number swimmer, consider three spheres of radii a_i ($i = 1, 2, 3$) that are separated by two arms of lengths L_1 and L_2 . Each sphere exerts a force F_i on, and experiences a force $-F_i$ from, the fluid that we assume to be along the swimmer axis. In the limit $a_i/L_j \ll 1$, we can use the Oseen tensor (5.15) to relate the forces and the velocities as

$$v_1 = \frac{F_1}{6\pi\mu a_1} + \frac{F_2}{4\pi\mu L_1} + \frac{F_3}{4\pi\mu(L_1 + L_2)}, \quad (5.23a)$$

$$v_2 = \frac{F_1}{4\pi\mu L_1} + \frac{F_2}{6\pi\mu a_2} + \frac{F_3}{4\pi\mu L_2}, \quad (5.23b)$$

$$v_3 = \frac{F_1}{4\pi\mu(L_1 + L_2)} + \frac{F_2}{4\pi\mu L_2} + \frac{F_3}{6\pi\mu a_3}. \quad (5.23c)$$

⁸For arbitrary sphere positions $\mathbf{X}(t)$, replace $\mathbf{x} \rightarrow \mathbf{x} - \mathbf{X}(t)$.

Note that in this simple one dimensional case, the tensorial structure of the hydrodynamic Green's function (Oseen tensor) does not enter the calculations as all the forces and velocities are parallel to each other and to the position vectors. The swimming velocity of the whole object is the mean translational velocity, namely

$$V_0 = \frac{1}{3}(v_1 + v_2 + v_3). \quad (5.24)$$

We are seeking to study autonomous net swimming, which requires the whole system to be force-free (i.e. there are no external forces acting on the spheres). This means that the above equations are subject to the constraint

$$F_1 + F_2 + F_3 = 0. \quad (5.25)$$

Eliminating F_2 using Eq. (5.25), we can calculate the swimming velocity from Eqs. (5.23a), (5.23b), (5.23c), and (5.24) as

$$\begin{aligned} V_0 = & \frac{1}{3} \left[\left(\frac{1}{a_1} - \frac{1}{a_2} \right) + \frac{3}{2} \left(\frac{1}{L_1 + L_2} - \frac{1}{L_2} \right) \right] \left(\frac{F_1}{6\pi\mu} \right) + \\ & \frac{1}{3} \left[\left(\frac{1}{a_3} - \frac{1}{a_2} \right) + \frac{3}{2} \left(\frac{1}{L_1 + L_2} - \frac{1}{L_1} \right) \right] \left(\frac{F_3}{6\pi\mu} \right), \end{aligned} \quad (5.26)$$

where the subscript 0 denotes the force-free condition. To close the system of equations, we should either prescribe the forces (stresses) acting across each linker, or alternatively the opening and closing motion of each arm as a function of time. We choose to prescribe the motion of the arms connecting the three spheres, and assume that the velocities

$$\dot{L}_1 = v_2 - v_1, \quad (5.27a)$$

$$\dot{L}_2 = v_3 - v_2, \quad (5.27b)$$

are known functions. We then use Eqs. (5.23a), (5.23b), (5.23c), and (5.25) to solve for F_1 and F_3 as a function of \dot{L}_1 and \dot{L}_2 . Putting the resulting expressions for F_1 and F_3 back in Eq. (5.26), and keeping only terms in the leading order in a_i/L_j consistent with our original scheme, we find the average swimming velocity to the leading order.

5.3.2 Swimming velocity

The above calculations yield a lengthy expression summarized in Eq. (B.1) of the Appendix. This result (B.1) is suitable for numerical studies of swimming cycles with arbitrarily large deformations. For the simple case where all the spheres have the same radii, namely $a = a_1 = a_2 = a_3$, Eq. (5.26) simplifies to

$$V_0 = \frac{a}{6} \left[\left(\frac{\dot{L}_2 - \dot{L}_1}{L_1 + L_2} \right) + 2 \left(\frac{\dot{L}_1}{L_2} - \frac{\dot{L}_2}{L_1} \right) \right], \quad (5.28)$$

plus terms that average to zero over a full swimming cycle. Equation (5.28) is also valid for arbitrarily large deformations.

We can also consider relatively small deformations and perform an expansion of the swimming velocity to the leading order. Using

$$L_1 = \ell_1 + u_1(t), \quad (5.29)$$

$$L_2 = \ell_2 + u_2(t), \quad (5.30)$$

in Eq. (B.1), and expanding to the leading order in u_i/ℓ_j , we find the average swimming velocity as

$$\overline{V}_0 = \frac{K}{2} \overline{(u_1 \dot{u}_2 - \dot{u}_1 u_2)}, \quad (5.31)$$

where

$$K = \frac{3 a_1 a_2 a_3}{(a_1 + a_2 + a_3)^2} \left[\frac{1}{\ell_1^2} + \frac{1}{\ell_2^2} - \frac{1}{(\ell_1 + \ell_2)^2} \right]. \quad (5.32)$$

In the above result, the averaging is performed by time integration over a full cycle. Note that terms proportional to $u_1 \dot{u}_1$, $u_2 \dot{u}_2$, and $u_1 \dot{u}_2 + \dot{u}_1 u_2$ are eliminated because they are full time derivatives and they average out to zero in a cycle. Equation (5.31) shows that the average swimming velocity is proportional to the enclosed area that is swept in a full cycle in the configuration space [i.e. in the (u_1, u_2) space]. This result, which is valid within the perturbation theory, is inherently related to the geometrical structure of theory the low Reynolds number swimming studied by Shapere and Wilczek [SW87]. Naturally, the swimmer can achieve higher velocities if it can maximize this area by introducing sufficient phase difference between the two deformation cycles (see below).

5.3.3 Harmonic deformations

As a simple explicit example, consider harmonic deformations of the two arms, with identical frequencies ω and a mismatch in phases,

$$u_1(t) = d_1 \cos(\omega t + \varphi_1), \quad (5.33)$$

$$u_2(t) = d_2 \cos(\omega t + \varphi_2). \quad (5.34)$$

The average swimming velocity from Eq. (5.31) reads

$$\overline{V}_0 = \frac{K}{2} d_1 d_2 \omega \sin(\varphi_1 - \varphi_2). \quad (5.35)$$

This result shows that the maximum velocity is obtained when the phase difference is $\pi/2$, which supports the picture of maximizing the area covered by the trajectory of the swimming cycle in the parameter space of the deformations. A phase difference of 0 or π , for example, will create closed trajectories with zero area, or just lines.

5.3.4 Force-velocity relation and stall force

The effect of an external force or load on the efficiency of the swimmer can be easily studied within the linear theory of Stokes hydrodynamics. When the swimmer is under the effect of an applied external force F , Eq. (5.25) should be changed as

$$F_1 + F_2 + F_3 = F. \quad (5.36)$$

Following through the calculations of Sec. 5.3.1 above, we find that the following changes take place in Eqs. (5.23a), (5.23b), (5.23c), and (5.24):

$$v_1 \mapsto v_1 - \frac{F}{4\pi\mu L_1}, \quad (5.37)$$

$$v_2 \mapsto v_2 - \frac{F}{6\pi\mu a_2}, \quad (5.38)$$

$$v_3 \mapsto v_3 - \frac{F}{4\pi\mu L_2}, \quad (5.39)$$

$$V \mapsto V - \frac{1}{3} \left(\frac{1}{6\pi\mu a_2} + \frac{1}{4\pi\mu L_1} + \frac{1}{4\pi\mu L_2} \right) F. \quad (5.40)$$

These lead to the changes

$$\dot{L}_1 \mapsto \dot{L}_1 - \left(\frac{1}{6\pi\mu a_2} - \frac{1}{4\pi\mu L_1} \right) F, \quad (5.41)$$

$$\dot{L}_2 \mapsto \dot{L}_2 - \left(\frac{1}{4\pi\mu L_2} - \frac{1}{6\pi\mu a_2} \right) F, \quad (5.42)$$

in Eq. (B.1), which together with correction coming from Eq. (5.40) leads to the average swimming velocity

$$\bar{V}(F) = \bar{V}_0 + \frac{F}{18\pi\mu a_R}, \quad (5.43)$$

to the leading order, where a_R is an effective (renormalized) hydrodynamic radius for the three-sphere swimmer. To the zeroth order, we have $a_R = \frac{1}{3}(a_1 + a_2 + a_3)$ for the general case and there are a large number of correction terms at higher orders that we should keep in order to be consistent in our perturbation theory. Instead of reporting the lengthy expression for the general case, we provide the expression for $a_1 = a_2 = a_3 = a$, which reads

$$\frac{1}{a_R} = \frac{1}{a} + \frac{1}{L_1} + \frac{1}{L_2} + \frac{1}{L_1 + L_2} - \frac{a}{2} \left(\frac{1}{L_1} - \frac{1}{L_2} \right)^2 - \frac{a}{2(L_1 + L_2)^2}. \quad (5.44)$$

The force-velocity relation given in Eq. (5.43), which could have been expected based on linearity of hydrodynamics, yields a *stall force*

$$F_s = -18\pi\mu a_R \bar{V}_0. \quad (5.45)$$

Using the zeroth order expression for the hydrodynamic radius, one can see that this is equal to the Stokes force exerted on the three spheres moving with a velocity \bar{V}_0 .

5.3.5 Power consumption and efficiency

Because we know the instantaneous values for the velocities and the forces, we can easily calculate the power consumption in the motion of the spheres through the viscous fluid. The rate of power consumption at any time is given as

$$\mathcal{P} = F_1 v_1 + F_2 v_2 + F_3 v_3 = F_1(-\dot{L}_1) + F_3(\dot{L}_2), \quad (5.46)$$

where the second expression is the result of enforcing the force-free constrain of Eq. (5.25). Using the expressions for F_1 and F_3 as a function of \dot{L}_1 and \dot{L}_2 , one finds for $a_1 = a_2 = a_3 = a$

$$\begin{aligned} \mathcal{P} &= 4\pi\mu a \left[1 + \frac{a}{L_1} - \frac{1}{2} \frac{a}{L_2} + \frac{a}{L_1 + L_2} \right] \dot{L}_1^2 + \\ &4\pi\mu a \left[1 - \frac{1}{2} \frac{a}{L_1} + \frac{a}{L_2} + \frac{a}{L_1 + L_2} \right] \dot{L}_2^2 + \\ &4\pi\mu a \left[1 - \frac{1}{2} \frac{a}{L_1} - \frac{1}{2} \frac{a}{L_2} + \frac{5}{2} \frac{a}{L_1 + L_2} \right] \dot{L}_1 \dot{L}_2. \end{aligned} \quad (5.47)$$

We can now define a Lighthill hydrodynamic efficiency as

$$\mu_L \equiv \frac{18\pi\mu a_R \overline{V_0^2}}{\overline{\mathcal{P}}}, \quad (5.48)$$

for which we find to the leading order

$$\mu_L = \frac{9}{8} \frac{a_R}{a} \frac{K^2 \overline{(u_1 \dot{u}_2 - \dot{u}_1 u_2)^2}}{C_1 \overline{\dot{u}_1^2} + C_2 \overline{\dot{u}_2^2} + C_3 \overline{\dot{u}_1 \dot{u}_2}}, \quad (5.49a)$$

where

$$C_1 = 1 + \frac{a}{\ell_1} - \frac{1}{2} \frac{a}{\ell_2} + \frac{a}{\ell_1 + \ell_2}, \quad (5.49b)$$

$$C_2 = 1 - \frac{1}{2} \frac{a}{\ell_1} + \frac{a}{\ell_2} + \frac{a}{\ell_1 + \ell_2}, \quad (5.49c)$$

$$C_3 = 1 - \frac{1}{2} \frac{a}{\ell_1} - \frac{1}{2} \frac{a}{\ell_2} + \frac{5}{2} \frac{a}{\ell_1 + \ell_2}. \quad (5.49d)$$

It is interesting to note that for harmonic deformations with a single frequency, Eq. (5.49a) is independent of the frequency and scales like $a^2 d^2 / \ell^4$, which reflects the generally low hydrodynamic efficiency of low Reynolds number swimmers. In this case, it is possible to find an optimal value for the phase difference that maximizes the efficiency.

5.4 Dimensionality

We saw above that, in 3D, the fundamental solution to the Stokes equations for a point force at the origin is given by the Oseen solution

$$u_i(\mathbf{x}) = G_{ij}(\mathbf{x}) F_j, \quad p(\mathbf{x}) = \frac{F_j x_j}{4\pi|\mathbf{x}|^3} + p_\infty, \quad (5.50a)$$

where

$$G_{ij}(\mathbf{x}) = \frac{1}{8\pi\mu|\mathbf{x}|} \left(\delta_{ij} + \frac{x_i x_j}{|\mathbf{x}|^2} \right), \quad (5.50b)$$

It is interesting to compare this result with corresponding 2D solution

$$u_i(\mathbf{x}) = J_{ij}(\mathbf{x}) F_j, \quad p = \frac{F_j x_j}{2\pi|\mathbf{x}|^2} + \partial_\infty, \quad \mathbf{x} = (x, y) \quad (5.51a)$$

where

$$J_{ij}(\mathbf{x}) = \frac{1}{4\pi\mu} \left[-\delta_{ij} \ln\left(\frac{|\mathbf{x}|}{a}\right) + \frac{x_i x_j}{|\mathbf{x}|^2} \right] \quad (5.51b)$$

with a being an arbitrary constant fixed by some intermediate flow normalization condition. Note that (5.51) decays much more slowly than (5.50), implying that hydrodynamic interactions in 2D freestanding films are much stronger than in 3D bulk solutions.

To verify that (5.51) is indeed a solution of the 2D Stokes equations, we first note that generally

$$\partial_j |\mathbf{x}| = \partial_j (x_i x_i)^{1/2} = x_j (x_i x_i)^{-1/2} = \frac{x_j}{|\mathbf{x}|} \quad (5.52a)$$

$$\partial_j |\mathbf{x}|^{-n} = \partial_j (x_i x_i)^{-n/2} = -n x_j (x_i x_i)^{-(n+2)/2} = -n \frac{x_j}{|\mathbf{x}|^{n+2}}. \quad (5.52b)$$

From this, we find

$$\partial_i p = \frac{F_i}{2\pi|\mathbf{x}|^2} - 2 \frac{F_j x_j x_i}{2\pi|\mathbf{x}|^4} = \frac{F_j}{2\pi|\mathbf{x}|^2} \left(\delta_{ij} - 2 \frac{x_j x_i}{|\mathbf{x}|^2} \right) \quad (5.53)$$

and

$$\begin{aligned} \partial_k J_{ij} &= \frac{1}{4\pi\mu} \partial_k \left[-\delta_{ij} \ln\left(\frac{|\mathbf{x}|}{a}\right) + \frac{x_i x_j}{|\mathbf{x}|^2} \right] \\ &= \frac{1}{4\pi\mu} \left[-\delta_{ij} \frac{1}{|\mathbf{x}|} \partial_k |\mathbf{x}| + \partial_k \left(\frac{x_i x_j}{|\mathbf{x}|^2} \right) \right] \\ &= \frac{1}{4\pi\mu} \left[-\delta_{ij} \frac{x_k}{|\mathbf{x}|^2} + \left(\delta_{ik} \frac{x_j}{|\mathbf{x}|^2} + \delta_{jk} \frac{x_i}{|\mathbf{x}|^2} - 2 \frac{x_i x_j x_k}{|\mathbf{x}|^4} \right) \right]. \end{aligned} \quad (5.54)$$

To check the incompressibility condition, note that

$$\begin{aligned}
\partial_i J_{ij} &= \frac{1}{4\pi\mu} \left[-\delta_{ij} \frac{x_i}{|\mathbf{x}|^2} + \left(\delta_{ii} \frac{x_j}{|\mathbf{x}|^2} + \delta_{ji} \frac{x_i}{|\mathbf{x}|^2} - \frac{x_i x_j x_i}{2|\mathbf{x}|^4} \right) \right] \\
&= \frac{1}{4\pi\mu} \left(-\frac{x_j}{|\mathbf{x}|^2} + 2\frac{x_j}{|\mathbf{x}|^2} + \frac{x_j}{|\mathbf{x}|^2} - 2\frac{x_j}{|\mathbf{x}|^2} \right) \\
&= 0,
\end{aligned} \tag{5.55}$$

which confirms that the solution (5.51) satisfies the incompressibility condition $\nabla \cdot \mathbf{u} = 0$. Moreover, we find for the Laplacian

$$\begin{aligned}
\partial_k \partial_k J_{ij} &= \frac{\partial_k}{4\pi\mu} \left[-\delta_{ij} \frac{x_k}{|\mathbf{x}|^2} + \delta_{ik} \frac{x_j}{|\mathbf{x}|^2} + \delta_{jk} \frac{x_i}{|\mathbf{x}|^2} - 2\frac{x_i x_j x_k}{|\mathbf{x}|^4} \right] \\
&= \frac{1}{4\pi\mu} \left[-\delta_{ij} \partial_k \left(\frac{x_k}{|\mathbf{x}|^2} \right) + \delta_{ik} \partial_k \left(\frac{x_j}{|\mathbf{x}|^2} \right) + \delta_{jk} \partial_k \left(\frac{x_i}{|\mathbf{x}|^2} \right) - 2\partial_k \left(\frac{x_i x_j x_k}{|\mathbf{x}|^4} \right) \right] \\
&= \frac{1}{4\pi\mu} \left[-\delta_{ij} \left(\frac{\delta_{kk}}{|\mathbf{x}|^2} - 2\frac{x_k x_k}{|\mathbf{x}|^4} \right) + \delta_{ik} \left(\frac{\delta_{jk}}{|\mathbf{x}|^2} - 2\frac{x_j x_k}{|\mathbf{x}|^4} \right) + \delta_{jk} \left(\frac{\delta_{ik}}{|\mathbf{x}|^2} - 2\frac{x_i x_k}{|\mathbf{x}|^4} \right) - \right. \\
&\quad \left. 2 \left(\frac{\delta_{ik} x_j x_k}{|\mathbf{x}|^4} + \frac{x_i \delta_{jk} x_k}{|\mathbf{x}|^4} + \frac{x_i x_j \delta_{kk}}{|\mathbf{x}|^4} - 4\frac{x_i x_j x_k x_k}{|\mathbf{x}|^6} \right) \right] \\
&= \frac{1}{4\pi\mu} \left[-\delta_{ij} \left(\frac{2}{|\mathbf{x}|^2} - 2\frac{1}{|\mathbf{x}|^2} \right) + \left(\frac{\delta_{ij}}{|\mathbf{x}|^2} - 2\frac{x_j x_i}{|\mathbf{x}|^4} \right) + \left(\frac{\delta_{ij}}{|\mathbf{x}|^2} - 2\frac{x_i x_j}{|\mathbf{x}|^4} \right) - \right. \\
&\quad \left. 2 \left(\frac{x_j x_i}{|\mathbf{x}|^4} + \frac{x_i x_j}{|\mathbf{x}|^4} + 2\frac{x_i x_j}{|\mathbf{x}|^4} - 4\frac{x_i x_j}{|\mathbf{x}|^4} \right) \right] \\
&= \frac{1}{2\pi\mu} \left(\frac{\delta_{ij}}{|\mathbf{x}|^2} - 2\frac{x_j x_i}{|\mathbf{x}|^4} \right)
\end{aligned} \tag{5.56}$$

Hence, by comparing with (5.53), we see that indeed

$$-\partial_i p + \mu \partial_k \partial_k u_i = -\partial_i p + \mu \partial_k \partial_k J_{ij} F_j = 0. \tag{5.57}$$

The difference between 3D and 2D hydrodynamics has been confirmed experimentally for *Chlamydomonas* algae [GJG10, DGM⁺10].

5.5 Force dipole and dimensionality

In the absence of external forces, microswimmers must satisfy the force-free constraint. This simplest realization is a force-dipole flow, which provides a very good approximation for the mean flow field generated by an individual bacterium [DDC⁺11] but not so much for an alga [DGM⁺10].

To construct a force dipole, consider two opposite point-forces $\mathbf{F}^+ = -\mathbf{F}^- = F \mathbf{e}_x$ located at positions $\mathbf{x}^+ = \pm \ell \mathbf{e}_x$. Due to linearity of the Stokes equations the total flow at

some point \mathbf{x} is given by

$$\begin{aligned}
u_i(\mathbf{x}) &= \Gamma_{ij}(\mathbf{x} - \mathbf{x}^+) F_j^+ + \Gamma_{ij}(\mathbf{x} - \mathbf{x}^-) F_j^- \\
&= [\Gamma_{ij}(\mathbf{x} - \mathbf{x}^+) - \Gamma_{ij}(\mathbf{x} - \mathbf{x}^-)] F_j^+ \\
&= [\Gamma_{ij}(\mathbf{x} - \ell \mathbf{e}_x) - \Gamma_{ij}(\mathbf{x} + \ell \mathbf{e}_x)] F_j^+
\end{aligned} \tag{5.58}$$

where $\Gamma_{ij} = J_{ij}$ in 2D and $\Gamma_{ij} = G_{ij}$ in 3D. If $|\mathbf{x}| \gg \ell$, we can Taylor expand Γ_{ij} near $\ell = 0$, and find to leading order

$$\begin{aligned}
u_i(\mathbf{x}) &\simeq \{[\Gamma_{ij}(\mathbf{x}) - \Gamma_{ij}(\mathbf{x})] - [x_k^+ \partial_k \Gamma_{ij}(\mathbf{x}) - x_k^- \partial_k \Gamma_{ij}(\mathbf{x})]\} F_j^+ \\
&= -2x_k^+ [\partial_k \Gamma_{ij}(\mathbf{x})] F_j^+
\end{aligned} \tag{5.59}$$

2D case Using our above result for $\partial_k J_{ij}$, and writing $\mathbf{x}^+ = \ell \mathbf{n}$ and $\mathbf{F}^+ = F \mathbf{n}$ with $|\mathbf{n}| = 1$, we find in 2D

$$\begin{aligned}
u_i(\mathbf{x}) &= -\frac{x_k^+}{2\pi\mu} \left[-\delta_{ij} \frac{x_k}{|\mathbf{x}|^2} + \left(\delta_{ik} \frac{x_j}{|\mathbf{x}|^2} + \delta_{jk} \frac{x_i}{|\mathbf{x}|^2} - 2 \frac{x_i x_j x_k}{|\mathbf{x}|^4} \right) \right] F_j^+ \\
&= -\frac{F\ell}{2\pi\mu} \left(-n_i \frac{x_k n_k}{|\mathbf{x}|^2} + n_i \frac{x_j n_j}{|\mathbf{x}|^2} + n_k n_k \frac{x_i}{|\mathbf{x}|^2} - 2 \frac{n_k x_i x_j x_k n_j}{|\mathbf{x}|^4} \right)
\end{aligned}$$

and, hence,

$$\mathbf{u}(x) = \frac{F\ell}{2\pi\mu|\mathbf{x}|} [2(\mathbf{n} \cdot \hat{\mathbf{x}})^2 - 1] \hat{\mathbf{x}} \tag{5.60}$$

where $\hat{\mathbf{x}} = \mathbf{x}/|\mathbf{x}|$.

3D case To compute the dipole flow field in 3D, we need to compute the partial derivatives of the Oseen tensor

$$G_{ij}(\mathbf{x}) = \frac{1}{8\pi\mu|\mathbf{x}|} (1 + \hat{x}_i \hat{x}_j), \quad \hat{x}_k = \frac{x_k}{|\mathbf{x}|}. \tag{5.61}$$

Defining the orthogonal projector (Π_{ik}) for \hat{x}_k by

$$\Pi_{ik} := \delta_{ik} - \hat{x}_i \hat{x}_k, \tag{5.62}$$

we have

$$\partial_k |\mathbf{x}| = \frac{x_k}{|\mathbf{x}|} = \hat{x}_k, \tag{5.63a}$$

$$\partial_k \hat{x}_i = \frac{\delta_{ik}}{|\mathbf{x}|} - \frac{x_k x_i}{|\mathbf{x}|^3} = \frac{\Pi_{ik}}{|\mathbf{x}|}, \tag{5.63b}$$

$$\partial_n \Pi_{ik} = -\frac{1}{|\mathbf{x}|} (\hat{x}_i \Pi_{nk} + \hat{x}_k \Pi_{ni}), \tag{5.63c}$$

and from this we find

$$\begin{aligned}\partial_k G_{ij} &= -\frac{\hat{x}_k}{|\mathbf{x}|} G_{ij} + \frac{\kappa}{|\mathbf{x}|^2} (\Pi_{ik} \hat{x}_j + \Pi_{jk} \hat{x}_i) \\ &= \frac{\kappa}{|\mathbf{x}|^2} (-\hat{x}_k \delta_{ij} + \hat{x}_j \delta_{ik} + \hat{x}_i \delta_{jk} - 3\hat{x}_k \hat{x}_i \hat{x}_j).\end{aligned}\quad (5.64)$$

Inserting this expression into (5.59), we obtain the far-field dipole flow in 3D

$$\mathbf{u}(\mathbf{x}) = \frac{F\ell}{4\pi\mu|\mathbf{x}|^2} [3(\mathbf{n} \cdot \hat{\mathbf{x}})^2 - 1] \hat{\mathbf{x}}. \quad (5.65)$$

As shown in Ref. [DDC⁺11], Eq. (5.65) agrees well with the mean flow-field of a bacterium.

Upon comparing Eqs. (5.60) and (5.65), it becomes evident that hydrodynamic interactions between bacteria in a free-standing 2D film are much longer-ranged than in a 3D bulk solution. This is a nice illustration of the fact that the number of available space dimensions can have profound effects on physical processes and interactions in biological systems.

5.6 Boundary effects

5.6.1 Hagen-Poiseuille flow

Many swimming cells and microorganisms operate in the vicinity of solid boundaries that can substantially affect the self-propulsion and the hydrodynamic interactions of the organisms. To illustrate the effects of no-slip boundaries on the fluid motion, let us consider pressure driven flow along a cylindrical pipe of radius R pointing along the x -axis. Assume that the flow is rotationally symmetric about the x -axis and constant in x -direction, $\mathbf{u} = u_x(r)\mathbf{e}_x$, where $r = \sqrt{y^2 + z^2}$ is the distance from the center. For such a flow, the incompressibility condition $\nabla \cdot \mathbf{u} = 0$ is automatically satisfied, and the Stokes equation in cylindrical coordinates (r, ϕ, x) reduces to

$$0 = -\partial_x p + \frac{\mu}{r} \partial_r (r \partial_r u_x). \quad (5.66)$$

Integrating twice over x , the general solution u_x of this equation can be written as

$$u_x(r) = \frac{1}{4\mu} (\partial_x p) r^2 + c_1 \ln r + c_2, \quad (5.67)$$

where c_1 and c_2 are constants to be determined by the boundary conditions. For a no-slip boundary with $u_x(R) = 0$ and finite flow speed at $r = 0$, one then finds

$$u_x(r) = -\frac{1}{4\mu} (\partial_x p) (R^2 - r^2). \quad (5.68)$$

If we assume a linear pressure difference $\Delta P = P(L) - P(0)$ over a length L , then simply

$$p(x) = [P(L) - P(0)]\frac{x}{L} \quad \Rightarrow \quad \partial_x p = -\frac{P(0) - P(L)}{L}. \quad (5.69)$$

The flow speed is maximal at center of the pipe

$$u_x^+ = \frac{P(0) - P(L)}{4\mu L} R^2 \quad (5.70)$$

and the average transport velocity is

$$\bar{u}_x = \frac{1}{\pi R^2} \int_0^R u_x(r) 2\pi r dr = 0.5u_x^+. \quad (5.71)$$

Note that, for fixed pressure difference and channel length, the transport velocity \bar{u}_x decreases quadratically with the channel radius, signaling that the presence of boundaries can substantially suppress hydrodynamic flows. To illustrate this further, we next consider a useful approximation that can help to speed up numerical simulations through an effective reduction from 3D to 2D flow.

5.6.2 Hele-Shaw flow

Consider two quasi-infinite parallel walls located at $z = 0$ and $z = H$. This setting is commonly encountered in experiments that study microbial swimming in flat microfluidic chambers. Looking for a 2D approximation of the Stokes equation, we may assume constant pressure along the z -direction, $p = P(x, y)$, and neglect possible flow components in the vertical direction, $u_z = 0$. Furthermore, using the above results for Hagen-Poiseuille flow as guidance, we can make the ansatz

$$\mathbf{u}(x, y, z) = \frac{6z(H-z)}{H^2} [U_x(x, y)\mathbf{e}_x + U_y(x, y)\mathbf{e}_y] \equiv \frac{6z(H-z)}{H^2} \mathbf{U}(x, y), \quad (5.72)$$

corresponding to a parabolic flow profile in the vertical direction that accounts for no-slip boundaries at the walls; in particular, in the mid-plane

$$\mathbf{u}(x, y, h/2) = \frac{3}{2} \mathbf{U}(x, y). \quad (5.73)$$

We would like to obtain an effective equation for the effective 2D flow $\mathbf{U}(x, y)$. This can be achieved by inserting ansatz (5.72) into the Stokes equations and subsequently averaging along the z -direction, yielding

$$0 = \nabla \cdot \mathbf{U}, \quad 0 = -\nabla P + \mu \nabla^2 \mathbf{U} - \kappa \mathbf{U} \quad (5.74)$$

where $\kappa = 12\mu/H^2$ and ∇ is now the 2D gradient operator. Note that compared with unconfined 2D flow in a free film, the appearance of the κ -term leads to an exponential damping of hydrodynamic excitations. This is analogous to the exponential damping in the Yakawa-potential (mediated by massive bosons) compared to a Columb potential (mediated by massless photons). That is, due to the presence of the no-slip boundaries, effective 2D hydrodynamic excitations acquire an effective mass $\propto 1/H^2$.

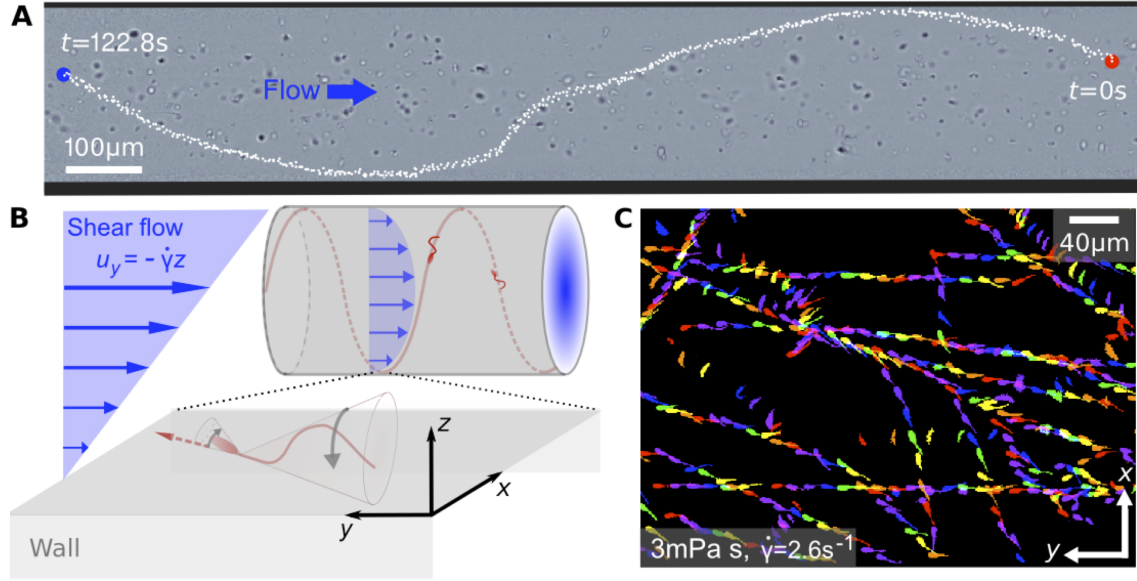


Figure 5.2: Sperm rheotaxis [KDBG14]. (A) Track of a sperm cell swimming upstream on a helical trajectory against a Poiseuille flow. (B) Schematic of shear flow and sperm close to a planar surface. (C) Tracks of sperms cells swimming near a planar surface (flow in negative y -direction).

5.7 Rheotaxis and resistive force theory

The results in Sec. 5.6.1 show that the presence of a boundary typically induces a flow gradient. Many swimming cells, like sperm or bacteria, tend to accumulate at surfaces due to their approximately conical or rod-like body geometry and, hence, can be strongly affected by such flow gradients. In this section, we derive simplified 2D equations of motion governing the reorientation sperm swimming under shear flow close to a solid surface. It is useful to consider non-chiral particles first. Corrections due to chirality will be discussed subsequently.

5.7.1 Non-chiral swimmer

We assume a geometry as depicted in Fig. 5.2B and shear-flow near the boundary given by

$$\mathbf{u} = \begin{pmatrix} 0 \\ \sigma\dot{\gamma}z \\ 0 \end{pmatrix}, \quad (5.75)$$

where $\dot{\gamma} > 0$ is the shear rate and $\sigma = \pm 1$ depending on flow direction. The corresponding vorticity pseudo-vector $\boldsymbol{\omega}$ and rate-of-strain tensor $\boldsymbol{\mathcal{E}}$ read

$$\boldsymbol{\omega} = \nabla \times \mathbf{u} = -\sigma\dot{\gamma} \begin{pmatrix} 1 \\ 0 \\ 0 \end{pmatrix}, \quad \boldsymbol{\mathcal{E}} = \frac{1}{2} (\nabla^T \mathbf{u} + \nabla \mathbf{u}^T) = \frac{\sigma\dot{\gamma}}{2} \begin{pmatrix} 0 & 0 & 0 \\ 0 & 0 & 1 \\ 0 & 1 & 0 \end{pmatrix}. \quad (5.76)$$

We describe the orientation of the cells by the 3D orientation vector $\mathbf{n} = (n_x, n_y, n_z)$ and denote the associated orthogonal projector by

$$\mathcal{P}(\mathbf{n}) = \mathcal{J} - \mathbf{n}\mathbf{n}, \quad (5.77)$$

where \mathcal{J} is the 3×3 unit matrix. According to Eq. (2.4) of Pedley and Kessler [PK92], reorientation of elliptical (or rod-like) particles in shear flow \mathbf{u} is governed to leading order by

$$\dot{\mathbf{n}} = a\boldsymbol{\omega} \times \mathbf{n} + 2b\mathbf{n} \cdot \boldsymbol{\mathcal{E}} \cdot \mathcal{P}(\mathbf{n}), \quad (5.78)$$

where $a = 1/2$ and $b = 0$ for spherical particles. Note that the structure of Eq. (5.80) is such that it conserves the length of \mathbf{n} .

Moreover, we may identify the cross-product $\boldsymbol{\omega} \times \mathbf{n}$ with a matrix multiplication $\mathcal{W} \cdot \mathbf{n}$, where the components of the antisymmetric matrix \mathcal{W} are given by

$$\begin{aligned} 2\mathcal{W}_{mn} &:= -(\boldsymbol{\omega} \times)_{mn} \\ &= -\epsilon_{min}(\epsilon_{ijk}\partial_j u_k) = \epsilon_{imn}(\epsilon_{ijk}\partial_j u_k) = (\delta_{mj}\delta_{nk} - \delta_{mk}\delta_{nj})\partial_j u_k \\ &= \partial_m u_n - \partial_n u_m, \end{aligned} \quad (5.79)$$

using a component notation with sum convention for repeated Latin indices $i, j, \dots = 1, 2, 3$. This allows us to rewrite Eq. (5.78) as

$$\dot{n}_i = 2a\mathcal{W}_{ij}n_j + 2bn_m\mathcal{E}_{mj}(\delta_{ji} - n_j n_i). \quad (5.80)$$

For the flow field in (5.75) we find

$$\dot{\mathbf{n}} = -a\sigma\dot{\gamma} \begin{pmatrix} 0 \\ -n_z \\ n_y \end{pmatrix} - b\sigma\dot{\gamma} \begin{pmatrix} 2n_x n_y n_z \\ (2n_y^2 - 1)n_z \\ (2n_z^2 - 1)n_y \end{pmatrix}, \quad (5.81)$$

with a, b encoding information about the cell-shape.

Now assume that after a collision with the boundary and subsequent alignment, the sperm points into the wall due to steric contact interactions between surface and flagellum, so that $n_z = \text{const} < 0$. This means that the wall must exert a balancing torque such that (i) $\dot{n}_z = 0$ and (ii) $n_x^2 + n_y^2 = (1 - n_z^2)$ is conserved. Assuming cylindrical symmetry of the swimmer around its axis of swimming, the contact interaction leads to rotation of the swimmer in the plane spanned by \mathbf{n} and the wall normal $\mathbf{e}_z = (0, 0, 1)$. The change in orientation per unit time due to wall interactions can therefore be written as $c\mathbf{n} + d\mathbf{e}_z$, which needs to be added to the rhs. of Eqs. (5.78), (5.80) and (5.81), if the sperm is contact with the surface. The coefficient d can be fixed by condition (i), but is not relevant for the motion in the (x, y) -plane parallel to the surface, which becomes governed by

$$\begin{pmatrix} \dot{n}_x \\ \dot{n}_y \end{pmatrix} = -a\sigma\dot{\gamma}n_z \begin{pmatrix} 0 \\ -1 \end{pmatrix} - b\sigma\dot{\gamma}n_z \begin{pmatrix} 2n_x n_y \\ 2n_y^2 - 1 \end{pmatrix} + c \begin{pmatrix} n_x \\ n_y \end{pmatrix}. \quad (5.82)$$

Condition (ii) then gives

$$c = \sigma \dot{\gamma} \frac{n_z [b(1 - 2n_z^2) - a]}{1 - n_z^2} n_y. \quad (5.83)$$

Keeping in mind that n_z and $n_x^2 + n_y^2$ are constant, we thus find the reduced 2D equations of motion

$$\begin{pmatrix} \dot{n}_x \\ \dot{n}_y \end{pmatrix} = -\sigma \dot{\gamma} (a + b) \frac{n_z}{n_x^2 + n_y^2} \begin{pmatrix} n_x n_y \\ n_y^2 - (1 - n_z^2) \end{pmatrix} \quad (5.84)$$

The fixed point criterium $(\dot{n}_x, \dot{n}_y) = 0$ gives

$$n_x = 0, \quad n_y = \pm \sqrt{1 - n_z^2}, \quad (5.85)$$

This result implies that, depending on the effective shape parameter

$$\alpha = -(a + b)n_z, \quad (5.86)$$

the combination of shear flow and wall interaction aligns the swimmer either parallel or anti-parallel to the flow direction. This result also indicates that, to explain the transverse velocity component observed in the experiments (Fig. 5.2A,C), we have to account for the chirality of the flagellar beat, which has been neglected so far. Before discussing chiral effects in the next section, let us still note that we may rewrite Eq. (5.84) in terms of the 2D unit vector

$$\mathbf{N} = \begin{pmatrix} N_x \\ N_y \end{pmatrix} = \frac{1}{\sqrt{1 - n_z^2}} \begin{pmatrix} n_x \\ n_y \end{pmatrix} \quad (5.87)$$

as

$$\begin{pmatrix} \dot{N}_x \\ \dot{N}_y \end{pmatrix} = \sigma \dot{\gamma} \alpha \begin{pmatrix} N_x N_y \\ N_y^2 - 1 \end{pmatrix}, \quad (5.88)$$

where $\sigma = \pm 1$ accounts for the flow direction and constant geometric prefactors have been absorbed in the ‘shape’ coefficient

$$\alpha = -(a + b)n_z. \quad (5.89)$$

Note that α is positive for sperm-type swimmers that point into the surface, for in this case one has $n_z < 0$.

5.7.2 Chiral swimmers

To identify how chirality of the flagellar beat might affect the reorientation rate of sperm in shear flow, we consider as a simplified sperm model a rigid 3D conical helix $\mathbf{C}(s)$ in

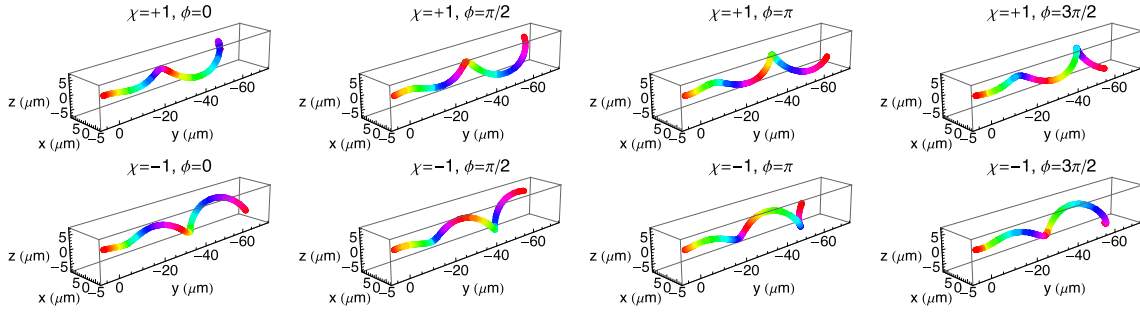


Figure 5.3: Rigid conical helices, as defined in Eq. (5.90), for different handedness $\chi = \pm 1$ and different ‘initial’ phases ϕ in their body-fixed frames, where the head rests at the origin. Colors encode windings. Parameters: $S = 4\pi$, $\epsilon_1 = \epsilon_2 = 0.1$, $\lambda = 5\mu\text{m}$.

contact with a wall that defines the (x, y) -plane of the lab frame $\Sigma = \{\mathbf{e}_x, \mathbf{e}_y, \mathbf{e}_z\}$, which is again chosen as in Fig. 5.2B.

We denote by $\mathbf{n} = (n_x, n_y, n_z)$ the orientation of the conical helix in the lab frame Σ . The head position is identified with tip of the cone. In the body-fixed frame $\hat{\Sigma} = \{\hat{\mathbf{e}}_x, \hat{\mathbf{e}}_y, \hat{\mathbf{e}}_z\}$, the head rests at the origin and the tail points in the $-\hat{\mathbf{e}}_y$ -direction (Fig. 5.3). Specifically, we assume that, in the body-fixed frame $\hat{\Sigma}$, the helix is described by the curve

$$\hat{\mathbf{C}}(s) = \begin{pmatrix} \hat{X}(s) \\ \hat{Y}(s) \\ \hat{Z}(s) \end{pmatrix} = \lambda s \begin{pmatrix} \chi \epsilon_1 \cos(s - \phi) \\ -1 \\ -\epsilon_2 \sin(s - \phi) \end{pmatrix}, \quad s \in [0, S]. \quad (5.90)$$

The length parameter λ scales the size of the flagellum. The parameters $\epsilon_1 > 0$ and $\epsilon_2 > 0$ determine the lateral shape of the helix, and they can also be used to interpolate between helical and planar beat patterns. The phase angle ϕ sets the ‘initial’ direction of the flagellum relative to the head. The chirality parameter $\chi = \pm 1$ determines the handedness, defined here such that $\chi = +1$ corresponds to a right-handed spiral when viewed from the head (Fig. 5.4).

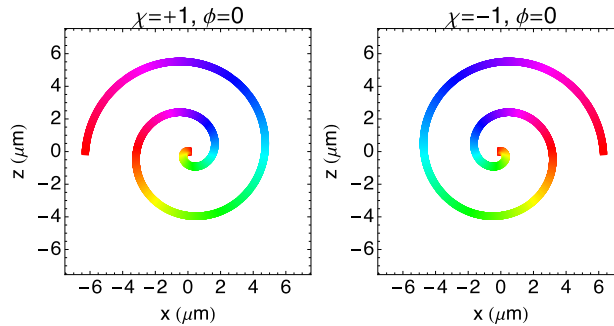


Figure 5.4: Rigid conical helices from Fig. 5.3 as viewed from the head, using the same color coding as in Fig. 5.3.

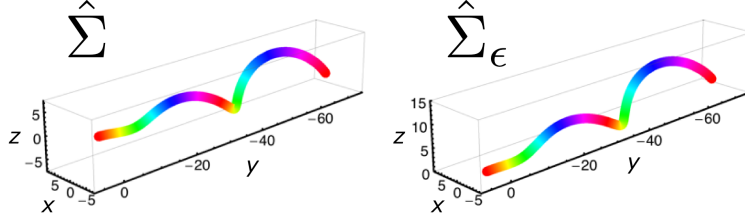


Figure 5.5: Body-centered frame $\hat{\Sigma}$ and tilted body-centered frame $\hat{\Sigma}_\epsilon$ are related by a rotation about the x -axis. After alignment with the wall, which is assumed to lie in the $(z = 0)$ -plane of $\hat{\Sigma}_\epsilon$, the orientation of the sperm in the lab frame Σ (not shown) is obtained by an additional rotation of $\hat{\Sigma}_\epsilon$ about the vertical axis .

To simplify calculations, we henceforth focus on symmetric spirals with $\epsilon_1 = \epsilon_2 = \epsilon$. In this case, the enveloping cone is given by

$$\hat{\mathbf{C}}(s, \phi) = \lambda s \begin{pmatrix} \epsilon \cos \phi \\ -1 \\ -\epsilon \sin \phi \end{pmatrix}, \quad s \in [0, S], \phi \in [0, 2\pi) \quad (5.91)$$

with half-opening angle

$$\theta_\epsilon = \arctan \epsilon. \quad (5.92)$$

Assume that the spiral is in contact with the surface along its envelope. By rotating through $-\theta$ about the $\hat{\mathbf{e}}_x$ -axis, we obtain the tilted body-centered frame $\hat{\Sigma}_\epsilon$ (Fig. 5.5) which is defined such that the channel surface is located at $z = 0$ in both $\hat{\Sigma}_\epsilon$ and the lab frame. In $\hat{\Sigma}_\epsilon$, the helix is given by

$$\hat{\mathbf{C}}_\epsilon(s) = \mathcal{R}_x(\theta_\epsilon) \cdot \hat{\mathbf{C}}(s), \quad \mathcal{R}_x(\theta_\epsilon) = \begin{pmatrix} 1 & 0 & 0 \\ 0 & \cos \theta_\epsilon & \sin \theta_\epsilon \\ 0 & -\sin \theta_\epsilon & \cos \theta_\epsilon \end{pmatrix}. \quad (5.93)$$

Using $\chi^2 = 1$, the tangent vectors in the body-fixed frame $\hat{\Sigma}$ are found as

$$\begin{aligned} \hat{\mathbf{t}}(s) &:= \frac{d\hat{\mathbf{C}}(s)/ds}{\|d\hat{\mathbf{C}}(s)/ds\|} \\ &= \frac{1}{\sqrt{1 + (1 + s^2) \epsilon^2}} \begin{pmatrix} \epsilon \chi [\cos(s - \phi) - s \sin(s - \phi)] \\ -1 \\ -\epsilon [s \cos(s - \phi) + \sin(s - \phi)] \end{pmatrix}. \end{aligned} \quad (5.94)$$

and, accordingly, after alignment with the wall in $\hat{\Sigma}_\epsilon$ as

$$\hat{\mathbf{t}}_\epsilon(s) = \mathcal{R}_x(\theta_\epsilon) \cdot \hat{\mathbf{t}}(s). \quad (5.95)$$

Due to our chosen parameterisation (5.90), the tangent vectors point away from the head. The length Λ of the curve $\mathbf{C}(s)$ is obtained as

$$\begin{aligned}\Lambda &= \int_0^S ds \left\| \frac{d\hat{\mathbf{C}}(s)}{ds} \right\| \\ &= \int_0^S ds \sqrt{\hat{X}'(s)^2 + \hat{Y}'(s)^2 + \hat{Z}'(s)^2} \\ &= S\lambda \left[1 + \frac{\epsilon^2}{6}(3 + S^2) \right] + \mathcal{O}(\epsilon^4).\end{aligned}\tag{5.96}$$

Thus, to leading order, one can identify $\Lambda \simeq S\lambda$ with the length of a flagellum, and $A = \Lambda\epsilon$ with the beat amplitude.

After averaging over all initial conditions ϕ , the mean geometric center of the helix in the body-fixed frame $\hat{\Sigma}_\epsilon$ is found as

$$\begin{aligned}\hat{\mathbf{C}}_\epsilon &:= \frac{1}{2\pi} \int_0^{2\pi} d\phi \left[\frac{1}{\Lambda} \int_0^S ds \left\| \frac{d\hat{\mathbf{C}}(s)}{ds} \right\| \hat{\mathbf{C}}_\epsilon(s) \right] \\ &= \frac{S\lambda}{2} \begin{pmatrix} 0 \\ -1 \\ \epsilon \end{pmatrix} + \mathcal{O}(\epsilon^2).\end{aligned}\tag{5.97}$$

The orientation $\hat{\mathbf{n}}_\epsilon$ in the wall-aligned body-fixed frame $\hat{\Sigma}_\epsilon$ is defined by

$$\hat{\mathbf{n}}_\epsilon := -\frac{\hat{\mathbf{C}}_\epsilon}{\|\hat{\mathbf{C}}_\epsilon\|} = \begin{pmatrix} 0 \\ 1 \\ -\epsilon \end{pmatrix} + \mathcal{O}(\epsilon^2),\tag{5.98}$$

which is normalised up to terms of order $\mathcal{O}(\epsilon^2)$. Recalling that the z -axes of $\hat{\Sigma}_\epsilon$ and lab-frame Σ coincide, the negative z -component means that the swimming direction points into the wall.

Let us assume, as before, that the shear fluid flow in the lab frame Σ is along the \mathbf{e}_y -direction,

$$\mathbf{u} = \sigma\dot{\gamma}z\mathbf{e}_y,\tag{5.99}$$

where $\dot{\gamma} > 0$ is the shear rate and $\sigma = \pm 1$ determines the flow direction. Measuring the orientation angle ψ of the swimmer wrt. \mathbf{e}_y in counterclockwise direction, we obtain the coordinates $\mathbf{C}(t, s)$ of the helix with head position $\mathbf{R}(t) = (X(t), Y(t), 0)$ in the lab frame Σ by

$$\mathbf{C}(t, s) = \mathbf{R}(t) + \mathcal{R}(\psi(t)) \cdot \hat{\mathbf{C}}_\epsilon(s),\tag{5.100}$$

where

$$\mathcal{R}(\psi) = \begin{pmatrix} \cos \psi & -\sin \psi & 0 \\ \sin \psi & \cos \psi & 0 \\ 0 & 0 & 1 \end{pmatrix}\tag{5.101}$$

represents a rotation about the \mathbf{e}_z -axis. By applying the rotation matrix $\mathcal{R}(\psi)$ to the orientation vector $\hat{\mathbf{n}}_\epsilon$ in $\hat{\Sigma}_\epsilon$, we find that, to leading order in ϵ , the 3D orientation vector \mathbf{n} in the lab frame Σ is given by

$$\mathbf{n} = \begin{pmatrix} \mathbf{N} \\ -\epsilon \end{pmatrix} + \mathcal{O}(\epsilon^2), \quad \mathbf{N} = \begin{pmatrix} N_x \\ N_y \end{pmatrix} = \begin{pmatrix} -\sin \psi \\ \cos \psi \end{pmatrix}, \quad (5.102)$$

where \mathbf{N} is the normalised (projected) 2D orientation vector in the (x, y) -plane. This allows us to rewrite the rotation matrix as

$$\mathcal{R}_\mathbf{N} = \begin{pmatrix} N_y & N_x & 0 \\ -N_x & N_y & 0 \\ 0 & 0 & 1 \end{pmatrix}. \quad (5.103)$$

The tangent vectors of \mathbf{C} in Σ are given by $\mathbf{t}(s) = \mathcal{R}_\mathbf{N} \cdot \mathcal{R}_x(\theta_\epsilon) \cdot \hat{\mathbf{t}}(s)$ with $\hat{\mathbf{t}}(s)$ from Eq. (5.94).

Assuming that the head position $\mathbf{R}(t)$ of the helix performs a quasi-2D motion along the surface, $\mathbf{R}(t) = X(t)\mathbf{e}_x + Y(t)\mathbf{e}_y$, we are interested in obtaining simplified effective equations for the mean drag velocity $\dot{\mathbf{R}} = \mathbf{U}(\mathbf{N})$ and the change in the orientation $\dot{\mathbf{N}}(t)$ due to the action of the flow gradient on the rigid helical curve \mathbf{C} . As we shall discuss next, such equations can be derived from resistive force theory (RFT).

From Eq. (5.100), the velocity of some point $s \in [0, S]$ on the helix can be decomposed as⁹

$$\dot{\mathbf{C}}(s) = \dot{\mathbf{R}} + \dot{\mathcal{R}}_\mathbf{N} \cdot \hat{\mathbf{C}}_\epsilon = \mathbf{U} + \dot{\mathcal{R}}_\mathbf{N} \cdot \hat{\mathbf{C}}_\epsilon. \quad (5.104)$$

Given the shear flow profile \mathbf{u} , RFT assumes that the force line-density (force per unit length) can be split as

$$\begin{aligned} \mathbf{f}(s) = & \zeta_{\parallel} \left\{ \left[\mathbf{u}(\mathbf{C}(s)) - \dot{\mathbf{C}}(s) \right] \cdot \mathbf{t}(s) \right\} \mathbf{t}(s) + \\ & \zeta_{\perp} \left\{ \left[\mathbf{u}(\mathbf{C}(s)) - \dot{\mathbf{C}}(s) \right] \cdot [\mathbf{I} - \mathbf{t}(s)\mathbf{t}(s)] \right\} \end{aligned} \quad (5.105)$$

where ζ_{\parallel} and ζ_{\perp} are tangential and perpendicular drag coefficients. The drag ratio

$$\kappa = \frac{\zeta_{\perp}}{\zeta_{\parallel}}, \quad (5.106)$$

which equals 2 for rigid rods, takes values $\kappa \simeq 1.4 - 1.7$ for realistic flagella. Combining the RFT ansatz (5.105) with the zero-force and zero-torque conditions of the over-damped Stokes-regime

$$0 = F_i = \int_0^S ds \left\| \frac{d\hat{\mathbf{C}}(s)}{ds} \right\| f_i(s), \quad (5.107)$$

$$0 = \tau_i = \int_0^S ds \left\| \frac{d\hat{\mathbf{C}}(s)}{ds} \right\| \epsilon_{ijk} [C_j(s) - X_j^*] f_k(s), \quad (5.108)$$

⁹For quasi-2D motions along the surface, the contact angle θ_ϵ remains constant and, hence, $\dot{\mathcal{R}}_x = 0$.

with \mathbf{X}^* denoting the center of rotation, yields a 6×6 -linear system which could be solved to obtain exact RFT- results for \mathbf{U} and $\dot{\mathbf{N}}$. However, the resulting expressions are very complicated and do not offer much insight. Fortunately, it is possible to obtain simple analytical formulas for \mathbf{U} and $\dot{\mathbf{N}}$, that capture the essential parts of their dynamics, by focussing on the two limit cases $\mathbf{U} \gg \dot{\mathcal{R}}_{\mathbf{N}} \cdot \hat{\mathbf{C}}$ (translation-dominated regime) and $\mathbf{U} \ll \dot{\mathcal{R}}_{\mathbf{N}} \hat{\mathbf{C}}$ (rotation-dominated regime).

To estimate \mathbf{U} , note that steric interactions between flagellum and channel wall compensate drag forces in vertical directions, so that only the (x, y) -components of the velocity are non-zero. Considering the translation-dominated regime $\mathbf{U} \gg \dot{\mathcal{R}}_{\mathbf{N}} \cdot \hat{\mathbf{C}}$, the zero-force conditions (5.108) in the (x, y) -directions, $F_1 = 0$ and $F_2 = 0$, can be solved for $\mathbf{U} = (U_x, U_y)$. After averaging over ϕ with a uniform angular distribution, we find for $\epsilon \ll 1$ and $\kappa \simeq 1$ to leading order¹⁰

$$\mathbf{U} \simeq \frac{1}{2}\epsilon\sigma\dot{\gamma}\lambda S \begin{pmatrix} 0 \\ 1 \end{pmatrix} - \frac{\chi}{3}\epsilon^2(\kappa - 1)\sigma\dot{\gamma}\lambda S^2 \begin{pmatrix} 0 \\ N_x N_y \end{pmatrix}, \quad (5.109)$$

where $\Lambda \simeq S\lambda$ is the approximate length of the flagellum. The first term is the mean drag on the geometric center of the conical helix, and the second is an orientation-dependent drag contribution due to chirality χ . For passive chiral objects, such as dead bacterial cells, both terms can be important, although the first term is likely more relevant for self-swimming sperm cells. For completeness, we mention that the leading-order transverse-drag term (not shown) appears at next order in $(\kappa - 1)$ and is found to be proportional to $-\chi\sigma(\kappa - 1)^2\epsilon^2 S^2 \dot{\gamma}\lambda$.

Guided by Eq. (5.109), we simulate the position dynamics of sperm cells that swim at self-swimming speed V in the direction of their 2D orientation \mathbf{N} by implementing a minimal dynamics of the form

$$\dot{\mathbf{R}} = V\mathbf{N} + \mathbf{U} = V\mathbf{N} + \sigma\dot{\gamma}\epsilon\eta \begin{pmatrix} 0 \\ 1 \end{pmatrix}, \quad (5.110)$$

where $\eta > 0$ is a geometric prefactor with dimensions of length. Neglecting the translational chirality-effects in Eq. (5.110) is indeed a reasonable approximation since, for sufficiently fast sperm cells, the beat chirality acts predominantly through the rotation dynamics of \mathbf{N} , which becomes amplified by multiplication with V in Eq. (5.110).

To obtain an equation of motion for $\dot{\mathbf{N}}$, we first remark that due to conservation of $|\mathbf{N}|^2 = 1$, the dynamics of the components \dot{N}_x and \dot{N}_y are coupled by

$$0 = |\dot{\mathbf{N}}|^2 = 2(N_x\dot{N}_x + N_y\dot{N}_y). \quad (5.111)$$

¹⁰The first term in Eq. (5.109) could also have been obtained by simply computing the mean drag velocity

$$\bar{\mathbf{u}} = \frac{1}{2\pi} \int_0^{2\pi} d\phi \left[\frac{1}{\Lambda} \int_0^S ds \left\| \frac{d\hat{\mathbf{C}}(s)}{ds} \right\| \mathbf{u}(\mathbf{C}(s)) \right].$$

Thus, only one of the three zero-torque conditions (5.108) is needed to determine both \dot{N}_x and \dot{N}_y . For sperm swimming next to a solid surface, only rotations parallel to the surface are possible and, therefore, the relevant condition is $\tau_3 = 0$. Whilst a passive helix would rotate around its center of mass, the rotation axis is shifted towards the head position \mathbf{R} for real sperm cells due to the presence of the cell head, which has been omitted thus far in our discussion of the rigid-spiral model. To account at least partially for the influence of the head on the rotation dynamics, we approximate $\mathbf{X}^* \simeq (\mathbf{R}, 0)$ in Eq. (5.108) and focus on the rotation dominated regime, $\mathbf{U} \ll \mathcal{R}_N \cdot \hat{\mathbf{C}}$. Adopting these simplifications and averaging over ϕ , one finds for small $\epsilon \ll 1$ from the vanishing τ_3 -component of Eq. (5.108) the leading order result

$$\dot{\psi} = \epsilon \dot{\gamma} \sigma \sin \psi + \frac{\chi}{4} \epsilon^2 \frac{\kappa - 1}{\kappa} \dot{\gamma} \sigma S \cos \psi. \quad (5.112)$$

Recalling that $\mathbf{N} = (N_x, N_y) = (-\sin \psi, \cos \psi)$, this can be rewritten as

$$\dot{\mathbf{N}} = \sigma \dot{\gamma} \epsilon \begin{pmatrix} N_x N_y \\ N_y^2 - 1 \end{pmatrix} + \frac{\chi}{4} \epsilon^2 \frac{\kappa - 1}{\kappa} \dot{\gamma} \sigma S \begin{pmatrix} N_x^2 - 1 \\ N_x N_y \end{pmatrix}. \quad (5.113)$$

The first term represents alignment against the flow due to the conical shape of the flagellar envelope, in agreement with Eq. (5.88). The second term describes chirality-induced deviations from exact anti-alignment, leading to a non-vanishing transversal velocity component, as observed in the experiments.

We may now summarize the quasi-2D model. Assuming as before that the shear flow is along the y -axis (Fig. 5.2B), Eqs. (5.110) and (5.113) imply the following minimal 2D model for the quasi-2D motion of a sperm with position $\mathbf{R}(t) = (X(t), Y(t))$ and orientation $\mathbf{N}(t) = (N_x(t), N_y(t))$ in the vicinity of the surface

$$\dot{\mathbf{R}} = V \mathbf{N} + \sigma \bar{U} \mathbf{e}_y, \quad (5.114a)$$

$$\dot{\mathbf{N}} = \sigma \dot{\gamma} \alpha \begin{pmatrix} N_x N_y \\ N_y^2 - 1 \end{pmatrix} + \sigma \dot{\gamma} \chi \beta \begin{pmatrix} N_x^2 - 1 \\ N_x N_y \end{pmatrix} + (2D)^{1/2} (\mathbf{I} - \mathbf{N} \mathbf{N}) \cdot \boldsymbol{\xi}(t). \quad (5.114b)$$

Here, $V > 0$ is the self-swimming speed, $\sigma = \pm 1$ defines the flow direction, $\dot{\gamma} > 0$ is the shear rate, $\bar{U} > 0$ the mean flow speed experienced by the cell, and $\chi \in \{0, \pm 1\}$ the beat chirality. The dimensionless geometry parameters $\alpha > 0, \beta > 0$ encode details of the shape of the flagellar beat, and the coefficient D determines the strength of the two-dimensional Gaussian white noise $\boldsymbol{\xi}$, interpreted here in the Stratonovich-sense and included to account for variability in sperm swimming.

Clearly, the model of a rigid conical helix, as discussed here, is a relatively crude approximation to the full swimming dynamics of a sperm cell, for it neglects dynamical aspects of the flagellar beat (exact wave form, etc.) as well as hydrodynamic effects due to translation and rotation of the cell's head. Notwithstanding, on time scales larger than the typical beat period, Eqs. (5.114) provides a useful coarse-grained description of sperm swimming near a surface, as the model captures the main symmetries of the problem [KDBG14].

Chapter 6

Network models

6.1 Graphs

Many biological systems and their interactions can be represented through graphs. Examples include, but are not restricted to, gene regulatory networks, phylogenetic trees, cytoskeletal networks, mucus, neuronal networks and hydrodynamic transport systems in plants and mammals. In this part, we survey basic mathematical concepts to describe and characterize graphs and transport on them. A main idea is to represent a network through suitable matrices and to relate their spectral characteristics to the properties of the underlying graph.¹

6.1.1 Basic definitions

A graph is collection $\mathcal{G} = (V, E)$ of vertices $V = \{v_1, v_2\}$ and edges $E = \{e_1, e_2, \dots\}$. We denote by $|V|$ and $|E|$ the number of vertices and edges, respectively. Undirected edges can be identified with disordered pairs of vertices, e.g., $e_1 = (v_1, v_2) = (v_2, v_1)$. A *simple* graph is an undirected graph that has no loops and at most one edge between any two vertices (Fig. 6.1a,b). A simple *undirected graph* with $|V|$ vertices can have at most $|E| = |V|(|V| - 1)/2$ edges; in this case the graph is called *complete* (Fig. 6.1b). A *directed graph* or *digraph* is collection $\vec{\mathcal{G}} = (V, \vec{E})$ of vertices $V = \{v_1, v_2\}$ and ordered edges $\vec{E} = \{\vec{e}_1, \vec{e}_2, \dots\}$, such that for example $\vec{e}_1 = (v_1, v_2) \neq (v_2, v_1)$ (Fig. 6.1c).

A *planar* graph is a graph that can be embedded in the plane in such a way that its edges intersect only at their endpoints. That is, a planar graph can be drawn in such a way that no edges cross each other (Fig 6.2). The *dual graph* \mathcal{G}^* of a plane graph \mathcal{G} is a graph that has a vertex corresponding to each face of \mathcal{G} , and an edge joining two neighboring faces for each edge in \mathcal{G} (Fig 6.2d). If \mathcal{G} is connected and \mathcal{G}^* is dual to \mathcal{G} , then \mathcal{G} is also dual to \mathcal{G}^* , $(\mathcal{G}^*)^* = \mathcal{G}$.

¹For a more detailed introduction, we refer to Dan Spielman's course on Spectral Graph Theory <http://www.cs.yale.edu/homes/spielman/561/>.

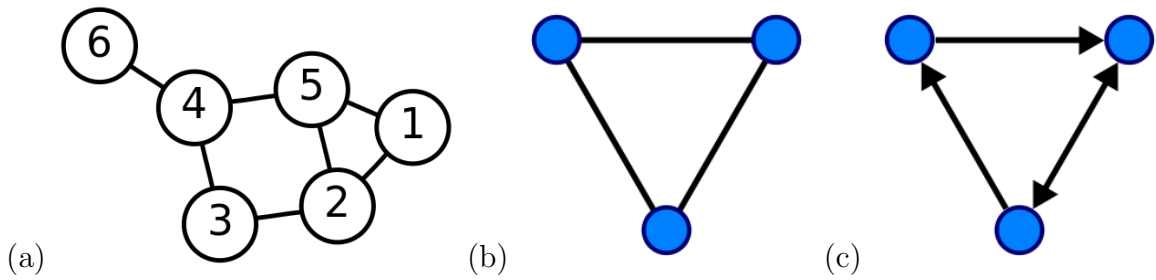


Figure 6.1: (a) Graph with six vertices and 7 edges. (b) Complete undirected graph. (c) Directed graph. Image source: wiki.

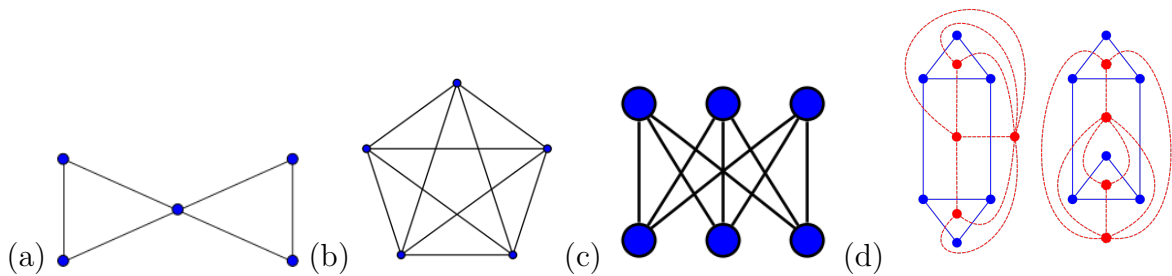


Figure 6.2: Planar, non-planar and dual graphs. (a) Plane ‘butterfly’ graph. (b, c) Non-planar graphs. (d) The two red graphs are both dual to the blue graph but they are not isomorphic. Image source: wiki.

Given a graph \mathcal{G} , its *line graph* or *derivative* $\mathcal{L}[\mathcal{G}]$ is a graph such that (i) each vertex of $\mathcal{L}[\mathcal{G}]$ represents an edge of \mathcal{G} and (ii) two vertices of $\mathcal{L}[\mathcal{G}]$ are adjacent if and only if their corresponding edges share a common endpoint (‘are incident’) in \mathcal{G} (Fig. ??). This construction can be iterated to obtain higher-order line (or derivative) graphs.

6.1.2 Adjacency and incidence

Adjacency matrix Two vertices v_1 and v_2 of a graph are called *adjacent*, if they are connected by an edge. The adjacency matrix $\mathbf{A}(\mathcal{G}) = (A_{ij})$ is a $|V| \times |V|$ -matrix that lists all the connections in a graph. If the graph is simple, then \mathbf{A} is symmetric and has only entries 0 or 1. For example, for the graph in Fig. 6.3a, we have

$$\mathbf{A} = \begin{pmatrix} 0 & 1 & 1 & 1 & 0 \\ 1 & 0 & 0 & 0 & 1 \\ 1 & 0 & 0 & 1 & 0 \\ 1 & 0 & 1 & 0 & 1 \\ 0 & 1 & 0 & 1 & 0 \end{pmatrix} \quad (6.1)$$

If the graph is simple, then the diagonal elements of \mathbf{A} are zero.

The column (row) sum defines the *degree* (connectivity) of the vertex

$$\deg(v_i) = \sum_j A_{ij} \quad (6.2)$$

and the volume of the graph is given by

$$\text{vol}(\mathcal{G}) = \sum_V \deg(v_i) = \sum_{ij} A_{ij} \quad (6.3)$$

The degree matrix $\mathbf{D}(\mathcal{G})$ is defined as the diagonal matrix

$$\mathbf{D}(\mathcal{G}) = \text{diag}(\deg(v_1), \dots, \deg(v_{|V|})) \quad (6.4)$$

For the graph in Fig. 6.3a, one has

$$\mathbf{D} = \begin{pmatrix} 3 & 0 & 0 & 0 & 0 \\ 0 & 2 & 0 & 0 & 0 \\ 0 & 0 & 2 & 0 & 0 \\ 0 & 0 & 0 & 3 & 0 \\ 0 & 0 & 0 & 0 & 2 \end{pmatrix} \quad (6.5)$$

The degree distribution is an important characteristics of random graphs, and we will return to this topic further below.

If the graph is directed, we may still define a signed adjacency matrix $\vec{\mathbf{A}}$ with elements

$$\vec{A}_{ij} = \begin{cases} -1, & \text{if edge goes from } v_i \text{ to } v_j \\ +1, & \text{if edge goes from } v_j \text{ to } v_i \\ 0, & \text{otherwise} \end{cases} \quad (6.6)$$

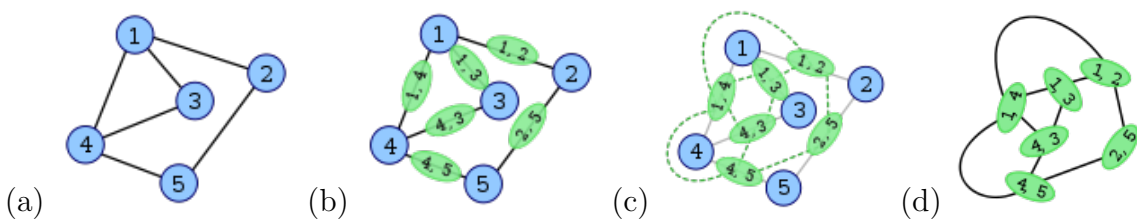


Figure 6.3: Construction of a line graph. These figures show a graph (a, with blue vertices) and its line graph (d, with green vertices). Each vertex of the line graph is shown labeled with the pair of endpoints of the corresponding edge in the original graph. For instance, the green vertex on the right labeled 1,3 corresponds to the edge on the left between the blue vertices 1 and 3. Green vertex 1,3 is adjacent to three other green vertices: 1,4 and 1,2 (corresponding to edges sharing the endpoint 1 in the blue graph) and 4,3 (corresponding to an edge sharing the endpoint 3 in the blue graph). Image and text source: wiki.

The *characteristic polynomial of a graph* is defined as the characteristic polynomial of the adjacency matrix

$$p(\mathcal{G}; x) = \det(\mathbf{A} - x\mathbf{I}) \quad (6.7)$$

For the graph in Fig. 6.3a, we find

$$p(\mathcal{G}; x) = -x(4 - 2x - 6x^2 + x^4) \quad (6.8)$$

Characteristic polynomials are *not* diagnostic for graph isomorphism, i.e., two nonisomorphic graphs may share the same characteristic polynomial.

Incidence matrix The incidence matrix \mathbf{C} of graph \mathcal{G} is a $|V| \times |E|$ -matrix with $C_{is} = 1$ if edge v_i is contained in edge e_s , and $C_{is} = 0$ otherwise. For the graph in Fig. 6.3a, with $i = 1, \dots, 5$ vertices and $s = 1, \dots, 6$ edges, we have

$$\mathbf{C} = \begin{pmatrix} 1 & 1 & 1 & 0 & 0 & 0 \\ 1 & 0 & 0 & 1 & 0 & 0 \\ 0 & 1 & 0 & 0 & 1 & 0 \\ 0 & 0 & 1 & 0 & 1 & 1 \\ 0 & 0 & 0 & 1 & 0 & 1 \end{pmatrix} \quad (6.9)$$

The incidence matrix $\mathbf{C}(\mathcal{G})$ of a graph \mathcal{G} and the *adjacency matrix* $A(\mathcal{L}[\mathcal{G}])$ of its *line graph* $\mathcal{L}[\mathcal{G}]$ are related by

$$\mathbf{A}(\mathcal{L}[\mathcal{G}]) = \mathbf{C}(\mathcal{G})^\top \cdot \mathbf{C}(\mathcal{G}) - 2\mathbf{I} \quad \Leftrightarrow \quad A(\mathcal{L}[\mathcal{G}])_{rs} = C_{ir}C_{is} - 2\delta_{rs} \quad (6.10)$$

For the example in Fig. 6.3, we thus find

$$\mathbf{A}(\mathcal{L}[\mathcal{G}]) = \begin{pmatrix} 0 & 1 & 1 & 1 & 0 & 0 \\ 1 & 0 & 1 & 0 & 1 & 0 \\ 1 & 1 & 0 & 0 & 1 & 1 \\ 1 & 0 & 0 & 0 & 0 & 1 \\ 0 & 1 & 1 & 0 & 0 & 1 \\ 0 & 0 & 1 & 1 & 1 & 0 \end{pmatrix} \quad (6.11)$$

yielding the characteristic polynomial

$$p(\mathcal{L}[\mathcal{G}]; x) = (x + 2)(x^2 + x - 1)[(x - 3)x^2 - x + 2] \quad (6.12)$$

Directed incidence matrix In addition to the undirected incidence matrix \mathbf{C} , we still define a directed $|V| \times |E|$ -matrix $\vec{\mathbf{C}}$ as follows

$$\vec{C}_{is} = \begin{cases} -1, & \text{if edge } e_s \text{ departs from } v_i \\ +1, & \text{if edge } e_s \text{ arrives at } v_i \\ 0, & \text{otherwise} \end{cases} \quad (6.13)$$

For undirected graphs, the assignment of the edge direction is arbitrary – we merely have to ensure that the columns $s = 1, \dots, |E|$ of $\vec{\mathbf{C}}$ sum to 0. For the graph in Fig. 6.3a, one finds

$$\vec{\mathbf{C}} = \begin{pmatrix} -1 & -1 & -1 & 0 & 0 & 0 \\ 1 & 0 & 0 & -1 & 0 & 0 \\ 0 & 1 & 0 & 0 & -1 & 0 \\ 0 & 0 & 1 & 0 & 1 & -1 \\ 0 & 0 & 0 & 1 & 0 & 1 \end{pmatrix} \quad (6.14)$$

6.1.3 Laplacian

The $|V| \times |V|$ -Laplacian matrix $\mathbf{L}(\mathcal{G})$ of a graph \mathcal{G} , often also referred to as Kirchhoff matrix, is defined as the difference between degree matrix and adjacency matrix

$$\mathbf{L} = \mathbf{D} - \mathbf{A} \quad (6.15a)$$

Hence

$$L_{ij} = \begin{cases} \deg(v_i), & \text{if } i = j \\ -1, & \text{if } v_i \text{ and } v_j \text{ are connected by edge} \\ 0, & \text{otherwise} \end{cases} \quad (6.15b)$$

As we shall see below, this matrix provides an important characterization of the underlying graph.

The $|V| \times |V|$ -Laplacian matrix can also be expressed in terms of the *directed* incidence matrix $\vec{\mathbf{C}}$, as

$$\mathbf{L} = \vec{\mathbf{C}} \cdot \vec{\mathbf{C}}^\top \quad \Leftrightarrow \quad L_{ij} = \vec{C}_{ir} \vec{C}_{jr} \quad (6.16)$$

For the graph in Fig. 6.3a, one finds

$$\mathbf{L} = \begin{pmatrix} 3 & -1 & -1 & -1 & 0 \\ -1 & 2 & 0 & 0 & -1 \\ -1 & 0 & 2 & -1 & 0 \\ -1 & 0 & -1 & 3 & -1 \\ 0 & -1 & 0 & -1 & 2 \end{pmatrix} \quad (6.17)$$

Properties We denote the eigenvalues of \mathbf{L} by

$$\lambda_0 \leq \lambda_1 \leq \dots \leq \lambda_{|V|} \quad (6.18)$$

The following properties hold:

- (i) \mathbf{L} is symmetric.

- (ii) \mathbf{L} is positive-semidefinite, that is $\lambda_i \geq 0$ for all i .
- (iii) Every row sum and column sum of \mathbf{L} is zero.²
- (iv) $\lambda_0 = 0$ as the vector $\mathbf{v}_0 = (1, 1, \dots, 1)$ satisfies $\mathbf{L} \cdot \mathbf{v}_0 = \mathbf{0}$.
- (v) The multiplicity of the eigenvalue 0 of the Laplacian equals the number of connected components in the graph.
- (vi) The smallest non-zero eigenvalue of \mathbf{L} is called the spectral gap.
- (vii) For a graph with multiple connected components, \mathbf{L} can be written as a block diagonal matrix, where each block is the respective Laplacian matrix for each component.

Normalized Laplacian The associated normalized Laplacian $\bar{\mathbf{L}}(\mathcal{G})$ is defined as

$$\bar{\mathbf{L}} = \mathbf{D}^{-1/2} \cdot \mathbf{L} \cdot \mathbf{D}^{-1/2} = \mathbf{I} - \mathbf{D}^{-1/2} \cdot \mathbf{A} \cdot \mathbf{D}^{-1/2} \quad (6.19a)$$

with elements

$$\bar{L}_{ij} = \begin{cases} 1, & \text{if } i = j \text{ and } \deg(v_i) \neq 0 \\ -1/\sqrt{\deg(v_i) \deg(v_j)}, & \text{if } i \neq j \text{ and } v_i \text{ and } v_j \text{ are connected by edge} \\ 0, & \text{otherwise} \end{cases} \quad (6.19b)$$

One can write $\bar{\mathbf{L}}(\mathcal{G})$ as, cf. Eq. (6.16),

$$\bar{\mathbf{L}}(\mathcal{G}) = \vec{\mathbf{B}} \cdot \vec{\mathbf{B}}^\top \quad (6.20a)$$

where $\vec{\mathbf{B}}$ is an $|V| \times |E|$ -matrix where

$$\vec{B}_{is} = \begin{cases} -1/\sqrt{\deg(v_i)}, & \text{if edge } e_s \text{ departs from } v_i \\ +1/\sqrt{\deg(v_i)}, & \text{if edge } e_s \text{ arrives at } v_i \\ 0, & \text{otherwise} \end{cases} \quad (6.20b)$$

A ‘0-chain’ is a real-valued vertex function $g : V \rightarrow \mathbb{R}$, and a ‘1-chain’ is a real-valued edge function $E \rightarrow \mathbb{R}$. Then $\vec{\mathbf{B}} = (\vec{B}_{is})$ can be viewed as *boundary operator* that maps 1-chains onto 0-chains, while the transposed matrix $\vec{\mathbf{B}}^\top = (\vec{B}_{si})$ is a *co-boundary operator* that maps 0-chains onto 1-chains. Accordingly $\bar{\mathbf{L}}$ can be viewed as an operator that maps a vertex functions \mathbf{g} , which can be viewed as $|V|$ -dimensional column vector, onto another vertex function $\bar{\mathbf{L}} \cdot \mathbf{g}$, such that

$$(\bar{\mathbf{L}} \cdot \mathbf{g})(v_i) = \frac{1}{\sqrt{\deg(v_i)}} \sum_{v_j \sim v_i} \left[\frac{g(v_i)}{\sqrt{\deg(v_i)}} - \frac{g(v_j)}{\sqrt{\deg(v_j)}} \right] \quad (6.21)$$

²The degree of the vertex is summed with a -1 for each neighbor

where $v_j \sim v_i$ denotes the set of adjacent nodes.

We denote the eigenvalues of $\overline{\mathbf{L}}$ by

$$0 = \bar{\lambda}_0 \leq \bar{\lambda}_1 \leq \dots \leq \bar{\lambda}_{|V|-1} \quad (6.22)$$

Abbreviating $n = |V|$, one can show that

- (i) $\sum_i \bar{\lambda}_i \leq n$ with equality iff \mathcal{G} has no isolated vertices.
- (ii) $\bar{\lambda}_1 \leq n/(n-1)$ with equality iff \mathcal{G} is the complete graph on $n \geq 2$ vertices.
- (iii) If $n \geq 2$ and \mathcal{G} has no isolated vertices, then $\bar{\lambda}_{n-1} \geq n/(n-1)$.
- (iv) If \mathcal{G} is not complete, then $\bar{\lambda}_1 \leq 1$.
- (v) If \mathcal{G} is connected, then $\bar{\lambda}_1 > 0$.
- (vi) If $\bar{\lambda}_i = 0$ and $\bar{\lambda}_{i+1} > 0$, then \mathcal{G} has exactly $i+1$ connected components.
- (vii) For all $i \leq n-1$, we have $\bar{\lambda}_i \leq 2$, with $\bar{\lambda}_{n-1} = 2$ iff a connected component of \mathcal{G} is bipartite and nontrivial.
- (viii) The spectrum of a graph is the union of the spectra of its connected components.

See Chapter 1 in [Chu97] for proofs.

Examples:

- For a complete graph K_n on $n \geq 2$ vertices, the eigenvalues are 0 (multiplicity 1) and $n/(n-1)$ (multiplicity $n-1$)
- For a complete bipartite graph $K_{m,n}$ on $m+n$ vertices, the eigenvalues are 0 and 1 (multiplicity $m+n-2$) and 2.
- For the star S_n on $n \geq 2$ vertices, the eigenvalues are 0 and 1 (multiplicity $n-2$) and 2.
- For the path P_n on $n \geq 2$ vertices, the eigenvalues are $\bar{\lambda}_k = 1 - \cos[\pi k/(n-1)]$ for $k = 0, \dots, n-1$.
- For the cycle C_n on $n \geq 2$ vertices, the eigenvalues are $\bar{\lambda}_k = 1 - \cos[2\pi k/n]$ for $k = 0, \dots, n-1$.
- For the n -cube Q_n on 2^n vertices, the eigenvalues are $\bar{\lambda}_k = 2k/n$, with multiplicity $\binom{n}{k}$ for $k = 0, \dots, n$.

6.2 Trees and Kirchhoff's theorem

Definitions and basic properties A tree is connected undirected simple graph without cycles. Nodes with only one adjacent vertex are called leaves. A star graph is a tree which consists of a single internal vertex (and $n-1$ leaves), i.e., a star graph is with as many leaves as possible. A *forest* is a disjoint union of trees. A directed tree is a directed graph that would be a tree if edge directions are dropped.

Cayley's formula states that there are

$$t(n) = n^{n-2} \quad (6.23)$$

trees on n labeled vertices. For n unlabeled vertices only asymptotic estimates exist

$$t_u(n) = C a^n n^{-5/2}, \quad n \rightarrow \infty \quad (6.24)$$

where $C \simeq 0.5349 \dots$ and $a \simeq 2.9557 \dots$

We summarize a few properties:

- Every tree is a bipartite graph.
- Every connected graph \mathcal{G} admits a *spanning tree*, which is a tree that contains every vertex of \mathcal{G} and whose edges are edges of \mathcal{G} .
- Every finite tree with $n > 1$ vertices has at least two terminal vertices (leaves).
- For any three vertices in a tree, the three paths between them have exactly one vertex in common.

Kirchhoff's theorem A *spanning tree* is a tree that contains every vertex of \mathcal{G} and whose edges are edges of \mathcal{G} . That is, spanning trees are obtained by successively deleting edges from a graph in such a manner that all cycles are resolved but the connectivity remains intact. Kirchhoff's theorem answers the question how many spanning trees a given graph \mathcal{G} permits. Specifically, the theorem states that, for a simple connected graph with $n = |V|$ vertices and non-zero Laplacian eigenvalues $\lambda_1, \dots, \lambda_{n-1}$, the number $t(n)$ of spanning trees is given by the normalized product of those eigenvalues

$$t(n) = \frac{1}{n} \lambda_1 \cdots \lambda_{n-1}. \quad (6.25)$$

Finding an optimal spanning tree for a weighted network is a commonly encountered optimization problem, e.g., if one wants to lay pipes or communication cables along a preexisting road network such that all vertices are connected at a minimal cost. Note, however, that trees are not robust as deleting a single edge disconnects the tree.

6.3 Transport

6.3.1 Max-Flow Min-Cut

Capacity and flow Consider a directed network $\vec{\mathcal{G}} = (V, \vec{E})$ with $|V| = n + 2$ vertices labelled v_0, \dots, v_n . We identify the first node as a source, $s = v_0$, and the last node as the ‘terminal’ sink $t = v_n$.

The *edge capacity* is a map $c : \vec{E} \rightarrow \mathbb{R}_+$, corresponding to an $|E|$ -dimensional vector $\mathbf{c} = (c_r) = (c(v_i, v_j))$. Similarly, the *flow* is a map $f : \vec{E} \rightarrow \mathbb{R}_+$, corresponding to an $|E|$ -dimensional vector $\mathbf{f} = (f_r) = (f(v_i, v_j))$.

We assume that transport through the network satisfies the capacity constraint

$$f_r \leq c_r, \quad \forall r = 1, \dots, |E| \quad (6.26a)$$

as well as the flow (‘mass’) conservation constraint

$$\sum_{u:(u,v) \in \vec{E}} f(u, v) = \sum_{u:(v,u) \in \vec{E}} f(v, u), \quad \forall v \in \{v_1, \dots, v_{n-1}\} \quad (6.26b)$$

The *value of flow* is defined as the total input entering through the source

$$|\mathbf{f}| = \sum_{u:(s,u) \in \vec{E}} f(s, u) \quad (6.27)$$

where $s = v_0$ is the source.

Max-Flow problem Maximize $|\mathbf{f}|$ for a given a capacity \mathbf{c} ; that is, to route as much flow as possible from source s to sink t .

Min-Cut An s - t cut $C = (V_s, V_t)$ is a partition of V such that $s \in V_s$ and $t \in V_t$. The *cut-set* of C is the set of edges connecting from V_s to V_t

$$\vec{E}_C = \{(v_i, v_j) \in \vec{E} : v_i \in V_s, v_j \in V_t\} \quad (6.28)$$

These are the edges that are deleted during the cutting procedure.

The capacity of the s - t cut is defined as

$$c_{s,t} = \sum_{\vec{E}_c} c(v_i, v_j) \quad (6.29)$$

Min-Cut problem Minimize $c_{s,t}$; that is, to determine V_s and V_t such that the capacity of the cut is minimal.

Max-Flow Min-Cut Theorem The maximum value of an s - t flow is equal to the minimum capacity over all s - t cuts.

Appendix A

Stochastic integrals and calculus

This appendix summarizes the most commonly considered stochastic integral definitions and the corresponding rules of stochastic calculus. For a more rigorous and comprehensive introduction, we refer to, e.g., Refs. [KS91, Gri02, Gar02, RF96].

We consider a Wiener process (standard Brownian motion) $B(t)$ as defined in Section 1.2.1; i.e., the increments $dB(t) := B(t + dt) - B(t)$ are stochastically independent [KS91, Gri02] and characterized by the Gaussian distribution

$$\mathbb{P}\{dB(t) \in [y, y + dy]\} = (2\pi dt)^{-1/2} \exp[-y^2/(2dt)] dy. \quad (\text{A.1})$$

We are interested in defining integrals of the form

$$I = \int_0^t f(Y(s)) \odot dB(s), \quad (\text{A.2})$$

where $f(y)$ is some real-valued function, $Y(s)$ a real-valued time-dependent process, and \odot signals different discretization rules to be discussed below. If $B(s)$ were some ordinary differentiable function of $s \in [0, t]$, then the integral in Eq. (A.2) would simply be given by¹

$$I = \int_0^t f(Y(s)) \dot{B}(s) ds, \quad (\text{A.3})$$

where $\dot{B} = dB/ds$. Unfortunately, $\dot{B}(s)$ is not well-defined for the Wiener process [Gar02, KS91], but it is possible to generalize the concept of integration to also include the Wiener process as well as other stochastic processes [KS91, Gri02, Gar02]. However, in contrast to the standard Riemann-Stieltjes integral (A.3), the integral with respect to a stochastic process may depend on the choice of the discretization scheme \odot and, in particular, also require modifications of differential calculus.

¹By writing Eq. (A.3), it is implicitly assumed that $f(y)$, Y and \dot{B} are sufficiently smooth functions so that this integral exists in the sense of Riemann-Stieltjes; in this case, the value of the integral (A.3) is independent of the underlying discretization scheme [Gri02].

To illustrate these aspects for the most commonly considered stochastic integral definitions, we will always consider the following equidistant partition $\{t_0, t_1, \dots, t_N\}$ of the time interval $[0, t]$:

$$\Delta t = t_k - t_{k-1} = t/N, \quad k = 1, \dots, N, \quad t_0 = 0, \quad t_N = t. \quad (\text{A.4})$$

A.1 Ito integral

We first summarize the properties of Ito's stochastic integral [Ito44, Ito51]. Its relationship to other stochastic integrals is discussed in Section A.4.

A.1.1 One-dimensional case

The Ito stochastic integral of some real-valued function $f(Y(t))$ with respect to a standard Brownian motion process $B(t)$ over the time-interval $[0, t]$ can be defined by

$$\int_0^t f(Y(s)) * dB(s) := \lim_{N \rightarrow \infty} \sum_{k=0}^{N-1} f(Y(t_k)) [B(t_{k+1}) - B(t_k)], \quad (\text{A.5})$$

where the partition $\{t_0, \dots, t_N\}$ is given by (A.4). The peculiar, defining feature of this integral is that, on the rhs. of Eq. (A.5), the argument of the function f must be evaluated at the lower boundary points t_k of the discrete intervals $[t_k, t_{k+1}]$; i.e., the definition of the Ito integral is *non-anticipatory*. Accordingly, the Ito discretization scheme is also known as the *pre-point* rule.

Now consider a stochastic process $Y(t)$ which, for two given functions $A(y)$ and $C(y)$, is defined by

$$Y(t) = Y(0) + \int_0^t A(Y(s)) ds + \int_0^t C(Y(s)) * dB(s), \quad (\text{A.6})$$

and where the last term is interpreted as an Ito integral (A.5). Stochastic integral equations like Eq. (A.6) are usually abbreviated by rewriting them as an Ito *stochastic differential equation* (I-SDE)

$$dY(t) = A(Y) dt + C(Y) * dB(t), \quad (\text{A.7})$$

complemented by the initial condition $Y(0)$. From the non-anticipatory definition (A.5) of the Ito integral and the properties of the Wiener process it follows that [Gar02]²

$$\mathbb{E}[C(Y) * dB(t) \mid Y(t) = y] = 0. \quad (\text{A.8})$$

² $\mathbb{E}[\cdot \mid Y(t) = y]$ denotes the conditional expectation with respect to the Gaussian measure of the Wiener process $B(t)$.

The Fokker-Planck equation for the PDF $f(t, y)$ of the stochastic process defined by Eq. (A.7) reads

$$\frac{\partial f}{\partial t} = \frac{\partial}{\partial y} \left[-Af + \frac{1}{2} \frac{\partial}{\partial y} (C^2 f) \right], \quad (\text{A.9})$$

where $A = A(y)$ and $C = C(y)$. A deterministic initial condition $Y(0) = y_0$ translates into $f(0, y) = \delta(y - y_0)$.

Finally, an important peculiarity arises when one considers nonlinear transformations G of the stochastic process $Y(t)$. More precisely, assuming that Y is defined by the I-SDE (A.7), then the differential change of the process $Z(t) := G(Y(t))$ is given by (see, e.g., Section 4.3.2 in [Gar02])

$$\begin{aligned} dZ(t) &= G'(Y) * dY + \frac{1}{2} C(Y)^2 G''(Y) dt \\ &= \left[A(Y) G'(Y) + \frac{1}{2} C(Y)^2 G''(Y) \right] dt + C(Y) G'(Y) * dB(t), \end{aligned}$$

where $G'(y) = dG(y)/dy$ and $G''(y) = d^2G(y)/dy^2$. Within ordinary differential calculus, the term containing G'' is absent. Equation (A.10) is usually referred to as *Ito formula*.

A.1.2 The n -dimensional case

Consider the n -dimensional stochastic process $\mathbf{Y}(t) = (Y^1(t), \dots, Y^n(t))$, defined by the following n -dimensional generalization of Eq. (A.7):

$$dY^i(t) = A^i(\mathbf{Y}) dt + C_r^i(\mathbf{Y}) * dB^r(t), \quad (\text{A.10})$$

where $i = 1, \dots, n$ and $r = 1, \dots, K$. In Eq. (A.10), the Wiener processes $B^r(t)$ represent K independent noise sources, and each term $C_r^i(\mathbf{Y}) * dB^r(t)$ symbolizes an Ito integral. The Fokker-Planck equation for the PDF $f(t, y^1, \dots, y^n)$ reads

$$\frac{\partial f}{\partial t} = \frac{\partial}{\partial y^i} \left[-A^i f + \frac{1}{2} \frac{\partial}{\partial y^j} (C_r^i C_r^j f) \right]. \quad (\text{A.11})$$

The generalized Ito-formula reads (see, e.g., Section 4.3.2 in [Gar02])

$$dG[\mathbf{Y}(t)] = \left[A^i \partial_i G + \frac{1}{2} C_r^i C_r^j \partial_i \partial_j G \right] dt + C_r^i \partial_i G * dB^r(t), \quad (\text{A.12})$$

where $\partial_i := \partial/\partial y^i$.

A.2 Stratonovich-Fisk integral

Next, we summarize the properties of an alternative stochastic integral definition proposed by Stratonovich [Str64, Str66, Str68] and Fisk [Fis63, Fis65]. In contrast to the non-anticipatory Ito integral, the Stratonovich-Fisk (SF) integral is *semi-anticipatory*, but satisfies the rules of ordinary stochastic calculus.

A.2.1 One-dimensional case

The SF stochastic integral of some real-valued function $f(Y(t))$ with respect to a standard Brownian (Wiener) motion process $B(t)$ over the time-interval $[0, t]$ can be defined by

$$\int_0^t f(Y(s)) \circ dB(s) := \lim_{N \rightarrow \infty} \sum_{k=0}^{N-1} \frac{1}{2} [f(Y(t_{k+1})) + f(Y(t_k))] \times [B(t_{k+1}) - B(t_k)], \quad (\text{A.13})$$

where the partition $\{t_0, \dots, t_N\}$ is given by (A.4). In contrast to Ito's integral (A.5), the SF definition (A.13) uses the mean of the boundary values of f on the intervals $[t_k, t_{k+1}]$; i.e., the definition of the SF integral is *semi-anticipatory*. This discretization scheme is also known as the *mid-point* rule.

Similar to Eq. (A.6), we may consider a stochastic process $Y(t)$ defined by

$$Y(t) = Y(0) + \int_0^t A(Y(s)) ds + \int_0^t C(Y(s)) \circ dB(s), \quad (\text{A.14})$$

where now the last term is interpreted as an SF integral (A.13). The integral equation (A.14) can be abbreviated in terms of the equivalent SF stochastic differential equation (SF-SDE)

$$dY(t) = A(Y) dt + C(Y) \circ dB(t), \quad (\text{A.15})$$

with initial condition $Y(0)$. From the semi-anticipatory definition (A.13) of the SF integral and the properties of the Wiener process it follows that [Gar02]

$$\mathbb{E}[C(Y) \circ dB(t) \mid Y(t) = y] = \frac{1}{2} C(y) C'(y) dt, \quad (\text{A.16})$$

where $C'(y) = dC(y)/dy$. The Fokker-Planck equation for the PDF $f(t, y)$ of the stochastic process (A.15) reads

$$\frac{\partial f}{\partial t} = \frac{\partial}{\partial y} \left[-A f + \frac{1}{2} C \frac{\partial}{\partial y} (C f) \right] \quad (\text{A.17})$$

where $A = A(y)$, and $C = C(y)$. The deterministic initial condition $Y(0) = y_0$ translates into $f(0, y) = \delta(y - y_0)$.

It can be shown [Gar02, Gri02] that the SF integral definition preserves the rules of ordinary stochastic calculus; i.e., if $Y(t)$ is defined by the SF-SDE (A.15), then the differential change of the process $Z(t) := G(Y(t))$ is given by (see, e.g., Section 4.3.2 in [Gar02])

$$\begin{aligned} dZ(t) &= G'(Y) \circ dY \\ &= A(Y) G'(Y) dt + C(Y) G'(Y) \circ dB(t), \end{aligned} \quad (\text{A.18})$$

where $G'(y) = dG(y)/dy$.

However, as will be discussed in Section A.4, for a given SF-SDE with sufficiently smooth coefficient functions A and C , one can always find an I-SDE that yields the same Fokker-Planck equation. Hence, in order to describe a certain physical process, one may choose that integral definition that is most convenient for the problem under consideration.

A.2.2 The n -dimensional case

Consider the n -dimensional stochastic process $\mathbf{Y}(t) = (Y^1(t), \dots, Y^n(t))$, defined by the following n -dimensional generalization of Eq. (A.15):

$$dY^i(t) = A^i(\mathbf{Y}) dt + C^i_r(\mathbf{Y}) \circ dB^r(t), \quad (\text{A.19})$$

where $i = 1, \dots, n$ and $r = 1, \dots, K$. In Eq. (A.19), the Wiener processes $B^r(t)$ represent K independent noise sources, and each term $C^i_r(\mathbf{Y}) \circ dB^r(t)$ symbolizes an SF integral. The Fokker-Planck equation for the PDF $f(t, y^1, \dots, y^n)$ reads

$$\frac{\partial f}{\partial t} = \frac{\partial}{\partial y^i} \left[- \left(A^i + \frac{1}{2} C^j_r \frac{\partial}{\partial y^j} C^i_r \right) f + \frac{1}{2} \frac{\partial}{\partial y^j} (C^i_r C^j_r f) \right], \quad (\text{A.20})$$

and the transformation rules of ordinary differential calculus apply.

A.3 Backward Ito integral

We still consider a third stochastic integral definition which is also known as the backward Ito (BI) integral [KS91, Jr.69]. Its relationship to the other stochastic integrals is discussed in Section A.4.

A.3.1 One-dimensional case

The BI stochastic integral of some real-valued function $f(Y(t))$ with respect to $B(t)$ over the time-interval $[0, t]$ can be defined by

$$\int_0^t f(Y(s)) \bullet dB(s) := \lim_{N \rightarrow \infty} \sum_{k=0}^{N-1} f(Y(t_{k+1})) [B(t_{k+1}) - B(t_k)], \quad (\text{A.21})$$

where the partition $\{t_0, \dots, t_N\}$ is given by (A.4). On the rhs. of Eq. (A.21), in contrast to the Ito and SF integrals, the argument of the function f must be evaluated at the upper boundary points t_{k+1} of the discrete intervals $[t_k, t_{k+1}]$; i.e., the definition of this integral is *anticipatory*. This discretization scheme is also known as the *post-point* rule.

Similar to above, we may consider a stochastic process $Y(t)$ which, for two given functions $A(y)$ and $C(y)$, is defined by

$$Y(t) = Y(0) + \int_0^t A(Y(s)) ds + \int_0^t C(Y(s)) \bullet dB(s), \quad (\text{A.22})$$

and where the last term is now interpreted as a BI integral (A.21). Equation (A.6) can be abbreviated by rewriting it as a backward Ito stochastic differential equation (BI-SDE)

$$dY(t) = A(Y) dt + C(Y) \bullet dB(t), \quad (\text{A.23})$$

complemented by the deterministic initial condition $Y(0)$. From the anticipatory definition (A.21) of the BI integral and the properties of the Wiener process it follows that [Gar02]

$$\mathbb{E}[C(Y) \bullet dB(t) \mid Y(t) = y] = C(y) C'(y) dt. \quad (\text{A.24})$$

The Fokker-Planck equation for the PDF $f(t, y)$ of the stochastic process defined by Eq. (A.23) reads

$$\frac{\partial f}{\partial t} = \frac{\partial}{\partial y} \left[-A f + \frac{1}{2} C^2 \frac{\partial}{\partial y} f \right], \quad (\text{A.25})$$

where $A = A(y)$ and $C = C(y)$. The deterministic initial condition $Y(0) = y_0$ translates into $f(0, y) = \delta(y - y_0)$.

It can be shown that, similar to the Ito integral, also the BI integral requires a modification of differential calculus. More precisely, assuming that Y is defined by the BI-SDE (A.23), the differential change of the process $Z(t) := G(Y(t))$ is given by

$$\begin{aligned} dZ(t) &= G'(Y) \bullet dY - \frac{1}{2} C(Y)^2 G''(Y) dt \\ &= \left[A(Y) G'(Y) - \frac{1}{2} C(Y)^2 G''(Y) \right] dt + C(Y) G'(Y) \bullet dB(t), \end{aligned} \tag{A.26}$$

where $G'(y) = dG(y)/dy$ and $G''(y) = d^2G(y)/dy^2$.

A.3.2 The n -dimensional case

Consider the n -dimensional stochastic process $\mathbf{Y}(t) = (Y^1(t), \dots, Y^n(t))$, defined by the following n -dimensional generalization of Eq. (A.23):

$$dY^i(t) = A^i(\mathbf{Y}) dt + C^i_r(\mathbf{Y}) \bullet dB^r(t), \tag{A.27}$$

where $i = 1, \dots, n$ and $r = 1, \dots, K$. In Eq. (A.27), the Wiener processes $B^r(t)$ represent K independent noise sources, and each term $C^i_r(\mathbf{Y}) \bullet dB^r(t)$ symbolizes a BI integral. The Fokker-Planck equation for the associated PDF $f(t, y^1, \dots, y^n)$ reads

$$\frac{\partial f}{\partial t} = \frac{\partial}{\partial y^i} \left[- \left(A^i + C^j_r \frac{\partial}{\partial y^j} C^i_r \right) f + \frac{1}{2} \frac{\partial}{\partial y^j} (C^i_r C^j_r f) \right]. \tag{A.28}$$

The generalized backward Ito-formula reads

$$dG[\mathbf{Y}(t)] = \left[A^i \partial_i G - \frac{1}{2} C^i_r C^j_r \partial_i \partial_j G \right] dt + C^i_r \partial_i G \bullet dB^r(t), \tag{A.29}$$

where $\partial_i := \partial/\partial y^i$.

A.4 Comparison of stochastic integrals

As anticipated in the preceding sections, the three different stochastic integrals/SDEs may be transformed into each other. In particular, a given Fokker-Planck equation can usually be realized by any of three SDE types, upon choosing the coefficient functions appropriately. To illustrate this by example, we reconsider the n -dimensional SDEs from above, assuming identical noise coefficients C^i_r but different drift coefficients $A^i_{*\circ\bullet}(\mathbf{Y})$, respectively, i.e.

$$dY^i(t) = A^i_*(\mathbf{Y}) dt + C^i_r(\mathbf{Y}) * dB^r(t), \tag{A.30a}$$

$$dY^i(t) = A^i_\circ(\mathbf{Y}) dt + C^i_r(\mathbf{Y}) \circ dB^r(t), \tag{A.30b}$$

$$dY^i(t) = A^i_\bullet(\mathbf{Y}) dt + C^i_r(\mathbf{Y}) \bullet dB^r(t), \tag{A.30c}$$

where $i = 1, \dots, n$ and $r = 1, \dots, K$. We would like to determine the drift coefficients such that these three different types of SDEs describe the same n -dimensional stochastic process $\mathbf{Y}(t) = (Y^1(t), \dots, Y^n(t))$ on the level of the Fokker-Planck equations³, which can be compactly summarized as follows

$$\frac{\partial f_\circ}{\partial t} = \partial_i \left[- (A_\circ^i + \lambda_\circ C_r^j \partial_j C_r^i) f_\circ + \frac{1}{2} \partial_j (C_r^i C_r^j f_\circ) \right], \quad (\text{A.31})$$

where $\partial_i := \partial/\partial y^i$, and $\lambda_* = 0$, $\lambda_\circ = 1/2$, and $\lambda_\bullet = 1$. We distinguish three cases:

- (i) **Eq. (A.30a) is given.** In this case, Eq. (A.31) implies that Eqs. (A.30b) and (A.30c) describe the same process as Eq. (A.30a), if we fix

$$A_\circ^i = A_*^i - \frac{1}{2} C_r^j \partial_j C_r^i, \quad A_\bullet^i = A_*^i - C_r^j \partial_j C_r^i. \quad (\text{A.32})$$

- (ii) **Eq. (A.30b) is given.** In this case, Eqs. (A.30a) and (A.30c) describe the same process as Eq. (A.30b), if we fix

$$A_*^i = A_\circ^i + \frac{1}{2} C_r^j \partial_j C_r^i, \quad A_\bullet^i = A_\circ^i - \frac{1}{2} C_r^j \partial_j C_r^i. \quad (\text{A.33})$$

- (iii) **Eq. (A.30c) is given.** In this case, Eqs. (A.30a) and (A.30b) describe the same process as Eq. (A.30c), if we fix

$$A_*^i = A_\bullet^i + C_r^j \partial_j C_r^i, \quad A_\circ^i = A_\bullet^i + \frac{1}{2} C_r^j \partial_j C_r^i. \quad (\text{A.34})$$

To summarize, by means of Eqs. (A.32), (A.33) and (A.34) one can change between the different forms of stochastic integration and stochastic differential calculus, respectively. Each SDE type has advantages and disadvantages: The Ito formalism is well suited for numerical simulations [RF96, KP06, Gla04] and yields a vanishing noise contribution to conditional expectations of the form (A.8). The Stratonovich-Fisk approach is more difficult to implement numerically, but preserves the rules of ordinary differential calculus (in contrast to Ito/backward Ito integration). Finally, within the backward Ito scheme, fluctuation dissipation relations may take a particularly elegant form (cf. Section 6.2 in Ref. [HT82], and Ref. [Kli94]).

A.5 Numerical integration

A detailed introduction to the numerical simulation of SDEs can be found in [RF96, KP06, Gla04]. A simple Monte-Carlo algorithm for numerically integrating Eqs. (A.30) follows

³For most practical purposes, two Markovian stochastic processes can be considered as physically equivalent if their PDFs are governed by the same Fokker-Planck equation.

directly from the definition of the stochastic integrals. The corresponding discretization scheme, which works sufficiently well for many purposes, reads

$$Y^i(t + \Delta t) - Y^i(t) = A_*^i(\mathbf{Y}(t)) \Delta t + C_r^i(\mathbf{Y}(t)) \Delta B^r(t), \quad (\text{A.35a})$$

$$Y^i(t + \Delta t) - Y^i(t) = A_\circ^i(\mathbf{Y}(t)) \Delta t +$$

$$\frac{1}{2}[C_r^i(\mathbf{Y}(t + \Delta t)) + C_r^i(\mathbf{Y}(t))] \Delta B^r(t),$$

$$Y^i(t + \Delta t) - Y^i(t) = A_\bullet^i(\mathbf{Y}(t)) \Delta t + C_r^i(\mathbf{Y}(t + \Delta t)) \Delta B^r(t). \quad (\text{A.35c})$$

Here, the $\Delta B^r(t)$ are random numbers, sampled from a Gaussian normal distribution with density

$$\mathbb{P}[\Delta B^r(t)] = \left(\frac{1}{2\pi\Delta t} \right)^{1/2} \exp \left\{ -\frac{[\Delta B^r(t)]^2}{2\Delta t} \right\}. \quad (\text{A.36})$$

As evident from Eqs. (A.35), for given functions A_*^i and C_r^i , the discretized I-SDE (A.35a) allows for calculating the values $Y^i(t + \Delta t)$ directly from the preceding values $Y^i(t)$. By contrast, the discretized SF-SDEs (A.35b) and BI-SDEs (A.35c) are implicit equations, which must be solved for $Y^i(t + \Delta t)$. The latter difficulty can be avoided by transforming a given SF/BI-SDE to the corresponding I-SDE by means of Eqs. (A.32), (A.33) and (A.34).

Appendix B

Swimming Velocity for Arbitrary Deformations

For the general case of a three-sphere swimmer based on the schematics in Fig. 1 of Ref. [GA07], Golestanian and Ajdari obtain the average swimming velocity to the leading order as

$$\begin{aligned}
V_0 = & \frac{(a_1 - a_2)(a_2 + a_3)}{3a_2(a_1 + a_2 + a_3)} \left[1 + \frac{3}{2} \left(\frac{a_1 a_2}{a_2 - a_1} \right) \left(\frac{1}{L_1 + L_2} - \frac{1}{L_2} \right) - 3 \left(\frac{a_2 a_3}{a_2 + a_3} \right) \frac{1}{L_2} \right. \\
& \left. + \frac{3}{a_1 + a_2 + a_3} \left(\frac{a_2 a_3}{L_2} + \frac{a_1 a_2}{L_1} + \frac{a_3 a_1}{L_1 + L_2} \right) \right] \dot{L}_1 \\
+ & \frac{a_3(a_1 - a_2)}{3a_2(a_1 + a_2 + a_3)} \left[1 + \frac{3}{2} \left(\frac{a_1 a_2}{a_2 - a_1} \right) \left(\frac{1}{L_1 + L_2} - \frac{1}{L_2} \right) - \frac{3}{2} \left(\frac{a_2}{L_1} + \frac{a_2}{L_2} - \frac{a_2}{L_1 + L_2} \right) \right. \\
& \left. + \frac{3}{a_1 + a_2 + a_3} \left(\frac{a_2 a_3}{L_2} + \frac{a_1 a_2}{L_1} + \frac{a_3 a_1}{L_1 + L_2} \right) \right] \dot{L}_2 \\
+ & \frac{a_1(a_2 - a_3)}{3a_2(a_1 + a_2 + a_3)} \left[1 + \frac{3}{2} \left(\frac{a_2 a_3}{a_2 - a_3} \right) \left(\frac{1}{L_1 + L_2} - \frac{1}{L_1} \right) - \frac{3}{2} \left(\frac{a_2}{L_1} + \frac{a_2}{L_2} - \frac{a_2}{L_1 + L_2} \right) \right. \\
& \left. + \frac{3}{a_1 + a_2 + a_3} \left(\frac{a_2 a_3}{L_2} + \frac{a_1 a_2}{L_1} + \frac{a_3 a_1}{L_1 + L_2} \right) \right] \dot{L}_1 \\
+ & \frac{(a_2 - a_3)(a_1 + a_2)}{3a_2(a_1 + a_2 + a_3)} \left[1 + \frac{3}{2} \left(\frac{a_2 a_3}{a_2 - a_3} \right) \left(\frac{1}{L_1 + L_2} - \frac{1}{L_1} \right) - 3 \left(\frac{a_1 a_2}{a_1 + a_2} \right) \frac{1}{L_1} \right. \\
& \left. + \frac{3}{a_1 + a_2 + a_3} \left(\frac{a_2 a_3}{L_2} + \frac{a_1 a_2}{L_1} + \frac{a_3 a_1}{L_1 + L_2} \right) \right] \dot{L}_2. \tag{B.1}
\end{aligned}$$

This expression can be used in numerical studies of the swimming motion for arbitrarily large deformations and geometric characteristics.

Bibliography

- [AT06] Igor S. Aranson and Lev S. Tsimring. Patterns and collective behavior in granular media: Theoretical concepts. *Rev. Mod. Phys.*, 78:641–692, 2006.
- [AZ79] M. J. Ablowitz and A. Zeppetella. Explicit solution of fisher’s equation for a special wave speed. *Bull. Math. Biol.*, 41, 1979.
- [BM08] A. Baskaran and M. C. Marchetti. Hydrodynamics of self-propelled hard rods. *Phys. Rev. E*, 77:011920, 2008.
- [BM09] A. Baskaran and M. C. Marchetti. Statistical mechanics and hydrodynamics of bacterial suspensions. *Proc. Natl. Acad. Sci.*, 106(37):15567–15572, 2009.
- [BPSV83] R. Benzi, G. Parisi, A. Suter, and A. Vulpiani. A theory of stochastic resonance in climatic change. *SIAM J. Appl. Math.*, 43:565–578, 1983.
- [BSLS00] Carlos Bustamante, Steven B. Smith, Jan Liphardt, and Doug Smith. Single-molecule studies of dna mechanics. *Current opinion in structural biology*, 10:279–285, 2000.
- [BTBL08] A. P. Berke, L. Turner, H. C. Berg, and E. Lauga. Hydrodynamic attraction of swimming microorganisms by surfaces. *Phys. Rev. Lett.*, 101(3):038102, 2008.
- [CCD⁺07] L. H. Cisneros, R. Cortez, C. Dombrowski, R. E. Goldstein, and J. O. Kessler. Fluid dynamics of self-propelled micro-organisms, from individuals to concentrated populations. *Exp. Fluids*, 43:737–753, 2007.
- [Chu97] Fan R. K. Chung. *Lectures on Spectral Graph Theory*. CBMS Regional Conference Series in Mathematics. AMS, 1997.
- [CKGG11] L. H. Cisneros, J. O. Kessler, S. Ganguly, and R. E. Goldstein. Dynamics of swimming bacteria: Transition to directional order at high concentration. *Phys. Rev. E*, 83:061907, 2011.
- [CPB08] E. A. Codling, M. J. Plank, and S. Benhamou. Random walk models in biology. *J. R. Soc. Interface*, 5:813–834, 2008.

- [DCC⁺04] C. Dombrowski, L. Cisneros, S. Chatkaew, R. E. Goldstein, and J. O. Kessler. Self-concentration and large-scale coherence in bacterial dynamics. *Phys. Rev. Lett.*, 93(9):098103, 2004.
- [DDC⁺11] K. Drescher, J. Dunkel, L. H. Cisneros, S. Ganguly, and R. E. Goldstein. Fluid dynamics and noise in bacterial cell-cell and cell-surface scattering. *Proc. Natl. Acad. Sci. USA*, 108(27):10940–10945, 2011.
- [DGM⁺10] K. Drescher, R. E. Goldstein, N. Michel, M. Polin, and I. Tuval. Direct measurement of the flow field around swimming microorganisms. *Phys. Rev. Lett.*, 105:168101, 2010.
- [DH09] J. Dunkel and P. Hänggi. Relativistic Brownian motion. *Physics Reports*, 471(1):1–73, 2009.
- [DHBG13] J. Dunkel, S. Heidenreich, M. Bär, and R. E. Goldstein. Minimal continuum theories of structure formation in dense active fluids. *New J. Phys.*, 15:045016, 2013.
- [DHD⁺13] J. Dunkel, S. Heidenreich, K. Drescher, H. H. Wensink, M. Bär, and R. E. Goldstein. Fluid dynamics of bacterial turbulence. *Phys. Rev. Lett.*, 110:228102, 2013.
- [DMCS12] J. Dunstan, G. Mino, E. Clement, and R. Soto. A two-sphere model for bacteria swimming near solid surfaces. *Phys. Fluids*, 24:011901, 2012.
- [DTM⁺05] Willow R. DiLuzio, Linda Turner, Michael Mayer, Piotr Garstecki, Douglas B. Weibel, Howard C. Berg, and George M. Whitesides. Escherichia coli swim on the right-hand side. *Nature*, 435:1271–1274, 2005.
- [EKG10] J. Elgeti, U. B. Kaupp, and G. Gompper. Hydrodynamics of sperm cells near surfaces. *Biophys. J.*, pages 1018–1026, 2010.
- [Fis30] R. A. Fisher. *The genetical theory of natural selection*. Oxford University Press, new edition 2000 edition, 1930.
- [Fis63] D. Fisk. *Quasi-martingales and stochastic integrals*. PhD thesis, Michigan State University, Dept. of Statistics, 1963.
- [Fis64] M. E. Fisher. Magnetism in one-dimensional systems—the Heisenberg model for infinite spin. *Amer. J. Phys.*, 32(5):343–346, 1964.
- [Fis65] D. Fisk. Quasimartingales. *Trans. Amer. Math. Soc.*, 120:369–389, 1965.
- [FSGB⁺02] J. A. Freund, L. Schimansky-Geier, B. Beisner, A. Neiman, D. F. Russell, T. Yakusheva, and F. Moss. Behavioral stochastic resonance: How the noise from a daphnia swarm enhances individual prey capture by juvenile paddlefish. *J. Theor. Biol.*, 214:71–83, 2002.

- [GA07] R. Golestanian and A. Ajdari. Simple swimmer at low Reynolds number: three linked spheres. *Phys. Rev. E*, 69, 2007.
- [Gar02] C. W. Gardiner. *Handbook of Stochastic Methods*. Springer Series in Synergetics. Springer, Berlin, 2 edition, 2002.
- [GHJM98] L. Gammaitoni, P. Hänggi, P. Jung, and F. Marchesoni. Stochastic resonance. *Rev. Mod. Phys.*, 70:223–288, 1998.
- [Gib80] B. H. Gibbins. Intermittent swimming of sea urchin sperm. *J. Cell Biol.*, 84(1):1–12, 1980.
- [GJG10] J. S. Guasto, K. A. Johnson, and J. P. Gollub. Oscillatory flows induced by microorganisms swimming in two dimensions. *Phys. Rev. Lett.*, 105:168102, 2010.
- [Gla04] P. Glasserman. *Monte Carlo Methods in Financial Engineering*. Number 53 in Applications of Mathematics. Springer, New York, 2004.
- [Gri02] M. Grigoriu. *Stochastic Calculus: Applications in Science and Engineering*. Birkhäuser, Boston, Basel, Berlin, 2002.
- [Hel73] W. Helfrich. Elastic properties of lipid bilayers—theory and possible experiments. *Z. Naturforsch. C*, 28:693–703, 1973.
- [HGBH03] N. J. Hadjiconstantinou, A. L. Garcia, M. Z. Bazant, and G. He. Statistical error in particle simulations of hydrodynamic phenomena. *J. Comp. Phys.*, 187:274–297, 2003.
- [HM09] P. Hänggi and F. Marchesoni. Artificial brownian motors: Controlling transport on the nanoscale. *Rev. Mod. Phys.*, 81:387–442, 2009.
- [HT82] P. Hänggi and H. Thomas. Stochastic processes: Time evolution, symmetries and linear response. *Phys. Rep.*, 88(4):207–319, 1982.
- [HTB90] P. Hänggi, P. Talkner, and M. Borkovec. Reaction Rate Theory: Fifty Years After Kramers. *Rev. Mod. Phys.*, 62:251–342, 1990.
- [Ito44] K. Ito. Stochastic integral. *Proc. Imp. Acad. Tokyo*, 20:519–524, 1944.
- [Ito51] K. Ito. On stochastic differential equations. *Mem. Amer. Mathem. Soc.*, 4:51–89, 1951.
- [Jar11] C. Jarzynski. Equalities and inequalities: Irreversibility and the second law of thermodynamics at the nanoscale. *Annu. Rev. Condens. Matter Phys.*, 2:329–351, 2011.
- [Jr.69] H. P. MacKean Jr. *Stochastic Integrals*. Academic Press, New York, 1969.

- [KDBG14] V. Kantsler, J. Dunkel, M. Blayney, and R. E. Goldstein. Rheotaxis facilitates upstream navigation of mammalian sperm cells. *eLife*, 3:02403, 2014.
- [Kli94] Yu. L. Klimontovich. Nonlinear Brownian Motion. *Physics-Uspekhi*, 37(8):737–766, 1994.
- [KP06] P. E. Kloeden and E. Platen. *Numerical Solution of Stochastic Differential Equations*, volume 23 of *Stochastic Modelling and Applied Probability*. Springer, 2006.
- [KS91] I. Karatzas and S. E. Shreve. *Brownian Motion and Stochastic Calculus*. Number 113 in Graduate Texts in Mathematics. Springer, New York, Berlin, 2 edition, 1991.
- [LT09] G. Li and J. X. Tang. Accumulation of microswimmers near a surface mediated by collision and rotational brownian motion. *Phys. Rev. Lett.*, 103(7):078101, 2009.
- [LTT08] G. Li, L.-K. Tam, and J. X. Tang. Amplified effect of brownian motion in bacterial near-surface swimming. *Proc. Natl. Acad. Sci. USA*, 105(47):18355–18359, 2008.
- [NN81] C. Nicolis and G. Nicolis. Stochastic aspects of climatic transitions - additive fluctuations. *Tellus*, 33:225–234, 1981.
- [OLXY99] Z.-C. Ou-Yang, J.-X. Liu, Y.-Z. Xie, and X. Yu-Zhang. *Geometric Methods in the Elastic Theory of Membranes in Liquid Crystal Phases*. World Scientific, Singapore, 1999.
- [Ped10] T. J. Pedley. Collective behaviour of swimming micro-organisms. *Experimental Mechanics*, 50:1293–1301, 2010.
- [PK92] T. J. Pedley and J. O Kessler. Hydrodynamic phenomena in suspensions of swimming microorganisms. *Annu. Rev. Fluid. Mech.*, 24:313–358, 1992.
- [POS97] Valery Petrov, Qi Ouyang, and Harry L. Swinney. Resonant pattern formation in a chemical system. *Nature*, 388:655–657, 1997.
- [Ram10] S. Ramaswamy. The mechanics and statistics of active matter. *Annu. Rev. Cond. Mat. Phys.*, 1:323–345, 2010.
- [Rei02] P. Reimann. Brownian motors: noisy transport far from equilibrium. *Phys. Rep.*, 361(2):57–265, 2002.
- [RF96] H. Risken and T. Frank. *The Fokker-Planck Equation: Methods of Solutions and Applications*. Springer Series in Synergetics. Springer, Berlin, 1996.

- [RKH05] I. H. Riedel, K. Kruse, and J. Howard. A self-organized vortex array of hydrodynamically entrained sperm cells. *Science*, 309:300–303, 2005.
- [SAKG07] A. Sokolov, I. S. Aranson, J. O. Kessler, and R. E. Goldstein. Concentration dependence of the collective dynamics of swimming bacteria. *Phys. Rev. Lett.*, 98:158102, 2007.
- [Sei97] U. Seifert. Configurations of fluid membranes and vesicles. *Adv. Phys.*, 46(1):13–137, 1997.
- [SH77] J. Swift and P. C. Hohenberg. Hydrodynamic fluctuations at the convective instability. *Phys. Rev. A*, 15(1):319–328, 1977.
- [SR02] R. A. Simha and S. Ramaswamy. Hydrodynamic fluctuations and instabilities in ordered suspensions of self-propelled particles. *Phys. Rev. Lett.*, 89(5):058101, 2002.
- [SS08] D. Saintillan and M. Shelley. Instabilities, pattern formation and mixing in active suspensions. *Phys. Fluids*, 20:123304, 2008.
- [Str64] R. L. Stratonovich. A New Representation for Stochastic Integrals and Equations. *Vestnik Moskov. Univ., Ser. I: Mat., Mekh.*, 1:3–12, 1964.
- [Str66] R. L. Stratonovich. A New Representation for Stochastic Integrals and Equations. *SIAM J. Control*, 4:362–371, 1966.
- [Str68] R. L. Stratonovich. *Conditional Markov processes and their application to the theory of optimal control*. American Elsevier Pub. Co., 1968.
- [SW87] A. Shapere and F. Wilczek. Self-propulsion at low Reynolds number. *Phys. Rev. Lett.*, 58(20):2051–2054, 1987.
- [TT98] J. Toner and Y. Tu. Flocks, herds, and schools: A quantitative theory of flocking. *Phys. Rev. E*, 58(4):4828–4858, 1998.
- [TTR05] J. Toner, Y. Tu, and S. Ramaswamy. Hydrodynamics and phases of flocks. *Ann. Phys.*, 318:170–244, 2005.
- [WDH⁺12] H. H. Wensink, J. Dunkel, S. Heidenreich, K. Drescher, R. E. Goldstein, H. Löwen, and J. M. Yeomans. Meso-scale turbulence in living fluids. *Proc. Natl. Acad. Sci. USA*, 109(36):14308–14313, 2012.
- [Wol08] C. W. Wolgemuth. Collective swimming and the dynamics of bacterial turbulence. *Biophys. J.*, 95:1564–1574, 2008.